Titre: Title:	Natural and mixed convection in a channel with perturbed boundaries
Auteur: Author:	Xiao Wang
Date:	1994
Type:	Mémoire ou thèse / Dissertation or Thesis
Référence: Citation:	Wang, X. (1994). Natural and mixed convection in a channel with perturbed boundaries [Thèse de doctorat, École Polytechnique de Montréal]. PolyPublie. https://publications.polymtl.ca/32752/

UNIVERSITÉ DE MONTRÉAL

NATURAL AND MIXED CONVECTION IN A CHANNEL WITH PERTURBED BOUNDARIES

par

Xiao Wang

DÉPARTEMENT DE GÉNIE MÉCANIQUE

ÉCOLE POLYTECHNIQUE

THÈSE PRÉSENTÉE EN VUE DE L'OBTENTION
DU GRADE DE PHILOSOPHIAE DOCTOR (Ph.D.)
(GÉNIE MÉCANIQUE)

Avril 1994

ISBN 0-315-97150-9

UNIVERSITÉ DE MONTRÉAL

ÉCOLE POLYTECHNIQUE

Cette thèse intitulée:

NATURAL AND MIXED CONVECTION IN A CHANNEL WITH PERTURBED BOUNDARIES

Présentée par: Xiao Wang

en vue de l'obtention du grade de: Philosophia Doctor (Ph.D.)

a été dûment acceptée par le jury d'examen constitué de:

M.	PELLETIER, Dominique	Ph.D., Président
M.	OOSTHUIZEN, Patrick. H.	Ph.D.
M.	KAHAWITA, René	Ph.D.
M.	ROBILLARD, Luc	Ph.D., Supervisor
M.	NGUYEN, T. Hung	Ph.D., Co-supervisor

Dedicated to my wife, my parents, my parents-in-law
and my uncle Zeng, Fan-you and my aunt Wang, Su-e

SOMMAIRE

Les cycles de vie réduits des produits et l'intense compétition globale dans le marché de la haute technologie ont modifié de façon fondamentale les procédés physiques de conception utilisés dans l'industrie éléctronique. Le développement des méthodes de conception éprouvées et d'équipements éléctroniques sans défaillance dépendent de la modélisation thermique adéquate et de l'application d'une méthodologie de conception physique reposant sur des bases scientifiques. En conséquence le contrôle thermique des composantes éléctroniques a été durant les dernières décades l'un des principaux champs d'application de techniques poussées en transfert thermique. Plusieurs des bénéfices associés à une fiabilité améliorée avec capacité de puissance accrue et à une miniaturisation physique sont le résutlat d'analyses et de conceptions thermiques améliorées qui permettent de stabiliser les températures des composantes au niveau désiré malgré les variations des conditions ambiantes où la présence d'un environnement hostile. Parmi les nombreux modèles de transfert de chaleur, la convection naturelle et la convection forcée continuent d'occuper une place importante dans la conception de boîtes életroniques à cause de leur coût peu élevé et de leur capacité d'adaptation aux normes environnementales.

Cette dissertation a pour objet de présenter notre travail de recherche actuel, lequel porte de façon générale sur la chaleur et le contrôle thermique des systèmes de refroidissement en électronique. Les aspects suivants sont considérés:

- l'environnement thermique des appareils éléctroniques modernes;

- les modèles mathématiques du transfert de chaleur dans des canalisations;
- le développement de simulation numérique;
- les test de comparaison avec des résultats approuvés;
- la convection mixte dans un canal horizontal;
- l'effet d'une onde thermique en mouvement sur la convection de Bénard dans une couche fluide;
- la convection mixte dans un canal incliné.

Plus spécifiquement, nous faisons l'investigation de la convection naturelle et mixte dans un canal à parois lisses dont les frontières sont soumises à des perturbations thermiques. C'est le genre de canal de base que l'on rencontre fréquement dans l'industrie électronique. On étudie numériquement l'interaction entre les rouleaux de convection résultant de l'instabilité classique de Bénard et le chauffage discontinu à intervalles réguliers (ou le cas d'une onde thermique spatialement périodique) imposé sur la frontière. L'intensité relative de l'écoulement forcé et les effets de poussée d'Archimède sont examinés pour une plage importante de nombres de Rayleigh, de Reynolds, et d'autre paramètres géométriques. Le problème est considéré comme étant bidimensionnel et l'on suppose des rouleaux transversaux. Les équations de base appropriées sont résolues numériquement par des techniques numériques. Des conditions périodiques sont imposées aux parois verticales distantes d'une longueur d'onde, de sorte que le domaine numérique peut être limité à une "fenêtre d'observation" d'une seule longueur d'onde qui peut être placée à une position quelconque le long du canal. Le domaine de calcul

peut aussi être étendu au canal tout entier, ce qui permet de considérer l'influence de l'entrée et de la sortie et de vérifier que l'hypothèse d'une solution périodique dont la longueur d'onde correspond à la perturbation est valide.

Les résultats numériques de la présente investigation révèlent que dans le cas de la convection mixte, il existe un seuil 1^0) au dessous duquel une solution permanente existe avec une position fixe des cellules convectives et 2^0) au-dessus duquel il n'y a pas d'état permament, les cellules de convection étant emportées vers l'aval à un rythme irrégulier, périodique dans le temps. Ce seuil a été déterminé pour des conditions variées incluant le cas où il n'y a pas d'écoulement forcé, l'onde thermique imposée à la frontière se déplaçant à une vitesse prédéterminée. Des analyses détaillées ont été effectuées pour les champs d'écoulement et de température, les taux de transfert de chaleur, les cisaillements et les gradients de pression. Dans des cas extrêmes, la précision du présent code numérique est comparée aux resultats provenant d'une analyse théorique.

Dans ce mémoire chaque chapitre reflète des projets de recherche relativement indépendants sur le sujet en question et, par conséquent, chaque chapitre est conçu pour être indépendant dans son contenu technique. Cependant, pour une vision efficace de la thèse dans son ensemble, on a utilisé dans la mesure du possible une nomenclature commune pour tous les chapitres. En plus, les symboles spécifiques à chaque chapitre sont immédiatement disponibles grâce à une liste de definitions additionnelle accompagnant chaque chapitre.

Le premier chapitre décrit de façon générale les types de contrôle thermique utilisés dans la conception de boites électroniques, avec emphase sur le mode de

refroidissement par circulation d'air, par convection naturelle, forcée et mixte. On y mentionne sommairement que le mode de refroidissement par convection naturelle joue un rôle important pour l'équipement en service dans un environnement thermique hostile où dans des endroits peu accessibles, là où la durée de vie des appareils servant à déplacer l'air est source d'inquiétude. Cette circulation d'air le long des composantes génératrices de chaleur a constitué l'une des méthodes les plus populaires de refroidissement. Aussi, un domaine dont l'intérêt est toujours actuel est l'étude d'écoulements combinant la convection naturelle et forcée qu'on désigne communément par le terme convection mixte.

Le chapitre 2 fournit un modèle mathematique de transfert de chaleur dans une couche fluide. Un ensemble d'équations couplées, elliptiques aux dérivées partielles est présenté, servant de base à une formulation aux variables primitives ainsi qu'à une formulation en termes de vorticité fonction de courant. Ces équations provennent des principes de conservation de masse, de conservation de quantité de mouvement et de conservation d'énergie. Des conditions aux limites appropriées y sont aussi discutées.

Le chapitre 3 présente les techniques numériques utilisées dans le présent travail, techniques deja appliquées a une large variété de problèmes de génie. Des méthodes de différences finies et de volume de contrôle y sont présentées. Certains aspects importants y sont discutés en profondeur, incluant la discrétisation des équations et des conditions aux limites. Des considérations sur l'algorithme utilisé pour des systèmes d'équations couplées, sur les conditions aux limites périodiques et sur les concepts de différentiation "upwind" y sont aussi discutées.

Dans le chapitre 4, la précision et la fiabilité du code numérique sont contrôlées par des tests de comparison avec des résultats existants approuvés, comme dans les cas d'un écoulement entrainé et de la convection naturelle dans une cavité carrée.

Le chapitre 5 considère la convection mixte dans un canal horizontal avec segments isothermes, ou sources de chaleur uniformes, régulièrement espacés et séparés par des parties isolées sur la frontière inférieure, alors que la frontière supérieure est froide. Cette idéalisation constitue un point de départ utile et commode pour explorer le transfert de chaleur qui survient dans le refroidissement de pièces électroniques. Le cas extreme d'une frontière inférieure portée entièrement à une tenpérature uniforme est examiné. En supposant que la solution est périodique le long d'un canal s'étendant à l'infini dans les deux directions, selon la périodicité de la perturbation thermique imposée à la frontière, le domaine numérique peu alors être limité à une "fenêtre d'observation" avec conditions périodiques imposées aux sections amont et aval. Cette "fenêtre" peut occuper une position quelconque le long du canal. L'intensité relative de l'écoulement forcé et les effets de poussée d'Archimède sont étudiés pour une plage importante des nombres de Rayleigh et Péclet (ou Reynolds). A des nombres de Reynolds faibles, les rouleaux des convection demeurent attachés aux éléments chauffants et donnent lieu à un état permanent. Au-delà d'un seuil en termes du nombre de Reynolds (ou de Péclet), les rouleaux sont emportés dans la direction aval avec une vitesse variable et selon une récurrence dans le temps. A cause du mouvement irrégulier des rouleaux de convection, toutes les autres variables physiques sont caractérisées par une dépendance du temps périodique. En particulier, le nombre

de Nusselt global relatif à la frontière supérieure et la température moyennée sur la couche fluide (cette température est une mesure de l'énergie contenue dans le fluide) ne sont pas en phase, tout en ayant une forte dépendance périodique du temps. Comme conséquence de ce déphasage, la chaleur produite par les éléments chauffants s'accumule dans la couche fluide avant d'être relachée à travers la frontière supérieure.

Dans le chapitre 6, le mouvement induit par une onde sinusoïdale se propagant dans une couche horizontale d'un fluide de Boussinesq est étudié numériquement. Dans le cas d'une onde thermique stationnaire, les résultats confirment ceux obtenus analytiquement dans le passé. Dans le cas d'une onde thermique en monvement, il existe une vitesse critique, fonction du nombre de Rayleigh et de l'amplitude de la pérturbation imposée, au-dessus de laquelle les rouleaux de Bénard sont emportés avec la perturbation, de sorte qu'une situation permanente peut être observée dans un référentiel se déplaçant avec l'onde. Au dela de cette vitesse critique, il n'y a plus de situation permanente et les rouleaux se déplacent avec une vitesse moyenne plus petite que celle de l'onde thermique. De fait, le comportement de l'écoulement est non permanent périodique et toutes les quantités physiques sont caractérisées par une dépendance cyclique du temps. En particulier, la chaleur est relachée par coups brusques à travers la frontière supérieure.

Dans le chapitre 7, la convection mixte dans un canal incliné avec chauffage discontinu sur le fond et paroi du haut isolée est étudiée numériquement. La plupart des resultats sont obtenus à partir d'un domaine numérique limité à une longueur d'onde de la périodicité imposée sur le fond et avec conditions limites

périodiques aux parois d'extrémité. Quelques résultats numériques sont aussi obtenus à partir d'un canal plus réaliste d'étendu limitée, comportant quelques éléments chauffants, avec conditions aux limites spécifiées à l'entrée et à la sortie. Des inversions d'écoulement locales et globales sont observées, lesquelles sont fonction des nombres de Rayleigh, de Reynolds et des angles d'inclinaison. Ces inversions d'écoulement peuvent modifier grandement la friction à la paroi, le gradient de pression, la distribution de température de même que le transfert de chaleur. Enfin, une solution analytique est obtenue pour le cas limite où la paroi tout entière est chauffée.

En résumé, le but principal de la thèse est d'étudier la convection naturelle et mixte dans des canaux dont les parois sont perturbées thermiquement et de déterminer ainsi l'effet combiné de la convection libre et de la convection forcée sur le transport de chaleur entre des plaques parallèles. Cette étude devrait permettre d'acquérir une vision en profondeur des mécanismes de refroidissement impliqués dans la conception de circuits électroniques.

ABSTRACT

Shrinking product life-cycles and intense global competition in the high-technology marketplace have fundamentally altered the physical design process used in the electronics industry. The development of correct-by-design and failure-free electronic systems is dependent on successful thermal modeling and the systematic application of a science-based physical design methodology. Consequently, thermal control of electronic components has been, for recent decades, one of the primary areas of application of advanced heat transfer techniques. Many of the benefits associated with improved reliability, increased power capability, and physical miniaturization can be traced directly to improved thermal analysis and design, which has allowed component temperatures to be stabilized at a desired level despite variations in ambient conditions or the presence of a hostile environment. Among the various heat transfer models, natural and forced convection continues to command substantial attention in electronic package design due to its lower cost and its environmentally friendly nature.

This dissertation presents our current research work in the subject of heat management and thermal control in electronic cooling system including:

- thermal environment of modern electronic devices
- mathematical model of heat transfer in channels
- numerical simulation development
- benchmark comparison test

- mixed convection in a horizontal channel
- effects of a moving thermal wave on Bénard convection in a horizontal fluid layer
- mixed convection in an inclined channel

In the present study, we investigate the behavior of natural and mixed convection in a smooth-walled channel with boundaries perturbed thermally, that is, the basic channel frequently encountered in electronic industry. The interaction between convective rolls resulting from classical Bénard instability and a regularly spaced discrete heating (or a spatially periodic thermal wave) imposed on the boundary is studied numerically. The relative strength of the forced flow and buoyancy effects are examined for a broad range of Rayleigh number, Reynolds number and geometric parameters.

The problem is considered two-dimensional and transverse rolls are assumed. The appropriate governing equations are solved numerically by computational techniques. Periodicity conditions are imposed on the vertical boundaries of one wavelength, from which the numerical domain is restricted to a one-wavelength "window" that can be located anywhere along the channel. The whole channel used as a computational domain is also calculated from which the influence of entrance and exit is considered and the assumption of periodic solution with a wavelength corresponding to the perturbation is validated.

The numerical results of the present investigation reveal that in the case of mixed convection, there exists a threshold 1^0 below which a steady state solution

exists with fixed location of the convective cell and 2^0 above which no steady state is possible with cells carried downstream at an irregular time-periodic rate. This type of the threshold has been determined for various conditions including the case for which no forced flow exist but the imposed thermal wave is moving at a predetermined velocity. Detailed analyses of flow and temperature fields, heat transfer rates and shear stress or pressure gradients have been conducted. In some extreme cases, the accuracy of present numerical code is verified by theoretical analysis.

ACKNOWLEDGEMENTS

First of all, I would like to express my greatest appreciation to professor Luc Robillard, my Ph.D program supervisor, for his encouragement and careful guidance during my research work and feel very pleased to have the opportunity to work under his supervision and counselling in all phases of my graduate studies at Ecole Polytechnique, University of Montreal. He has given me invaluable help in many ways.

Grateful acknowledgements are also expressed to professor T. Hung Nguyen, my co-supervisor, for his many helpful suggestions and discussions during my graduate study.

Many professors, fellow graduate students, colleagues and friends in the Mechanical Engineering Department of Ecole Polytechnique, University of Montreal have provided a lot of suggestions and personal help. My sincere thanks go to all, and I would like to mention specifically the help and advice that I received from professor P. Vasseur.

Also, acknowledgement is due to NSERC & FCAR for the research financial support as well as the Department of Mechanical Engineering at Ecole Polytechnique that provides a dynamic and exciting atmosphere together with good computer facilities.

TABLE OF CONTENTS

LIST OF FIGURES

LIST OF TABLES

LIST OF SYMBOLS

A	dimensionless length of heating elements
a	dimensional length of heating elements
B	dimensionless length of periodicity
b	dimensional length of periodicity
C	dimensionless increment of temperature for one wavelength
Fr	Froude number, $u_0/\sqrt{g\beta\Delta T h}$
g	gravitational acceleration, m/s^2
h	width of the channel, m
k	thermal conductivity, $W/(m.K)$
K'	dimensional wavenumber of thermal wave
K	dimensionless wavenumber of thermal wave
L	dimensionless length of whole channel
Nu	Nusselt number
Pe	Peclet number, hu_0/α
Pr	Prandtl number, ν/α
q	imposed heat flux on heating elements, $W/(m^2)$
q_r	flow reversal parameter (Eq. 7.14)
Ra	Rayleigh number, $g\beta\Delta T h^3/\mu\alpha$
Re	Reynolds number, hu_0/ν
t	dimensional time
T	dimensional temperature, K
V_a	dimensionless velocity of moving window

V_c	dimensionless velocity of transverse rolls
V_w	dimensionless velocity of thermal wave
ΔP	dimensionless pressure decrement in one wavelength
u, v	dimensional velocity components in x and y directions
U, V	dimensionless velocity components in X and Y directions
x, y	dimensional cartesian coordinates
X, Y	dimensionless cartesian coordinates, x/h, y/h

Greek Symbols

α	thermal diffusivity, m^2/s
β	thermal expansion coefficient, K^{-1}
θ	dimensionless temperature $(T - T_r)/\Delta T$
μ	dynamic viscosity of fluid, $kg/s.m$
ν	kinematic viscosity of fluid, m^2/s
ρ	fluid density, kg/m^3
σ	dimensional amplitude of the thermal wave
δ	dimensionless amplitude of thermal wave
τ	dimensionless time hu_0/ν
φ	inclination angle of the channel
ψ	dimensional stream function
Ψ	dimensionless stream function
ω	vorticity,
Ω	dimensionless vorticity

λ	imposed wavelength
Υ	dimensionless time period
γ	dimensional frequency of thermal wave
Γ	dimensionless frequency of thermal wave

Subscripts

av	refers to average value
b	refers to bottom wall
c	refers to convective property
cr	refers to critical value
ext	refers to extreme value
l	refers to left wall
r	refers to right wall
t	refers to top wall

Superscripts

$*$	refers to conductive property
$-$	refers to value averaged over one period
$\hat{}$	refers to moving coordinate system
$\tilde{}$	refers to value averaged over one wavelength

LIST OF APPENDICES

Chapter 1

INTRODUCTION

1.1 BACKGROUND

The growing use of electronics in both the military and civilian sectors leads to widespread recognition of the need for thermal packaging and design of electronic components. Particularly the rising level of overall power dissipation and high density of electronic components make the successful operation of electronic devices, ranging from microelectronic chips to large power tubes, critically dependent on efficient and reliable heat removed. Consequently, the choice of thermal control technology and the particular decisions made in the course of evolving the thermal packaging design often have far-reaching effects on both the reliability and cost of the electronic system.

Despite changing demands and the availability of new heat transfer technology, direct air cooling of electronic components continues to command substantial attention. A comprehensive overview of this subject may be found in the article given by Hannemann, R [1], where he concludes that natural and forced convection are still very popular in electronic cooling systems due to their lower cost bands as well as convenient user environments, and that research in creative packaging and cooling approaches using forced air will be beneficial in designing high performance microsystems.

1.1.1 Thermal Environment of Modern Electronic Devices

In the thermal control of modern electronic devices, it is necessary to provide an acceptable "microclimate", for a diversity of components that, while frequently in close proximity to each other, often display substantially different sensitivities to environmental factors and widely varying heat dissipation rates. Some knowledge of the possible range of component and environmental variations is thus a necessary prerequisite for successful design and development of thermal control systems and the rational interpretation of bench and prototype tests. A review of the aims of thermal control, commonly encountered thermal environment and the thermal characteristics of several classes of components are presented by Bar-Cohen [2].

Generally, the thermal management of a complex system like a computer can be divided into different structural levels. A typical configuration is shown in Fig. 1.1, where the chip is the smallest component of the system, the module, whose function is to isolate the chip(s) from the atmosphere and at the same time to provide the leads for transmission of signals to and from the chip(s), the supply of power, and the printed wiring board (PWB), which carries modules. Heat produced by the chip has to travel along multiple conduction paths inside the module, overcoming what is called internal thermal resistance. On the surface of the module, heat is transferred to the coolant, thereby overcoming the external thermal resistance. At the level of the PWB (printed wiring board), the temperature of the coolant increases as the coolant absorbs heat from the modules along its flow path. This is referred to as the system level thermal resistance. Modules near the exit of the coolant flow are subject to the most severe thermal environment

within the system due to the high temperature of the coolant surrounding them.

Figure 1.2 shows the data for heat loads on chips, modules, and PWBs (printed wiring boards). The horizontal axis gives the area on the components for chips and modules which is the projected area on the board. The data belong to the machines already in commercial operation in the field; those carrying open symbols represent air-cooling machines, and the shaded symbols represent machines where indirect water cooling is employed. The arrows indicate the trends of increasing heat load at all structural levels of the computer.

Figure 1.3 shows another view of the current state of the hardware design of computer. The vertical axis shows the rate of electrical power consumption by the computer system, which is approximately equal to the rate of heat generation by the system. This figure refers not only to the data of mainframes and supercomputers but also to medium-sized computers for office use. The shaded band covers the data for office computers, central processor volume (CPU) of some typical computers, and system volume of mainframes and supercomputer. Most of these data belong to the air-cooled machines, with only a few characterizing the indirect water-cooled machine. An examination of this data collection indicates that the volumetric power density of medium and small scale computers is comparable to that of large-scale computers. However, the design of air cooling for small computers is just an equally demanding task as for large systems.

Obviously, the knowledge base established with the past generations of electronic equipment serves as a vehicle for the development of future generations of equipments.

1.1.2 Natural Convection Cooling

With the spread of electronic equipment in many corners of our lives, the demands are growing for the elimination of acoustic noise inherent to forced air-cooling. As a consequent, natural convection cooling is playing an important role for equipment that operates in hostile thermal environments and in remote locations, where the service life of air-moving devices is a matter of concern.

In actual electronic equipments, however, the presence of components and other obstacles imposing constraints on the convection of air is almost the rule, particularly in equipments where increased packing density of components is inevitable. Figure 1.4 shows a situation commonly found in electronic equipments, where heat dissipating components are mounted on the plates and heat transfer from the array is influenced by free convection of the coolant, as well as by conduction in the plates and by radiation exchange between the plates and their surroundings. Although the manner in which heat is dissipated along the wall varies with specific packaging and operating conditions, many applications of interest are suitably approximated by smooth plates with symmetric isothermal or isoflux surfaces, or use of an isothermal/isoflux boundary together with an insulated boundary condition along the adjoining plate [3], [4], [5].

For vertical channels, buoyancy acts exclusively to induce motion in the streamwise direction and, boundary layers, beginning at inlet, develop on each surface. For short channels and/or large sparrings, independent boundary layer development occurs at each surface and conditions correspond to those for an isolated plate in an infinite quiescent medium. For large length/width, however,

boundary layers developing on opposing surfaces eventually merge to yield a fully developed condition. If the channel is inclined, there is a component of the buoyancy force acting normal, as well as parallel, to the streamwise direction, and conditions may lead to strong flow.

Beginning with the benchmark paper by Elenbaas [6], the vertical channel orientation has been studied extensively for symmetrically and asymmetrically heated plates with isothermal or isoflux surface conditions. For symmetrically heated, isothermal plates, Elenbaas obtained a semi-empirical correlation for the average Nusselt number $\overline{Nu_s}$ as a function of the parameter Ra_s. In the fully developed limit, the correlation is in excellent agreement with the predictions of Bodoia et al. [7], who numerically simulated the developing flow with uniform inlet velocity and temperature profile, and with the analytical fully developed flow solution of Aung [8]. Improved agreement was obtained by Aihara [9], whose numerical simulation accounted for the pressure defect created by the acceleration of the inviscid fluid at the channel inlet.

For symmetrically heated isoflux surfaces, local heat transfer coefficients have been measured by Siegel and Norris [10], and both fully developed and entry region solutions have been obtained by Aung et al. [8], [11]. Experiments performed by Wirtz and Stutzman [12] yielded a correlation for the maximum plate temperature, which is in good agreement with the predictions of Aung et al. [11].

For asymmetric heating Aung [8] obtained closed form solutions for fully developed flow, while Aung et al. [11] obtained numerical and experimental results for developing flow. It was also concluded that expressions obtained for isoflux

symmetric heating could be used to predict the maximum temperature on each of the asymmetrically heated surfaces. Miyatake and Fujii [13], [14], and Dalbert [15] extended the available results to include both asymmetric wall temperature and heat flux boundary conditions, including the single insulated wall.

Conditions corresponding to a single heated plate, with the other plate insulated, have received consideration. Numerical simulations (Miyatake and Fujii [13], Miyatake et al. [14]), as well as experiments (Sparrow et al., [16]; Miyamoto et al. [17]) have been performed for both isothermal and isoflux conditions at the heated plate. For modified Rayleigh numbers up to 3×10^{14}, Miyamoto et al. [17] observed transition to turbulence in upper portions of the channel, with an accompanying enhancement of the local Nusselt number at the heated (isoflux) surface.

Factors that may influence the applicability of the foregoing results to PCBs (printed circuit boards) include edge effects (Sparrow and Bahrami [18]), board conduction (Burch et al. [19]), and the effect of protruding components. Studies concerning applicability of isothermal or isoflux correlations to PCBs (printed circuit boards) with regular and irregular arrays of wall protrusions have yielded mixed results. Birnbrier [20] found that uniform heat flux correlations did not provide reliable predictions of component temperatures on a printed circuit board. Ortega and Moffat [21] measured heat transfer from a square in-line array of cubical elements mounted on one of opposing insulated boards, and average convection coefficients for air were as much as 50 percent larger than results for an equivalent parallel plate channel. With respect to the elements, flow due to global buoyancy was viewed as forced convection and heat transfer could be calculated from an

appropriate forced convection correlation.

Energy dissipated by an electronic component in a quiescent ambient air induces a buoyancy-driven flow that ascends from the component as a wake or plume. A common example concerns free convection heat transfer from a small rectangular component, flush-mounted to a vertical substrate. The problem was first considered by Baker [22], [23], who found that the heat transfer coefficient increased significantly with decreasing heater size and was underpredicted by accepted free convection correlations. Heat transfer coefficients in excess of standard predictions were also measured by Carey and Mollendorf [24] and Park and Bergles [25]. In the latter study, the coefficient increased with decreasing width, and the effect was attributed to an induced flow of ambient fluid at the sides of the heater.

For a vertical, in-line array of heat sources, the plume ascending from a lower source can strongly influence heat transfer at an upper source. For laminar, two-dimensional flow associated with two isolated sources flush mounted on a vertical wall, Sparrow and Faghri [26] numerically delineated the competing effects on heat transfer enhancement and degradation at the upper source due to fluid acceleration and preheating, respectively, by the lower source. The problem has been considered experimentally by Park and Bergles [25].

There exist numerous applications for which electronic components are packaged within rectangular enclosures. The components may be mounted to one wall of the enclosure, while one or more of the other walls is cooled. Buoyancy forces induce a recirculating flow within the enclosure, and heat is transferred by natural convection from the component surfaces.

Although the literature on natural convection in enclosures is voluminous, comparatively little has been reported on the effects of discrete heat sources. The first such study was performed by Chu et al. [27], who observed a two-dimensional numerical solution for a single, isothermal heater strip, flush-mounted to a vertical wall of the cavity. The opposite wall was cooled, while all other surfaces were adiabatic. Calculations were performed for air, with Grashof numbers and aspect ratios in the ranges $0 \leq Gr_H \leq 10^5$ and $0.4 \leq H/W \leq 5$. The heater size L and position S were also varied. Over the range of conditions considered, the average Nusselt number was found to increase as Gr_H^n, where $n \simeq 0.3$. It also increased with increasing L/H, exhibited a maximum for an optimal heater location of $S/H \simeq 0.4$, and was approximately independent in a subsequent numerical simulation for water [28]. Experiments performed in air for heating and cooling on opposite vertical walls [29], [30] confirmed the L/H, S/H, and H/W trends predicted by Chu et al. [27], but for larger Grashof number ($5\times10^6 \leq Gr_H \leq 9\times10^6$).

More recently, two-dimensional numerical simulations [31] and experiments [32] have been performed for an isothermal protruding heater mounted to one vertical wall of a rectangular cavity. The remainder of the heater wall and the opposing wall were insulated, while the top and bottom surfaces were cooled. At large Rayleigh numbers, Nusselt number data were in good agreement with the predictions, but at small Rayleigh numbers the data, which were characterized by large uncertainty, were significantly overpredicted. Irrespective of heater location, both the numerical simulations and visualizations revealed that the buoyancy-driven flow was concentrated in the region above the heater. A three-dimensional simulation has been performed for flow and heat transfer from a 3×3 array of

blocklike electronic components mounted to one vertical wall of a rectangular cavity filled with a dielectric liquid [33]. However, there is need for additional research to clarify the significance of three-dimensional effects and limitations associated with two-dimensional results.

For inclined channel, Kennedy and Kanehl [34] and Azevedo and Sparrow [35] performed experiments for inclined channels in air and water, respectively. For isoflux plates and $30^0 \leq \varphi \leq 90^0$, Kennedy and Kanehl found that bottom plate temperatures could be reduced by operating at a tilt angle of 75^0. They also observed three-dimensional longitudinal vortices driven by the normal component of the buoyancy force that resulted from bottom heating. For heated and insulated top and bottom plates, respectively, a two-dimensional recirculating flow was observed to exist near the unheated wall and the channel outlet. Data obtained for all experimental conditions, including vertical as well as inclined plates, were correlated to within ± 10 percent.

So far, the above and complementary studies emerge a unified picture of natural convection cooling in electronic equipments. In principle, these studies are within the scope of classical natural convection internal flow. From such a fundamental point of view, instabilities, transitions found in Rayleigh-Bénard convection and nonlinear phenomena are likely to be encountered. A comprehensive review of this subject is presented in the book of Bejan [36]. A number of studies consider the effect of thermal boundary conditions on convection in a horizontal layer. Mohanty [37] calculated the unsteady convection in horizontal channels with arbitrary temperatures through to steady state flow. An analytical and experimental study describes the instability of convection rolls in a layer

heated from below [38]. In the limit of very low Prandtl numbers, a square pattern of convection cells occurs [39]. Large-scale motion for low Prandtl number fluid is also predicted by Chapman and Proctor [40]. Linear stability theory has been used to predict the instability in a horizontal layer with suction through the boundaries [41], and the experimental results on the initial onset of flow for sudden heating from below were reported [42]. Also, a nonlinear stability analysis predicts a stable hexagons within a thin fluid layer having a sinusoidal variation of bottom wall temperature [43]. It was demonstrated recently that some natural convection flows may show steady-state solutions with flow in opposite directions [44]. This multiplicity of solutions is not merely theoretical, as there is experimental evidence for at least two different stably convective flows under identical heating and geometric conditions [45]. In a study by Robillard et al. [46] of free convection in horizontal porous layers with localized heating from below, a special emphasis is given on the multiple steady-state solutions that can take place within the cavity through the use of appropriate initial perturbations.

Unlike horizontal fluid layers, inclined layers generally do not have a critical Rayleigh number for the onset of flow. However, stability analyses are still of interest in such flow layers. Ozisik et al. [47] investigated the effect of boundary conditions on the stability of an inclined layer. A power integral analysis [48] estabilishes the parameters for instability and also describes the post-stability flow taking place in both inclined and vertical layers. It was shown that the inclination angle has an important role in determining the flow direction in a slanted open rectangular cavity [49]. At small inclination angles, the side wall of a cavity give rise to a secondary flow in the form of stationary transverse rolls with horizontal

axes parallel to the shorter side, as opposed to the longitudinal rolls predicted for an infinite layer [50]. The tilt angle and aspect ratio of an inclined layer strongly affect the critical Rayleigh number corresponding the transition threshold from steady to time varying flow.

1.1.3 Forced Convection Cooling

Blowing air past heat generating components has been the most popular method of cooling. In 1942, Mouromtseff [51] documented the design analysis for the cooling of a high-power vacuum tube, which was performed by applying the correlations presented by McAdams [52]. In most cases of cooling devices by forced convection of air, the thermal design involves the use of extended surfaces. Kraus [53] recently appraised Gardner's classic work [54] on the graphical presentations of the fin efficiency which was published in 1945. The technique of heat transfer enhancement by extended surfaces has also been useed for devices requiring high-power dissipation since the early years of electrical and electronics technology. An example is found in the report by London [55] on the use of louvered fins to improve the thermal design of a new type of vacuum tube (microwave) dissipating up to 25 kW. The now popular reference book by Kays and London [56] originated from the need to provide a database of heat transfer and flow friction for such design work.

With the advent of integrated circuit technology, new dimensions were added to the problem of air cooling. For instance, Fig. 1.5 shows a printed wiring board, 28 cm wide and 42 cm long, carrying 72 modules, and dissipating 512 W [57]. Such a device is common in present day air-cooled main frame computer. Grouped in

the middle of the board are the high-speed memory modules, and the rest are the logic modules. Heat sinks are designed to accommodate the heat dissipation, 6 W from the logic module, and 11 W from the memory module. A row of such boards is set in the housing where air is forced through by the blowers. Hence, the physical situation is described by a model where the modules rest on one side of the parallel plate channels, leaving free-flow space between the fin tips and the other side of the channel, and also between the columns of the modules. Heat transfer problems involved in this example embody the following generic issues for the present and future generations of electronic equipment.

Heat transfer from flush-mounted sources

The temperature distribution in a channel is complex since the air flow over the columns of the modules has only a finite rate of mass exchange with the air through the free flow areas between the module columns. The air temperature over the modules is higher than that in the adjacent free flow areas. The variation of air temperature in the channel is governed by the geometry of the channel, the size and structure of the module, the location of the modules, the rate of the heat dissipation from the modules, and the air velocity. It is important for the equipment designer to predict the distribution of air temperature in order to hold the temperature of modules below a tolerable level near the channel exit, as well as to constrain the temperature variation among the modules within a permissible range. Early experimental data available for such design work were obtained by Baker [22], [23].

Studies related to heat transfer from an array of discrete isothermal sources

flush-mounted to one wall of a rectangular channel have been performed by Incropera et al. [58]. The array consisted of four equally spaced rows, with three heaters in each row. Experiments were performed for water and FC-77 without the pin fins, and results were compared with predictions based on two-dimensional, conjugate forced convection models for laminar and turbulent flow. The data were significantly underpredicted in laminar flow, and differences were attributed to the effects of buoyancy on the experimental results. In turbulent flow, however, agreement between the predicted and measured results was good, suggesting that three-dimensional boundary layer effects were negligible. Due to the effects of upstream thermal boundary layer development, average Nusselt numbers in the second row were approximately 25 percent less than those of the first row, while Nusselt numbers in the third row were approximately 10 percent less than those of the second row. The decrease from the third to the fourth row was only 3 percent.

Heat transfer from protruding sources

A common electronic package is one that involves forced air cooling of protruding components on a printed circuit board. Typically, many such boards are stacked in a direction normal to the flow, forming parallel plate channels with the component covered board facing the smooth surface of an adjoining board. However, unlike the regular array of cubical components, components of varying dimensions are often arranged in an irregular pattern. Even for a regular arrangement of uniformly sized components, there is considerable geometric variability and there is no definitive characteristic length. Three-dimensional flow component edges, separation downstream of the components, and bypass around the

components. If the components occupy a large portion of the flow cross-section, the flow is partitioned into two streams, one of which passes through the array, contributing to its cooling, while the other passes over the array with little effect on cooling. In addition to being influenced by such flow phenomena, heat transfer from a downstream component may be strongly affected by incomplete mixing in the channel cross section and hence by the location of the downstream component in the thermal wake of an upstream component. Further complications may result from the existence of missing components and the use of barriers or ribs to enhance heat transfer from downstream components.

Despite the enormous variability of geometric conditions, systematic attempts have been made to determine component coefficients and to develop methodologies for treating the effect of component location in an array. In an early study, Buller and Kilburn [59] obtained heat transfer data for a single rectangular component and successfully correlated the data using a hybrid characteristic length based on features of both the flow and component geometries. In subsequent experiments, Sparrow and his co-workers considered an array of components and systematically examined the effect of row number, missing and irregular components, and barriers on the average convection coefficient for a single component in the array [60], [61]. Lemann and Wirtz [62] also considered the effect of rib spacing and channel height by placing ten unheated, repeating ribs upstream of a heated, two-dimensional, rectangular component. Conjugate heat transfer calculations for two-dimensional developing flow over three repeating, heated, rectangular components [63] revealed the effect of recirculating zones and the existence of an optimum component spacing.

Several investigators have suggested methodologies for treating downstream effects of nonuniform heating in an array of components. Arvizu and Moffat [64] proposed a superposition method to account for the effect of thermal wakes on the temperature rise of downstream components. In subsequent studies Moffat et al. [65] obtained thermal wake functions for an in-line array of cubical elements, while Bieber and Sammakia [66] applied a superposition method to an array of flat packs. An alternative was proposed by Ashiwake et al. [67], who found that the dispersion of thermal wakes and the reduction of downstream component temperatures improved when the components are staggered rather than in-line. Thermal wake dispersion is known to increase with increasing Reynolds number [64], [68].

Heat transfer enhancement with fins

The large convection coefficients associated with small surfaces render the use of single-phase forced convection an attractive method for the cooling of electronic devices. However, it is possible that additional enhancement may be realized by employing fins to augment the surface. Such augmentation can result in as much as an order-of-magnitude increase in the heat transfer rate without appreciably altering the heat transfer coefficient.

Experimental studies by Sparrow and Ramsey [69] for in-line and staggered arrays of pins with tip clearance revealed a row-by-row increase in the pin convection coefficient up to the fourth row, beyond which fully developed conditions were achieved. Convection coefficients and pressure drops were larger for the staggered array than for the in-line array. Van Fossen [70] studied heat transfer from

staggered arrays of short pin fins affixed between two heated copper plates and showed that the pins enhanced heat transfer by a factor of two over that for a plain channel with no fins. Simoneau and Van Fossen [71] reported results for in-line and staggered arrays of pins, and in both cases heat transfer from a row was enhanced by the presence of upstream rows. More recently, Steuber and Metzger [72] performed a comprehensive experimental study of more than 20 in-line and staggered pin fin arrangements, with and without tip clearance. The effect of pin fin configuration on local convection coefficients at the wall of a rectangular channel to which the pins are attached has been experimentally determined by Lau et al. [73].

Shrouded arrays of longitudinal fins may also be used to enhance heat transfer from electronic devices. Sparrow and Hsu [74] predicted local Nusselt number distributions on longitudinal fins for fully developed laminar flow. The results revealed highly nonuniform heat transfer distributions along the fin and base surfaces. With no tip clearance, the Nusselt number attained a maximum between the base and tip, and with tip clearance, the Nusselt number increased monotonically to the tip. Experiments have also been performed to assess the effect of longitudinal fins on heat transfer from discrete sources. Kishimoto et al. [75] obtained heat transfer data for longitudinal fins mounted to an array of chips, while Yokono et al. [76] obtained data for a single heater. In both cases, data were obtained for air flow over unshrouded fins of varying dimensions.

In some instances, heat transfer from electronic components can be enhanced through the use of boundary layer turbulators, which should be placed at appropriate locations on printed circuit cards to trip the flow and break up the boundary

layer. For a fixed air flow rate, the heat transfer coefficient on a module behind a turbulator is presented by Sparrow et al. [77]. Of course, the added pressure drop due to the turbulators will cause the blower to shift its operating points, and deliver less air flow. Taking this into account the actual improvement realized in heat transfer coefficient is around 15% [78] . Nonetheless, turbulator strips have been used in practice to achieve modest reductions in chip temperature.

Heat transfer enhancement may also be realized by modulating low Reynolds number laminar flows in a parallel plate channel. The process, known as resonant enhancement, may be affected in a grooved channel by actively modulating the flow rate at the natural frequency of the system or by achieving passive modulation through insertion of small vortex-shedding cylinders in crossflow [79] [80]. Significant heat transfer enhancement may be achieved with only a modest increase in pressure drop.

1.1.4 Mixed Convection Cooling

An area of continuing interest is the study of flows with combined natural and forced convection often called mixed convection. Under such conditions, flow is driven by an externally imposed pressure gradient, as well as by buoyancy forces. If the channel is vertical, buoyancy acts to augment or retard the flow, according to whether the buoyancy force aids or opposes the imposed flow. if the channel is horizontal and heating occurs at the bottom surface, buoyancy may induce a secondary flow which, in combination with the main flow, produces a system of longitudinal vortices. If the channel is inclined, the buoyancy force has two components, one parallel to the surface, acting to accelerate or decelerate flow in

the streamwise direction, and the other normal to the surface, acting to drive the secondary flow. The relative influence of these effects depends on the inclination angle.

Two-dimensional, elliptic models have been used to analyze laminar, mixed convection flow between vertical parallel plates with symmetric and asymmetric uniform wall temperature. The models have addressed both developing [81], [82] and fully developed [83] flow conditions. Due to local fluid acceleration effects, buoyancy enhances heat transfer in the entrance region, particularly for the hotter of the two walls, but buoyancy has no effect on heat transfer in the fully developed region. For asymmetric heating, flow reversal occurs when the parameter Gr/Re exceeds a threshold value, causing downflow along the cooler of the two walls. Heat transfer enhancement is most pronounced when the channel is horizontal and heat is transferred from the bottom surface. Gill and Del Casal [84] analysed the effect of buoyancy on fully developed laminar flow between parallel isothermal planes, and Beckett [85] considered the influence of viscous dissipation in the same problem.

In experiments performed for laminar flow between asymmetrically heated parallel plates [86], convection coefficients at the bottom plate were found to exceed those corresponding to pure forced convection by up to a factor of 6. Enhancement was due to buoyancy-driven flow, which replaced warmer particles of fluid ascending from the plate with cooler fluid descending from the main flow. In transitional and turbulent flows, The effects of buoyancy on heat transfer enhancement at the bottom plate are much less pronounced [87]. Criteria for predicting the onset of a secondary flow have been established [58], and a laminar, parabolic,

three-dimensional model has been used to predict the flow morphology [88]. In the absence of significant wall condition, the developing secondary flow causes longitudinal variations in the Nusselt number, which have been confirmed experimentally [89]. The strength of the secondary flow and the attendant Nusselt number oscillations decrease with increasing inclination angle [90]. Recent work has focused on the existence of travelling transverse waves resulting from the thermal instability caused by the temperature difference between the two horizontal plates. A large cross section of the fundamental research on this topic has been reviewed by Ouazzani et al. [91], Platten et al. [92] and Fukui et al. [93].

Studies of mixed convection heat transfer from discrete sources are documented by Kennedy and Zebib [94] and Tomimura and Fujii [95]. For small heater strips flush-mounted to the wall of a horizontal channel, Kennedy and Zebib observed the formation of longitudinal and spanwise vortices in air due to heating at the bottom and top surfaces, respectively. Tomimura and Fujii applied a laminar, two-dimensional model to air flow between parallel plates, with the top surface insulated and with an array of seven equally spaced discrete sources flush-mounted to the bottom surface. For vertical and near-vertical orientations, acceleration of the flow by the streamwise component of the buoyancy force enhances the local Nusselt number for each source significantly above that associated with forced convection. More recently, Hasnaoui et al. [96] investigated mixed convection in a horizontal layer with heating elements regularly spaced on the lower boundary. Their results show that at low Reynolds number, a steady state is possible for which the convective cells remain attached to the heating elements. Beyond a critical Reynolds number, the cells are carried downstream, reinforced

and weakened periodically.

1.2 OUTLINE OF THE THESIS

The variety in the geometry and packaging distribution of electronic components used in commercial and military equipment precludes a description of all the possible combinations of physical, thermal, and fluid parameters. It is nevertheless, useful to classify, in somewhat idealized form, the various configurations according to:

- Physical boundary condition (smooth, "sandgrain" roughness, protuberance)
- Thermal, circumferential boundary condition (symmetric, variable, one-side insulated)
- Thermal, axial boundary condition (isothermal, isoflux, axil temperature profile, axil flux profile)
- Flow regime (laminar, transition, turbulent)
- Fluid temperature profile in channel (developing, fully developed)
- Fluid velocity profile in channel (developing, fully developed)

This rather restricted, idealized classification contains more than 430 distinct combinations, and it is clearly not possible to analyse each one in detail with the limits of the present study. Instead, following a detailed exploration of thermal transport in a smooth-walled channel with fully developed laminar flow, that is, the basic channel, attention will be turned to the more common variations, including the particular contribution of thermal wave on the lower boundary. In this, we mainly focus on the following cases:

A. We consider in Chapter 5 the mixed convection in a horizontal channel with isothermal segment or isoflux segment regularly spaced and separated by insulated parts on the lower boundary and cooled isothermally at the top boundary. This idealization provides both a convenient and useful starting point for the exploration of heat transfer in electronic cooling applications. The approach here is two-dimensional and transverse rolls are assumed. Also periodicity conditions are applied on the vertical boundaries of the domain to be solved numerically. This domain is then equivalent to a "window" that can be located anywhere along the channel. Depending on the values of the Rayleigh and Péclet number (or Reynolds number), the flow may be steady or unsteady periodic, with or without rolls. Moreover, for the particular case of a lower boundary maintained everywhere at a uniform temperature, the thermal wave characterizing the mixed convection is carried downstream at a constant velocity and consequently it becomes possible, by the use of the galilean transformation applied to that window, to eliminate the time dependence of the solution.

B. In chapter 6, the motion induced by a sinusoidal thermal wave propagating in a horizontal layer of Boussinesq fluid is investigated numerically. In the case of a stationary thermal wave, the results corroborate those obtained analytically by Kelly and Pal [97]. In the case of a moving thermal wave, there exists a critical wave velocity for a given pair of values Rayleigh number and magnitude of perturbation, below which the cells remain attached to the thermal wave, so that a steady state is observed in a coordinate system moving with the wave. Above that critical value, the cells are entrained, but at lower velocity and a time periodic solution is obtained.

C. Finally, a fully developed opposing mixed convection in an inclined channel with discrete heating on the bottom and insulated top wall is numerically studied in chapter 7. Both overall and local recirculating flow are observed for different values of Rayleigh number, Reynolds number and inclination angle. These flow reversal could strongly affect velocity and temperature profiles as well as the stability of the heat transfer and fluid motion in channels.

The remainder of the thesis consists of three additional chapters and accompanying appendices.

In chapter 2, a mathematical model is presented based on a set of governing equations with appropriate boundary conditions, which expresses mass, momentum and energy conservation in the fluid layer. Chapter 3 discusses the numerical schemes used to solve the set of equations given in chapter 2. Both finite difference and control volume methods are undertaken with a vorticity-stream function formulation and a primitive variable approach respectively. In chapter 4, the validity and reliability of the numerical code is examined by validation tests of driven flow and natural convection in a square cavity.

In summary, the main objective of this thesis is to study the behavior of fluid motion and heat transfer in channels with boundaries perturbed thermally and to observe the effect of relative strength of free and forced convection on the characteristics of thermal transport between parallel plates.

Chapter 2

MATHEMATICAL MODEL

The problem considered in this thesis is a fully developed laminar flow in channels with perturbed thermal boundary conditions. The problem is considered two dimensional and is schematically described in Fig. 2.1, where the upper boundary is cooled or insulated while the lower boundary is heated at a constant temperature or through regularly spaced discrete heating elements at constant temperature or uniform heat flux, the remaining parts being adiabatic. Another thermal boundary condition on the lower boundary is adding a sinusoidal temperature distribution of arbitrary amplitude and velocity (thermal wave) to the uniform temperature of the lower boundary. Assuming that the resulting motion due to forced flow and buoyancy effects is spatially periodic with a wavelength corresponding to the imposed thermal perturbation, we restricted the domain of study to one wavelength λ with periodic boundary conditions imposed on upstream and downstream sections, as shown in Fig. 2.1 by a dotted rectangle ("window"). The hypothesis of a solution with a wavelength corresponding to the imposed wavelength on the lower boundary will be discussed later on. The horizontal and vertical cases can be recovered by setting the tilt angle to zero and $\pi/2$ respectively.

Basically, the dynamics of a general incompressible flow where buoyancy effects due to temperature differences are involved, can be described well by the

Navier-Stokes equations, together with the energy equation for conservation of energy and the continuity equation for conservation of mass. These form a set of nonlinear coupled partial differential equations (PDEs).

2.1 PRIMITIVE-VARIABLE FORMULATION

The governing equations are the momentum equation and energy equation as well as continuity equation in terms of the primitive variables.

Continuity Equation

$$\nabla \cdot \vec{v} = 0 \tag{2.1}$$

Momentum Equation

$$\rho \frac{D\vec{v}}{Dt} = -\nabla p + \mu \nabla^2 \vec{v} + \vec{f} \tag{2.2}$$

Energy Equation

$$\rho C_p \frac{DT}{Dt} = k\nabla^2 T + e + \beta T \frac{Dp}{Dt} + \mu\phi \tag{2.3}$$

where $\vec{v}$, p, T. $\vec{f}$ and e represent the velocity, pressure, temperature, body force and internal heat generation respectively. Other parameters ρ, C_p, k, μ, β, $\mu\phi$ are the fluid density, specific heat at constant pressure, thermal conductivity, dynamic viscosity of fluid, thermal expansion coefficient and the viscous dissipation.

Assuming that the laminar flow is incompressible with constant properties, zero internal heat generation, negligible viscous dissipation, and that the usual Boussinesq approximation holds, $(\rho - \rho_0)/\rho_0 = -\beta(T - T_0)$ with $|\beta(T - T_0)| \ll 1$,

we obtain from Eqs. (2.1), (2.2) and (2.3) the following 2-D governing equations in terms of Cartesian system

$$\frac{\partial u}{\partial x} + \frac{\partial v}{\partial y} = 0 \tag{2.4}$$

$$\frac{\partial u}{\partial t} + \frac{\partial u^2}{\partial x} + \frac{\partial vu}{\partial y} = -\frac{1}{\rho_0}\frac{\partial p}{\partial x} + \nu\left(\frac{\partial^2 u}{\partial x^2} + \frac{\partial^2 u}{\partial y^2}\right) + [1 - \beta(T - T_0)](-g\sin\varphi) \tag{2.5}$$

$$\frac{\partial v}{\partial t} + \frac{\partial uv}{\partial x} + \frac{\partial v^2}{\partial y} = -\frac{1}{\rho_0}\frac{\partial p}{\partial y} + \nu\left(\frac{\partial^2 v}{\partial x^2} + \frac{\partial^2 v}{\partial y^2}\right) + [1 - \beta(T - T_0)](-g\cos\varphi) \tag{2.6}$$

$$\frac{\partial T}{\partial t} + \frac{\partial uT}{\partial x} + \frac{\partial vT}{\partial y} = \frac{k}{\rho C_p}\left(\frac{\partial^2 T}{\partial x^2} + \frac{\partial^2 T}{\partial y^2}\right) \tag{2.7}$$

Here, u and v are velocity components aligned with the Cartesian coordinate direction x and y, respectively. Equations (2.4) – (2.7) may be solved simultaneously to provide a solution for u, v,p and T

The formulation of a problem requiring the solution of a partial differential equation also requires the specification of appropriate boundary and initial conditions. In the present mathematical model, boundary conditions are the following. At the solid walls, $y = 0$, h, the flow must satisfy the no-slip and impermeable-boundary conditions and the temperature or the heat flux must be prescribed. Hence $u = v = 0$ and T or T_y are prescribed at these boundaries. For the rectangular domain shown in Fig. 2.1 by dotted lines, periodic boundary conditions are assumed to prevail for the physical quantities, on the two arbitrary sections with respect to imposed wavelength. For a flow domain corresponding to a whole finite extent channel, velocity and temperature are specified at the entrance of the channel, while at the outlet, extrapolated values of the physical quantities may

be used, according to the procedure described by Tomimura and Fujii [95]. The initial condition is usually set to static state with $u = v = T = p = 0$, or it may correspond for instance to some known solution, such as pure conduction.

2.2 VORTICITY-STREAM FUNCTION FORMULATION

One of the main difficulties in determining the flow field via Eq. (2.2) is the unknown pressure field that appears in the form of pressure gradients in the momentum equation.

Since the pressure field is usually not of primary interest, it is eliminated by taking the "curl" of Eq. (2.2). Defining the vorticity as

$$\vec{\omega} = \nabla \times \vec{v} \tag{2.8}$$

we obtain the vorticity transport equation

$$\rho \frac{D\vec{\omega}}{Dt} = \mu \nabla^2 \vec{\omega} + \nabla \times \vec{f} \tag{2.9}$$

In the two-dimensional Cartesian system and for a Boussinesq-incompressible fluid, the above equation reads

$$\frac{\partial \omega}{\partial t} + \frac{\partial u\omega}{\partial x} + \frac{\partial v\omega}{\partial y} = \nu\left(\frac{\partial^2 \omega}{\partial x^2} + \frac{\partial^2 \omega}{\partial y^2}\right) + \rho g\left(\frac{\partial T}{\partial x}\cos\varphi - \frac{\partial T}{\partial y}\sin\varphi\right) \tag{2.10}$$

Using the definition of stream function

$$u = \frac{\partial \psi}{\partial y}, \qquad v = -\frac{\partial \psi}{\partial x} \tag{2.11}$$

the definition of vorticity in terms of the stream function is

$$\nabla^2 \psi = -\omega \tag{2.12}$$

the energy equation (2.7) remains unaltered; the velocity u and v appearing in it may be replaced on the basis of the stream function ψ using Eq. (2.11), if desired.

The no-slip condition and impermeability at solid boundaries lead to $\psi = 0$ and ψ =constant along the boundary, while thermal boundary conditions remain as given in section 2.1. Also the periodic boundary condition for the one-wavelength configuration or entrance and outlet boundary conditions for the whole channel configuration are handled in a similar way as the previous section, so are the initial conditions.

Unfortunately, it is difficult to determine the value of vorticity on the boundaries. Frequently, the vorticity equation (2.10) is not solved simultaneously with the stream-function equation (2.12). In that case, the wall boundary condition for vorticity is derived by evaluating Eq. (2.12) at the boundary, yielding

$$\omega|_{\text{wall}} = -\left.\frac{\partial^2 \psi}{\partial n^2}\right|_{\text{wall}} \tag{2.13}$$

where n is in outward direction normal to the boundary. There exist different approaches to derive the vorticity at the wall, which can be found in Roache [98]

Chapter 3

NUMERICAL APPROACH

Prediction of heat transfer and fluid flow processes can be obtained by experimental investigation or theoretical calculation. Analytical methods are largely pencil-and-paper procedures that attempt to provide solutions to problems through the use of simplifying assumptions. Many simplifying assumptions are necessary to make the problems tractable, but they severely limit the applicability of the results.

Experimental investigation can provide some information regarding a particular problem of interest. However, the limitation on hardware required for the model and the difficulty in simulating adequately the prototype, makes it an impractical means of obtaining results for many problems. Nevertheless, the information obtained from experiments is valuable in validating mathematical solutions of the governing equations. Thus, experimental data are used along with computational solutions of the equations.

The availability of the digital computer has stimulated the rapid growth of another approach to solving complex problems in heat transfer that has become known as the "numerical" or "computational" approach. With the advent of electronic digital computers, the introduction of newer numerical techniques are being proposed almost on a daily basis.

This chapter will provide an overview of the role and nature of the numerical

techniques in terms of finite difference and control volume approaches. This will be followed by a detailed description of a well-tested numerical procedure that can handle the present problem as well as a wide variety of engineering problems.

3.1 FINITE DIFFERENCE METHODS

3.1.1 Finite Difference Formulation

In the finite-difference approach, the flow domain is "discretized' so that the dependent variables are considered to exist only at discrete points. The typical two dimensional grids system is shown in Fig. 3.1, where (i, j), the grid point in Cartesian coordinate and superscript index n, the marching coordinate. Derivatives are approximated by differences resulting in an algebraic representation of the partial differential equation (PDE). The nature of the resulting system of algebraic equations depends on the character of the problem posed by the original PDE (or system of PDEs).

Usually, the second-order central difference approximation is a frequently used scheme for solving the governing equations described in the chapter 2. However, in the convection dominated flow (high Péclet, Reynolds, or Rayleigh numbers), using the second-order central difference approximation to discretize the convective terms in the governing equations may produce wiggly solution. An upwind and its modified schemes can eliminate these wiggles. Table 3.1 demonstrate central difference and different upwind schemes for a general finite difference representation of an arbitrary scalar function shown as below

$$\left.\frac{\partial uf}{\partial x}\right|_i = A^u f_{i-2} + B^u f_{i-1} + C^u f_i + D^u f_{i+1} + E^u f_{i+2} \tag{3.1}$$

where A^u, B^u, C^u, D^u and E^u are functions of u

Table 3.1 Coefficients of the different schemes

Scheme	A^u	B^u	C^u	D^u	E^u
Central difference	0	$-\frac{u}{2\Delta x}$	0	$\frac{u}{2\Delta x}$	0
1st upwind	0	$-\frac{\lvert u\rvert + u}{2\Delta x}$	$\frac{\lvert u\rvert}{\Delta x}$	$-\frac{\lvert u\rvert - u}{2\Delta x}$	0
2nd upwind	$\frac{\lvert u\rvert + u}{4\Delta x}$	$-\frac{\lvert u\rvert + u}{\Delta x}$	$\frac{3\lvert u\rvert}{2\Delta x}$	$-\frac{\lvert u\rvert - u}{\Delta x}$	$\frac{\lvert u\rvert - u}{4\Delta x}$
3rd upwind	$\frac{\lvert u\rvert + u}{12\Delta x}$	$-\frac{\lvert u\rvert + 2u}{3\Delta x}$	$\frac{\lvert u\rvert}{2\Delta x}$	$-\frac{\lvert u\rvert - 2u}{3\Delta x}$	$\frac{\lvert u\rvert - u}{12\Delta x}$

As shown in Table 3.1, the coefficients A^u and E^u of the central difference and the first-order upwind schemes are equal to zero. The remaining coefficients B^u, C^u and D^u of f_{i-1} , f_i and f_{i+1} form a tri-diagonal matrix. Using the higher order upwind schemes, the discretized equations are no longer represented by a tridiagonal matrix. Instead, the algebraic equations become a pentadiagonal matrix.

3.1.2 Discretization Governing Equations

For numerical computations, the governing differential equation (2.7), (2.10), (2.12) have to be cast in a discretized form. Owing to the moderate convection flow of present problem, all the convective and diffusive terms in the equations are discretized by the central difference scheme, while the time derivatives are approximated by forward differences. The discretization procedure is developed as follows.

The energy equation (2.7) can be discretized as

$$\frac{T_{i,j}^{n+1}-T_{i,j}^{n}}{(\Delta t)}+\frac{u_{i+1,j}^{n}T_{i+1,j}^{n+1}-u_{i-1,j}^{n}T_{i-1,j}^{n+1}}{2(\Delta x)}+\frac{v_{i,j+1}^{n}T_{i,j+1}^{n+1}-v_{i,j-1}^{n}T_{i,j-1}^{n+1}}{2(\Delta y)}$$
$$=\alpha[\frac{T_{i+1,j}^{n+1}-2T_{i,j}^{n+1}+T_{i-1,j}^{n+1}}{(\Delta x)^2}+\frac{T_{i,j+1}^{n+1}-2T_{i,j}^{n+1}+T_{i,j-1}^{n+1}}{(\Delta y)^2}]+$$
$$O[(\Delta t),(\Delta x)^2,(\Delta y)^2] \tag{3.2}$$

This formulation is implicit, since more than one unknown appears in the finite difference equation, from which it follows that

$$[\frac{(\Delta t)}{2(\Delta x)}u_{i+1,j}^{n}-\frac{\alpha(\Delta t)}{(\Delta x)^2}]T_{i+1,j}^{n+1}+[-\frac{(\Delta t)}{2(\Delta x)}u_{i-1,j}^{n}-\frac{\alpha(\Delta t)}{(\Delta x)^2}]T_{i-1,j}^{n+1}+$$
$$[1+\frac{2\alpha(\Delta t)}{(\Delta x)^2}+\frac{2\alpha(\Delta t)}{(\Delta y)^2}]T_{i,j}^{n+1}+[-\frac{(\Delta t)}{2(\Delta y)}v_{i,j-1}^{n}-\frac{\alpha(\Delta t)}{(\Delta y)^2}]T_{i,j-1}^{n+1}+$$
$$[\frac{(\Delta t)}{2(\Delta y)}v_{i,j+1}^{n}-\frac{\alpha(\Delta t)}{(\Delta y)^2}]T_{i,j+1}^{n+1}=T_{i,j}^{n} \tag{3.3}$$

By defining the coefficients of the unknowns as a, b, c, d and e, and the right-hand side by f, equation (3.3) may be written as

$$a_{i,j}T_{i+1,j}^{n+1}+b_{i,j}T_{i-1,j}^{n+1}+c_{i,j}T_{i,j}^{n+1}+d_{i,j}T_{i,j-1}^{n+1}+e_{i,j}T_{i,j+1}^{n+1}=f_{i,j} \tag{3.4}$$

It is obvious that the coefficient matrix is pentadiagonal in Eq.(3.4). The solution procedure for a pentadiagonal system of equations is very time-consuming. One way to overcome the shortcomings and inefficiency of the method described above, is to use a splitting method. This method is known as the alternating direction implicit method (ADI), which is proposed by Roache [98]. The algorithm produces two sets of tridiagonal simultaneous equations to be solved in sequence. The finite difference form of the energy equation in the ADI formulation is then

$$\frac{T_{i,j}^{n+\frac{1}{2}}-T_{i,j}^{n}}{(\frac{\Delta t}{2})}+\frac{u_{i+1,j}^{n}T_{i+1,j}^{n+\frac{1}{2}}-u_{i-1,j}^{n}T_{i-1,j}^{n+\frac{1}{2}}}{2(\Delta x)}+\frac{v_{i,j+1}^{n}T_{i,j+1}^{n}-v_{i,j-1}^{n}T_{i,j-1}^{n}}{2(\Delta y)}$$
$$=\alpha[\frac{T_{i+1,j}^{n+\frac{1}{2}}-2T_{i,j}^{n+\frac{1}{2}}+T_{i-1,j}^{n+\frac{1}{2}}}{(\Delta x)^2}+\frac{T_{i,j+1}^{n}-2T_{i,j}^{n}+T_{i,j-1}^{n}}{(\Delta y)^2}] \tag{3.5}$$

and

$$\frac{T_{i,j}^{n+1} - T_{i,j}^{n+\frac{1}{2}}}{(\frac{\Delta t}{2})} + \frac{u_{i+1,j}^{n} T_{i+1,j}^{n+\frac{1}{2}} - u_{i-1,j}^{n} T_{i-1,j}^{n+\frac{1}{2}}}{2(\Delta x)} + \frac{v_{i,j+1}^{n} T_{i,j+1}^{n+1} - v_{i,j-1}^{n} T_{i,j-1}^{n+1}}{2(\Delta y)}$$
$$= \alpha[\frac{T_{i+1,j}^{n+\frac{1}{2}} - 2T_{i,j}^{n+\frac{1}{2}} + T_{i-1,j}^{n+\frac{1}{2}}}{(\Delta x)^2} + \frac{T_{i,j+1}^{n+1} - 2T_{i,j}^{n+1} + T_{i,j-1}^{n+1}}{(\Delta y)^2}] \tag{3.6}$$

with the truncation error of order $[(\Delta t)^2, (\Delta x)^2, (\Delta y)^2]$ and is unconditionally stable. Equations (3.5) and (3.6) are written in the tridiagonal form as

$$A_1^T T_{i-1,j}^{n+\frac{1}{2}} + B_1^T T_{i,j}^{n+\frac{1}{2}} + C_1^T T_{i+1,j}^{n+\frac{1}{2}} = D_1^T \tag{3.7}$$

and

$$A_2^T T_{i,j-1}^{n+1} + B_2^T T_{i,j}^{n+1} + C_2^T T_{i,j+1}^{n+1} = D_2^T \tag{3.8}$$

where

$$\begin{aligned}
A_1^T &= -\frac{(\Delta t)}{4(\Delta x)} u_{i-1,j}^{n} - \frac{\alpha(\Delta t)}{2(\Delta x)^2} \\
B_1^T &= 1 + \frac{\alpha(\Delta t)}{(\Delta x)^2} \\
C_1^T &= \frac{(\Delta t)}{4(\Delta x)} u_{i+1,j}^{n} - \frac{\alpha(\Delta t)}{2(\Delta x)^2} \\
D_1^T &= [\frac{(\Delta t)}{4(\Delta y)} v_{i,j-1}^{n} + \frac{\alpha(\Delta t)}{2(\Delta y)^2}] T_{i,j-1}^{n} + \\
&\quad [1 - \frac{\alpha(\Delta t)}{(\Delta y)^2}] T_{i,j}^{n} + [-\frac{(\Delta t)}{4(\Delta y)} v_{i,j+1}^{n} + \frac{\alpha(\Delta t)}{2(\Delta y)^2}] T_{i,j+1}^{n} \\
A_2^T &= -\frac{(\Delta t)}{4(\Delta y)} v_{i,j-1}^{n} - \frac{\alpha(\Delta t)}{2(\Delta y)^2} \\
B_2^T &= 1 + \frac{\alpha(\Delta t)}{(\Delta y)^2} \\
C_2^T &= \frac{(\Delta t)}{4(\Delta y)} v_{i,j+1}^{n} - \frac{\alpha(\Delta t)}{2(\Delta y)^2} \\
D_2^T &= [\frac{\Delta t}{4(\Delta x)} u_{i-1,j}^{n} + \frac{\alpha(\Delta t)}{2(\Delta x)^2}] T_{i-1,j}^{n+\frac{1}{2}} + [1 - \frac{\alpha(\Delta t)}{(\Delta x)^2}] T_{i,j}^{n+\frac{1}{2}} + \\
&\quad [\frac{(\Delta t)}{4(\Delta x)} u_{i+1,j}^{n} + \frac{\alpha(\Delta t)}{2(\Delta x)^2}] T_{i+1,j}^{n+\frac{1}{2}}
\end{aligned}$$

The solution procedure starts with the solution of the tridiagonal system (3.7). The formulation of Eq. (3.7) is implicit in the x-direction and explicit in the y-direction; thus the solution at this stage is referred to as the x sweep. Solving the tridiagonal system of (3.7)provides the necessary data for the right-hand side of Eq. (3.8) to solve the tridiagonal system of (3.8). In this equation, the FDE is implicit in the y-direction and explicit in the x-direction, and it is referred to as the y sweep. Graphical presentation of the method is shown in Fig. 3.2.

Similarly, the vorticity-transportation equation (2.10) can be discretized in the tridiagonal form as

$$A_1^\omega \omega_{i-1,j}^{n+\frac{1}{2}} + B_1^\omega \omega_{i,j}^{n+\frac{1}{2}} + C_1^\omega \omega_{i+1,j}^{n+\frac{1}{2}} = D_1^\omega \tag{3.9}$$

and

$$A_2^\omega \omega_{i,j-1}^{n+1} + B_2^\omega \omega_{i,j}^{n+1} + C_2^\omega \omega_{i,j+1}^{n+1} = D_2^\omega \tag{3.10}$$

$$\begin{aligned}
A_1^\omega &= -\frac{(\Delta t)}{4(\Delta x)} u_{i-1,j}^n - \frac{\nu(\Delta t)}{2(\Delta x)} \\
B_1^\omega &= 1 + \frac{\nu(\Delta t)}{(\Delta x)^2} \\
C_1^\omega &= \frac{(\Delta t)}{4(\Delta x)} u_{i+1,j}^n - \frac{\nu(\Delta t)}{2(\Delta x)^2} \\
D_1^\omega &= [\frac{(\Delta t)}{4(\Delta y)} v_{i,j-1}^n + \frac{\nu(\Delta t)}{2(\Delta y)^2}]\omega_{i,j-1}^n + [1 - \frac{\nu(\Delta t)}{(\Delta y)^2}]\omega_{i,j}^n + \\
&\quad [-\frac{(\Delta t)}{4(\Delta y)} v_{i,j+1}^n + \frac{\nu(\Delta t)}{2(\Delta y)^2}]\omega_{i,j+1}^n + \\
&\quad \rho g[\frac{T_{i+1,j}^n - T_{i-1,j}^n}{2(\Delta x)} \cos\varphi - \frac{T_{i,j+1}^n - T_{i,j-1}^n}{2(\Delta y)} \sin\varphi] \\
A_2^\omega &= -\frac{(\Delta t)}{4(\Delta y)} v_{i,j-1} - \frac{\nu(\Delta t)}{2(\Delta y)^2} \\
B_2^\omega &= 1 + \frac{\nu(\Delta t)}{(\Delta y)^2}
\end{aligned}$$

$$
\begin{aligned}
C_2^{\omega} &= \frac{(\Delta t)}{4(\Delta y)} v_{i,j+1}^{n} - \frac{\nu(\Delta t)}{2(\Delta y)^2} \\
D_2^{\omega} &= [\frac{(\Delta t)}{4(\Delta x)} u_{i-1,j}^{n} + \frac{\nu(\Delta t)}{2(\Delta x)^2}]\omega_{i-1,j}^{n+\frac{1}{2}} + [1 - \frac{\nu(\Delta t)}{(\Delta x)^2}]\omega_{i,j}^{n+\frac{1}{2}} + \\
&\quad [-\frac{(\Delta t)}{4(\Delta x)} u_{i+1,j}^{n} + \frac{\nu(\Delta t)}{2(\Delta x)^2}]\omega_{i+1,j}^{n+\frac{1}{2}} + \\
&\quad \rho g[\frac{T_{i+1,j}^{n} - T_{i-1,j}^{n}}{2(\Delta x)} \cos\varphi - \frac{T_{i,j+1}^{n} - T_{i,j-1}^{n}}{2(\Delta y)} \sin\varphi]
\end{aligned}
$$

For the stream function equation (2.12), the central difference scheme produce the representation of FDE as

$$
\frac{\psi_{i+1,j} - 2\psi_{i,j} + \psi_{i-1,j}}{(\Delta x)^2} + \frac{\psi_{i,j+1} - 2\psi_{i,j} + \psi_{i,j-1}}{(\Delta y)^2} = -\omega_{i,j} \tag{3.11}
$$

From Eq. (3.11), a general recurrence formula for the line successive over-relaxation (L.S.O.R.) can be presented by introduction of the relaxation parameter β as

$$
\begin{aligned}
&\beta\psi_{i,j-1}^{n+1} - 2[\frac{(\Delta y)^2}{(\Delta x)^2} + 1]\psi_{i,j}^{n+1} + \beta\psi_{i,j+1}^{n+1} = -\beta\frac{(\Delta y)^2}{(\Delta x)^2}\psi_{i-1,j}^{n} - \\
&2(1-\beta)[\frac{(\Delta y)^2}{(\Delta x)^2} + 1]\psi_{i,j}^{n} - \beta\frac{(\Delta y)^2}{(\Delta x)^2}\psi_{i+1,j}^{n} - \beta(\Delta y)^2\omega_{i,j}^{n}
\end{aligned} \tag{3.12}
$$

There is no simple way to determine the value of optimum β. In practice, a trial and error approach is used to compute β_{opt} for a particular problem.

3.1.3 Boundary Condition Discretization

Since the no-slip and impermeable boundary conditions are imposed on the solid wall, the corresponding velocity components are set to zero value and the stream function are set to either zero or a constant value. The boundary conditions of the vorticity are determined from the stream function Eq.(2.13) at the solid wall and its discretized formula can be presented in terms of first order or second order forms:

First order form

$$\omega_w = -\frac{2(\psi_{w+1} - \psi_w - \vec{v_w} \cdot \Delta\vec{n})}{(\Delta n)^2} + O(\Delta n), \quad \vec{v} = [u, v]^T \tag{3.13}$$

Second order form (Woods method)

$$\omega_w = \frac{3(\psi_w - \psi_{w+1} + \vec{v_w} \cdot \Delta\vec{n})}{(\Delta n)^2} - \frac{1}{2}\omega_{w+1} + O(\Delta n^2), \quad \vec{v} = [u, v]^T \tag{3.14}$$

where $\Delta\vec{n}$ is the spatial increment vector normal to the boundary.

In the present study, the boundary conditions for the energy equation are either an imposed temperature or a specified heat flux. In dimensionless form, we have

$$\theta_w = \text{constant} \quad \text{or} \quad q_w = -\left.\frac{\partial\theta}{\partial n}\right|_w \tag{3.15}$$

The periodicity conditions are imposed on the vertical boundaries for any physical variable f yielding

$$f(x + \lambda, y, t) = f(x, y, t) \tag{3.16}$$

The treatment in the A.D.I. approach is done by a matrix partition procedure similar to that utilized by Phillps [99]. Details may be found in appendix A.

3.1.4 Program Procedure

The general solution procedure, as described by the flow chart in Fig. 3.3, consists of the following steps.

1. Generate grid according to a uniform or nonuniform mesh size.

2. Set initial values of all the variables $u_{i,j}$, $v_{i,j}$, $\omega_{i,j}$, $\psi_{i,j}$ and $T_{i,j}$.
3. Set boundary conditions for velocity, stream function, temperature or its derivative normal to the boundary.
4. Compute the temperature field by solving the energy equation, alternatively sweeping in x and y directions.
5. Compute vorticity on interior grid points by solving the vorticity-transportation equation and using velocity and updated temperature. An A.D.I. scheme is also used.
6. Solve the stream function by S.O.R. to obtain the $\psi_{i,j}$. Updated vorticity $\omega_{i,j}$ is used.
7. Calculate the vorticity on the boundary by using the stream function and vorticity at interior points as well as the velocity on the boundary.
8. Determine velocity components from updated stream function.
9. Return to step 4, and repeat the whole procedure until a converged solution is obtained. The convergence criterion is defined as following. One checks the continuity equation at each grid point. the other checks the fractional change of any variable between two time steps at any node.

$$\frac{|f_{i,j}^{n+1} - f_{i,j}^{n}|}{|f_{i,j}^{n}|} \leq \epsilon \tag{3.17}$$

CONTROL VOLUME DIFFERENCE METHOD

3.2 FINITE CONTROL VOLUME METHOD

The foregoing governing equations (2.4 – 2.7) can be considered as particular

cases of the general differential equation

$$\underbrace{\frac{\partial}{\partial t}(f)}_{\text{unsteady term}} + \underbrace{\nabla \cdot (\vec{v} f)}_{\text{convective term}} = \underbrace{\Gamma_k \nabla \cdot (\nabla f)}_{\text{diffusive term}} + \underbrace{S}_{\text{source term}} \quad (3.18)$$

where f is the general dependent variable which can represent velocity component, temperature and mass fraction, Γ_k is the generalized constant diffusion coefficient, and S is the source term. When a particular meaning is associated with f, the expressions for Γ_k and S are to be obtained by comparing the actual conservation for the chosen variable with the general equation, Eq. (3.18).

3.2.1 Domain Discretization

The numerical method to be described here is based on the control-volume formulation proposed by Pantankar [100]. the discretization equations (which are the algebraic counterparts of the differential equations) are derived by integrating the governing differential equation over a small region called the control volume. Each control volume is associated with a discrete point at which the dependent variables such as velocity, pressure, and temperature are to be calculated.

Figure 3.4 shows a rectangular calculation domain subdivided into control volumes. The dashed lines denote the faces of the control volumes; these lines are drawn parallel to the two coordinate directions x and y. the grid points are placed at the geometric centers of the control volumes. The filled circular dots in Fig. 3.4 represent these grid points, and the solid lines joining them are called the grid lines. A typical control volume around point P is shown shaded. The grid point P communicates with the four neighboring grid points through the four faces of the control volume. These points are denoted by E, W, N, and S, implying the east,

west, north, and south directions with respect to the center point P. It can be seen from Fig. 3.4 that the grid lines are extended to the boundaries of the calculation domain, and additional boundary grid points are placed at the ends of the grid lines. Such grid points on the boundary are shown by open circles; B denotes a typical boundary grid point. A typical near-boundary internal grid point is shown as I, and its control volume is also shaded. For this control volume, one faces coincides with the boundary of the calculation domain, and the boundary grid point B is placed at the center of this face. That both a control-volume face and a grid point are located at the boundary of the calculation domain makes it easy to treat different boundary conditions; the control volume around I can easily accept a given value of f at the boundary or a given flux through the boundary surface.

It is not necessary that the widths of all the control volumes be equal nor do the successive grid points have to maintain the same spacing between them. Indeed, a nonuniform grid spacing is often desirable, because it enables one to deploy a given number of grid points in an optimal manner. In general, a fine grid is required where the variation of f is steep, and a coarse grid is sufficient where f varies rather slowly.

3.2.2 Discretization of the General Equation

The basis of the numerical method is the conversion of the general differential equation, Eq. (3.18), into an algebraic equation relating the value of f at grid point P to the values at the neighboring grid points. This is done by integrating Eq. (3.18) over a typical control volume (Fig. 3.5) and approximating various

terms in the integration so that they are expressed in terms of the grid-point value of f. The resulting discretization equation becomes

$$a_P f_P = a_E f_E + a_W f_W + a_N f_N + a_S f_S + b \tag{3.19}$$

where coefficients a_P, a_E, a_W, a_N, a_S and b are given by Patankar [100]:

$$\begin{aligned}
a_E &= D_e A(|P_e|) + max(-F_e, 0) \\
a_W &= D_w A(|P_w|) + max(F_w, 0) \\
a_N &= D_n A(|P_n|) + max(-F_n, 0) \\
a_S &= D_s A(|P_s|) + max(F_s, 0) \\
a_P &= a_E + a_W + a_N + a_S + a_P^0 \\
b &= a_P^0 f_P^0 + \int_v S_P dv
\end{aligned} \tag{3.20}$$

with

$$\begin{aligned}
D_e &= \frac{\Gamma_k \Delta y}{\delta x_e}, \quad F_e = u_e \Delta y, \quad P_e = \frac{F_e}{D_e} \\
D_w &= \frac{\Gamma_k \Delta y}{\delta x_w}, \quad F_w = u_w \Delta y, \quad P_w = \frac{F_w}{D_w} \\
D_n &= \frac{\Gamma_k \Delta x}{\delta y_n}, \quad F_n = v_n \Delta x, \quad P_n = \frac{F_n}{D_n} \\
D_s &= \frac{\Gamma_k \Delta x}{\delta y_s}, \quad F_s = v_s \Delta x, \quad P_s = \frac{F_s}{D_s} \\
a_P^0 &= \frac{\Delta x \Delta y}{\Delta t}
\end{aligned} \tag{3.21}$$

The definition of $A(|P|)$ depends on the particular choice of the interpolation scheme for the calculation of f over the control volume considered. Expressions

for $A(|P|)$ are listed in Table 3.2. For the present work, we found that power-law scheme provide an extremely good approximation.

Table 3.2 The function $A(|P|)$ for different schemes

Scheme	Formula for $A(\|P\|)$
Central difference	$1 - 0.5\|P\|$
Upwind	1
Hybrid	$max(0.1 - 0.5\|P\|)$
Power law	$max(0, [1 - 0.1\|P\|]^5)$
Exponential	$\|P\|/[exp(\|P\|) - 1]$

It is well known that the general differential equation Eq. (3.18), has been cast into the discretization form with the understanding that the flow field u_i is known. The velocity components u_i are governed by the momentum equations, which are particular cases of the general equation Eq. (3.18). Thus, the fields of u_i can be obtained simply by solving for the general variable f, with its meaning set as the velocity component u, v. In that sense, a calculation procedure for the flow field has already been described. However, if the velocity components and the pressure are calculated for the same grid points, some physically unrealistic fields arise as solutions. These difficulties are discussed fully in the book given by Patankar [100]. A remedy for this ailment is the staggered grid in which the velocity components are calculated for the points that lie on the faces of the

control volumes.

Figure 3.6 shows a typical 6×6 control volume configuration and grid point distribution, where the appropriate control volumes for the velocity components u and v are also illustrated by light shaded areas. Circle marks indicate grids of temperature and pressure, while solid circles and triangular marks corresponds to grid points of velocity components u and v respectively. Location of the stream function values calculated from velocity are denoted by star marks.

3.2.3 Discretized Momentum Equations

The staggered locations for the velocity components determine the corresponding control volumes to be used for conservation of momentum. The two faces of the control volume around the velocity component u_e pass through the grid points P and E. The corresponding momentum equation can be written as

$$\begin{aligned} a_e u_e &= \sum a_{nb} u_{nb} + b + A_e(P_P - P_E) \\ a_n u_n &= \sum a_{nb} v_{nb} + b + A_n(P_P - P_N) \end{aligned} \tag{3.22}$$

where the term b includes the source terms other than the pressure gradient, and A_e, A_n is the area over which the pressure force acts. The coefficient expressions are identical to those given in Eqs. (3.20) and (3.21), except that the staggered geometry of the control volume must be taken into account in determining the diffusion conductance D and the flow rates F.

3.2.4 Pressure-Correction Equation

Let P' denote the pressure correction. The corresponding correction to the velocity component u^* and v^* are denoted by u' and v', where u^* and v^* are the

velocity field based on an estimated pressure field P^*, and satisfy the equation

$$\begin{aligned} a_e u_e^* &= \sum a_{nb} u_{nb}^* + b + A_e(P_P^* - P_E^*) \\ a_n v_n^* &= \sum a_{nb} v_{nb}^* + b + A_n(P_P^* - P_N^*) \end{aligned} \tag{3.23}$$

Thus

$$\begin{cases} P = P^* + P' \\ u = u^* + u' \\ v = v^* + v' \end{cases} \tag{3.24}$$

The velocity-correction formula can be written as

$$\begin{aligned} u_e &= u_e^* + d_e(P_P' - P_E'), \quad d_e = \frac{A_e}{a_e} \\ v_n &= v_n^* + d_n(P_P' - P_N'), \quad d_n = \frac{A_n}{a_n} \end{aligned} \tag{3.25}$$

The pressure-correction equation is obtained by substituting the velocity-correction formulas into the discretized form of the continuity equation, which can be written as

$$a_P P_P' = a_E P_E' + a_W P_W' + a_N P_N' + a_S P_S' + b \tag{3.26}$$

where

$$
\begin{aligned}
a_E &= \frac{(\Delta y)^2}{a_e} \\
a_W &= \frac{(\Delta y)^2}{a_w} \\
a_N &= \frac{(\Delta x)^2}{a_n} \\
a_S &= \frac{(\Delta x)^2}{a_s}
\end{aligned}
\tag{3.27}
$$

$$a_P = a_E + a_W + a_N + a_S$$

$$b = (u_w^* - u_e^*)\Delta y + (v_s^* - v_n^*)\Delta x$$

3.2.5 Boundary Conditions Setting

With reference to Figs. 3.4 and 3.6, it can be seen that there is a control volume around each internal grid point for the temperature, the pressure and the velocity components u and v, and that there will be a corresponding discretization equation such as Eq. (3.19). This equation can be regarded as an equation for determining f_P. For a near-boundary control volume such as the one around grid point I in Fig. 3.4, the discretization equation will contain the boundary value f_B as one of the neighbors. If f_B is known, no additional information is needed. On the other hand, if the boundary condition specifies the boundary flux in some manner, an additional equation must be written for the evaluation of the unknown value f_B. This equation is constructed simply by equating the given expression for the boundary flux J_B with the formula expressed in terms of f_B and f_I

$$J_B - F_B f_I = \{D_B A(|P_B|) + max(F_B, 0)\}(f_B - f_I) \tag{3.28}$$

Furthermore, this equation for f_B can be used to eliminate f_B from the control-volume equation for the grid point I. In this manner, the resulting set of equations will have only the f values at the internal grid points as the unknowns. There also exist a simple scheme in which we assume that the value f_B on the boundary is known in advance for the computation of interior points, then we use the flux formula and the updated interior points values to evaluate the value on the boundary.

3.2.6 Computation Procedure

As indicated in the foregoing sections, the general computation procedure is based on the solution of the general f equation. The momentum equations require a somewhat separate treatment because of the staggered grid and because the pressure term is handled in a special manner. The overall procedure is based on the SIMPLE algorithm proposed by Patankar [100]. An A.D.I. procedure is used for the time integration of momentum and energy equations while the pressure correction equation is solved by a point successive under-relaxation method (P.S.U.R.). It should be mentioned here that it is in some sense necessary to use an under-relaxation factor for the dependent variables and other auxiliary quantities to meet the requirement of convergence. Thus,

$$f = \beta f_{\text{new}} + (1 - \beta) f_{\text{old}} \tag{3.29}$$

Of course, the relaxation factor β appearing in Eq. (3.29) need not be the same, nor is it necessary to use the same value of β at every grid point.

Although different forms of under-relaxation method promote convergence, there is no unconditional guarantee that the iterative solution procedure will al-

ways converge for all kinds of nonlinearities and interlinkages. Also, there are no general formulas for choosing the optimum value of the under-relaxation factor. To this extent, obtaining a converged solution for a particular problem remains an art. With sufficient experience and insight, one is normally able to develop an under-relaxation procedure that produces a converged solution. But a successful outcome may sometimes be preceded by an experience of divergence.

The convergence criterion requires that the residual $|R|$ at each point defined as

$$|R| = |\sum a_{nb} f_{nb} + b - a_P f_P| \tag{3.30}$$

be less than a given value. There is a specific and efficient residual in terms of the mass conservation given by

$$max|(u^*_{i,j} - u^*_{i-1,j})dY_j + (v^*_{i,j} - v^*_{i,j-1})dX_i| \leq \epsilon$$
$$i = 1, ...M_{max}, \quad j = 1, ...N_{max} \tag{3.31}$$

Our results were mostly based on that last definition of the residual.

Chapter 4

BENCHMARK COMPARISON TEST

Two benchmark problems, the driven flow and the natural convection in a square cavity, are simulated numerically in this chapter. The purpose of the present study is to validate the computational techniques described in the previous chapter, and to test the accuracy and the reliability of the numerical code. Steady state results will be compared with those obtained by U. Ghia [101] and G. De Vahl Davis [102].

4.1 DRIVEN CAVITY FLOW

The laminar incompressible flow in a square cavity whose top wall moves with a uniform velocity in its own plane has served as a model problem for testing and evaluating numerical techniques, in spite of the singularities at two of its corners. The configuration of the problem is shown in Fig. 4.1.

4.1.1 Governing Differential Equations and Boundary Conditions

By introducing the scales h, u_0, h/u_0 for length, velocity, time and the pressure $P = (p + \rho_0 gy)/(\rho_0 u_0^2)$, the two-dimensional flow in the square cavity can be represented mathematically in terms of primitive variables as follows:

$$\frac{\partial U}{\partial X} + \frac{\partial V}{\partial Y} = 0 \tag{4.1}$$

$$\frac{\partial U}{\partial \tau} + \frac{\partial U^2}{\partial X} + \frac{\partial VU}{\partial Y} = \frac{1}{Re}\nabla^2 U - \frac{\partial P}{\partial X} \tag{4.2}$$

$$\frac{\partial V}{\partial \tau} + \frac{\partial UV}{\partial X} + \frac{\partial V^2}{\partial Y} = \frac{1}{Re}\nabla^2 V - \frac{\partial P}{\partial Y} \tag{4.3}$$

where $Re = u_0 h/\nu$ (Reynolds number)

The zero-slip and impermeable conditions are imposed on the boundaries as a result of

$$\begin{cases} X = 0,\ 1: & U = 0, \quad V = 0 \\ Y = 0: & U = 0, \quad V = 0 \\ Y = 1: & U = 1, \quad V = 0 \end{cases} \tag{4.4}$$

Similarly, the dimensionless governing equations with respect of the stream function and the vorticity are formulated in the form of

$$\frac{\partial^2 \Psi}{\partial X^2} + \frac{\partial^2 \Psi}{\partial Y^2} + \Omega = 0 \tag{4.5}$$

$$\frac{\partial \Omega}{\partial \tau} + \frac{\partial U\Omega}{\partial X} + \frac{\partial V\Omega}{\partial Y} = \frac{1}{Re}\nabla^2 \Omega \tag{4.6}$$

$$U = \frac{\partial \Psi}{\partial Y}, \quad V = -\frac{\partial \Psi}{\partial X} \tag{4.7}$$

Where the dimensionless scales for stream function and vorticity are $u_0 h$ and u_0/h respectively. The no-slip and impermeable wall condition impose a constant value of the stream function (Ψ arbitrarily set to zero) on all the boundaries. However, there is no direct condition for Ω at the walls. In practice, the boundary conditions for Ω are derived from the physical boundary conditions together with the definition of Ω as given by Eq. (4.5). Thus, at the moving wall $Y = 1$ ($j =$

NP)

$$\begin{cases} \Psi|_{Y=1} = 0 \\ \Omega|_{Y=1} = -\dfrac{\partial^2 \Psi}{\partial Y^2} = \dfrac{3(\Psi_{NP} - \Psi_N - U_{NP} \cdot \Delta Y)}{(\Delta Y)^2} - \dfrac{1}{2}\Omega_N + O(\Delta Y^2) \end{cases} \tag{4.8}$$

Expressions for Ω at other boundaries are obtained in an analogous manner deduced from Eq. (3.14).

4.1.2 Computational Procedure

For the control volume method, Eqs. (4.1) to (4.3) are discretized and integrated over each control volume. The detailed procedure described in chapter 3 is then applied. The imposed convergence criterion defined by Eq. (3.31) is that the mass conservation for each control volume should be satisfied with a residual less than 10^{-6}. A uniform mesh size of 40×40 is used for both X and Y directions. The time increment ranges from 0.001 to 0.1 and under-relaxation coefficients are chosen between 0.1 to 0.8 according to the values of the governing parameters.

The problem is also solved by stream function vorticity formulation based governing equations (4.5) to (4.7). The procedure is also described in chapter3, and the convergence criterion defined by Eq. (3.17) is set ϵ be less than10^{-5}. A uniform mesh size of 40×40 is used for both X and Y directions, and the time increment varied between 0.0001 to 0.001 corresponding to different Reynolds number.

4.1.3 Results

Figure 4.2 illustrates solutions for incompressible flow of driven cavity for the

cases of $Re = 100$, $Re = 400$ and $Re = 1000$. These results have been obtained by the control volume approach (results from the finite difference method are omitted for brevity). A view of the induced roll given by the streamlines is seen that this roll becomes stronger as the Reynolds number increases. This behavior has been noted in the article by U. Ghia et al. [101] Figure 4.3 shows the velocity profiles for U along vertical lines and V along horizontal lines passing through the geometric center of the cavity. Solid and dotted lines represent results from finite difference method and from control volume approach respectively. The solutions of U. Ghia et al. [101] using a fine mesh size of 129×129 are shown by circle marks. For $Re = 100$, all results agree well with one another, indicating that for this value of Re, the coarser grid of 40×40 of the present work was quite adequate. As Re increases, however, the inadequacy of coarse meshes gradually becomes apparent. This is particularly evident in the region near U_{min}, and V_{max}.

4.2 NATURAL CONVECTION IN A SQUARE CAVITY

We consider the two-dimensional flow of a Boussinesq fluid of Prandtl number 0.71 in an upright square cavity shown in Fig. 4.4. X and Y are dimensionless coordinates with the flow domain $0 \leq X \leq 1$, $0 \leq Y \leq 1$. Both velocity components are zero on all boundaries. Horizontal boundaries are insulated. Vertical boundaries are maintained at different uniform temperature.

4.2.1 Governing Equations

With h, α/h, h^2/α, ΔT for length, velocity, time, temperature and the pressure $P = h^2(p + \rho_0 gy)/(\rho_0 \alpha^2)$, the dimensionless governing equations are

$$\frac{\partial U}{\partial X} + \frac{\partial V}{\partial Y} = 0 \tag{4.9}$$

$$\frac{\partial U}{\partial \tau} + \frac{\partial U^2}{\partial X} + \frac{\partial VU}{\partial Y} = Pr\nabla^2 U - \frac{\partial P}{\partial X} \tag{4.10}$$

$$\frac{\partial V}{\partial \tau} + \frac{\partial UV}{\partial X} + \frac{\partial V^2}{\partial Y} = Pr\nabla^2 V - \frac{\partial P}{\partial Y} + PrRa\theta \tag{4.11}$$

$$\frac{\partial \theta}{\partial \tau} + \frac{\partial U\theta}{\partial X} + \frac{\partial V\theta}{\partial Y} = \nabla^2 \theta \tag{4.12}$$

where $Pr = \nu/\alpha$ (Prandtl number) and $Ra = g\beta\Delta h^3/\nu\alpha$ (Rayleigh number). The appropriate boundary conditions are

$$\begin{cases} X = 0: & U = 0, & V = 0, & \theta = 1 \\ X = 1: & U = 0, & V = 0, & \theta = 0 \\ Y = 0,\ 1: & U = 0, & V = 0, & \dfrac{\partial \theta}{\partial Y} = 0 \end{cases} \tag{4.13}$$

The dimensionless governing equations based on stream function vorticity formulation are illustrated as

$$\frac{\partial \theta}{\partial \tau} + \frac{\partial U\theta}{\partial X} + \frac{\partial V\theta}{\partial Y} = \nabla^2 \theta \tag{4.14}$$

$$\frac{\partial \Omega}{\partial \tau} + \frac{\partial U\Omega}{\partial X} + \frac{\partial V\Omega}{\partial Y} = Pr\nabla^2 \Omega + PrRa\frac{\partial \theta}{\partial X} \tag{4.15}$$

$$\nabla^2 \Psi = -\Omega \tag{4.16}$$

$$U = \frac{\partial \Psi}{\partial Y}, \quad V = -\frac{\partial \Psi}{\partial X} \tag{4.17}$$

where the dimensionless scales for stream function and vorticity are αh^2 and α respectively. The corresponding boundary conditions are

$$\begin{cases} X = 0: & \Psi = 0, & U = V = 0, & \theta = 1 \\ X = 1: & \Psi = 0, & U = V = 0, & \theta = 0 \\ Y = 0,\ 1: & \Psi = 0, & U = V = 0, & \dfrac{\partial \theta}{\partial Y} = 0 \end{cases} \tag{4.18}$$

The vorticity on the boundary is treated by Woods method described in Chapter 3.

4.2.2 Computational Procedure

The governing equations (4.9) to (4.12) are solved by the control volume approach; the stream function-vorticity based governing equations (4.14) to (4.17) are solved by the finite difference method. Uniform mesh sizes of (10×10), (20×20) and (40 × 40) are used to model the present problem.

Figure 4.5 shows the effects of Rayleigh number on the natural convection in a square cavity in terms of isotherms (right) and streamlines (left). Those temperature and flow patterns have been obtained from the control volume approach. Comparable temperature and flow patterns (omitted for brevity) have been obtained from the finite difference method. Tables 4.1 to 4.8 provide a quantitative comparison for a number of typical parameters. U_{max} and V_{max} are respectively the maximum horizontal velocity on the vertical mid-plane and the maximum vertical velocity on the horizontal mid-plane. The overall Nusselt number on the

left and right sides are defined respectively as

$$Nu_l = -\int_0^1 \frac{\partial\theta}{\partial X}\Big|_0 dY \qquad Nu_r = -\int_0^1 \frac{\partial\theta}{\partial X}\Big|_1 dY \tag{4.19}$$

Tables 4.1, 4.2, 4.3 and 4.4 are used for comparison between benchmark [102] and the present results based on the control volume approach; tables 4.5, 4.6, 4.7 and 4.8 compare the benchmark and the results based on the finite difference method. It may be found from those tables that the present results are very accurate for a fine-mesh size of (40×40), although, as expected, the deviation becomes larger as the Ra is increased. It also noticed that in table 4.4 the results for mesh size of 10×10 is smaller than the benchmark. This undershoot phenomenon at large Ra and very crude mesh size is found to occur from time to time.

Thus we have two numerical methods to solve the problems specified in the introduction. Most of the solutions coming in the next chapters will be based on the finite deference method.

It should be mentioned here that the galilean transformation used for the study of mixed convection in a horizontal channel with entirely heated bottom provides a way to check the accuracy of the time dependent numerical computation. We first solve the case of no forced flow, i.e., natural convection producing classical Bénard cells in a fixed frame. Secondly, we solve the same problem in a reference frame ("window") that moves at a predetermined velocity V_a; the problem becomes time dependent, and the transverse rolls move in the opposite direction at the same velocity. The results obtained from the moving frame can be transformed into values with respect to the fixed frame by Eq. (5.9). Those values can be compared with the values obtained numerically from the fixed frame. A

good agreement is then found with the maximum discrepancy within 1% for $\Psi_{i,j}$ at the moving velocity $V_a = 10$.

TABLE 4.1: Results for $Ra = 1 \times 10^3$

Parameters	Benchmark	10×10	Error (%)	40×40	Error (%)
Ψ_{max}	1.174	1.2561	6.99	1.1800	0.51
U_{max}	3.649	3.684	0.97	3.656	0.19
V_{max}	3.697	3.777	2.17	3.698	0.08
Nu_l	1.117	1.141	2.12	1.119	0.18
Nu_r	1.117	1.141	2.12	1.119	0.18

TABLE 4.2: Results for $Ra = 1 \times 10^4$

Parameters	Benchmark	10×10	Error (%)	40×40	Error (%)
Ψ_{max}	5.071	5.2633	3.79	5.0861	0.24
U_{max}	16.178	15.873	1.89	16.129	0.30
V_{max}	19.617	17.983	8.33	19.609	0.04
Nu_l	2.238	2.461	9.94	2.259	0.94
Nu_r	2.238	2.461	9.94	2.259	0.94

TABLE 4.3: Results for $Ra = 1 \times 10^5$

Parameters	Benchmark	10×10	Error (%)	40×40	Error (%)
Ψ_{max}	9.612	10.512	9.36	9.737	1.30
U_{max}	34.73	35.152	1.22	34.981	0.72
V_{max}	68.59	73.353	6.94	68.955	0.53
Nu_l	4.509	5.411	20.00	4.620	2.46
Nu_r	4.509	5.411	20.00	4.620	2.46

TABLE 4.4: Results for $Ra = 1 \times 10^6$

Parameters	Benchmark	10×10	Error (%)	40×40	Error (%)
Ψ_{max}	16.75	21.148	26.26	17.531	4.66
U_{max}	64.63	75.631	17.02	66.798	3.35
V_{max}	219.36	189.52	13.60	223.49	1.88
Nu_l	8.817	8.188	7.14	9.417	6.80
Nu_r	8.817	8.188	7.14	9.417	6.80

TABLE 4.5: Results for $Ra = 1 \times 10^3$

Parameters	Benchmark	20×20	Error (%)	40×40	Error (%)
Ψ_{max}	1.174	1.170	0.32	1.1722	0.15
U_{max}	3.649	3.569	2.21	3.617	0.89
V_{max}	3.697	3.594	2.79	3.673	0.64
Nu_l	1.117	1.122	0.44	1.121	0.31
Nu_r	1.117	1.122	0.44	1.121	0.31

TABLE 4.6: Results for $Ra = 1 \times 10^4$

Parameters	Benchmark	20×20	Error (%)	40×40	Error (%)
Ψ_{max}	5.071	5.111	0.78	5.0654	0.11
U_{max}	16.178	15.861	1.96	16.084	0.58
V_{max}	19.617	18.508	5.65	19.385	1.18
Nu_l	2.238	2.314	3.40	2.269	1.37
Nu_r	2.238	2.314	3.40	2.269	1.37

TABLE 4.7: Results for $Ra = 1 \times 10^5$

Parameters	Benchmark	20×20	Error (%)	40×40	Error (%)
Ψ_{max}	9.612	10.091	4.98	9.6592	0.49
U_{max}	34.73	36.015	3.70	34.865	0.39
V_{max}	68.59	57.790	15.71	66.168	3.53
Nu_l	4.509	4.873	8.07	4.6379	2.86
Nu_r	4.509	4.873	8.07	4.6379	2.86

TABLE 4.8: Results for $Ra = 1 \times 10^6$

Parameter	Benchmark	20×20	Error (%)	40×40	Error (%)
Ψ_{max}	16.75	20.675	23.43	17.472	4.31
U_{max}	64.63	78.613	21.64	67.223	4.01
V_{max}	219.36	191.75	12.59	200.25	8.71
Nu_l	8.817	9.7321	10.38	9.4578	7.27
Nu_r	8.817	9.7321	10.38	9.4578	7.27

Chapter 5

MIXED CONVECTION IN A HORIZONTAL CHANNEL

Mixed convection in a horizontal channel heated from below has received considerable attention due to its important application in electronic packaging design and other energy related industrial processes. Many past studies have been devoted to that subject with emphasis on thermal boundary conditions applied on the two walls. A large cross section of the fundamental research has been reviewed recently by Ouazzani et al. [91]. In those research, they found that the lower heated wall gives rise to transverse or longitudinal rolls according to the values of the Reynolds and Rayleigh number. Relatively little work has been done on mixed convection through a channel with discrete heating from below. Tomimura and Fujii [95] discussed the need for understanding such phenomena in order to predict accurately the maximum temperature encountered on the wiring board in electronic equipments. Kennedy and Zebib [34] presented numerical and experimental results on the effect of free convection on a forced laminar horizontal channel flow with a local heat source on the bottom surface. Numerical and experimental results have also been obtained by Incropera et al. [58] who determined convection heat transfer from discrete heat sources in a horizontal rectangular channel. Recently, the forced convective heat transfer between horizontal flat plates heated periodically from below has been studied numerically by Hasnaoui et al. [96].

The present work provides numerical solutions for mixed convection in a horizontal fluid layer cooled isothermally at the top and heated at the bottom either by heating elements of uniform temperature regularly spaced or by localized heating sources. The relative strength of the free and forced convection is numerically examined for a wide range of Rayleigh, Péclet (or Reynolds) numbers.

5.1 MATHEMATICAL FORMULATION

The geometry considered in this study is a two-dimensional fluid layer of infinite extent, bounded by two horizontal impermeable surfaces, as shown in Fig. 5.1. The upper surface is assumed to be cooled at constant temperature T_c, and the bottom is assumed to be heated with either uniform temperature T_h or uniform heat flux q generated from heating elements which are regularly spaced at distance b along the surface while the rest of them is adiabatic. Also we consider the existence of an externally imposed flow with average velocity u_0 within the layer. Assuming that the laminar flow is incompressible, that the fluid properties are constant, except for the density variation with temperature and that the Boussinesq approximation holds, we obtain the following set of dimensionless equations expressing the conservation of energy and momentum:

$$\frac{\partial \theta}{\partial \tau} + \frac{\partial U\theta}{\partial X} + \frac{\partial V\theta}{\partial Y} = \frac{1}{PrRe}\nabla^2\theta \tag{5.1}$$

$$\frac{\partial \Omega}{\partial \tau} + \frac{\partial U\Omega}{\partial X} + \frac{\partial V\Omega}{\partial Y} = \frac{1}{Re}\nabla^2\Omega + \frac{Ra}{PrRe^2}\frac{\partial \theta}{\partial X} \tag{5.2}$$

$$\Omega = -\nabla^2\Psi \tag{5.3}$$

$$U = \frac{\partial \Psi}{\partial Y}, \qquad V = -\frac{\partial \Psi}{\partial X} \tag{5.4}$$

The above equations are deduced using the following scales:

Length:	h
Velocity:	u_0
Time:	h/u_0
Temperature:	ΔT
Vorticity:	u_0/h
Stream function:	hu_0

The governing parameters are

the length of heating elements:	$A = a/h$
the periodicity of heating elements:	$B = b/h$
the Rayleigh number:	$Ra = g\beta\Delta T h^3/\nu\alpha$
the Prandtl number:	$Pr = \nu/\alpha$
the Reynolds number:	$Re = u_0 h/\nu$

Except for the limit case $A = B$, we assume that B, the regular space of heating elements, imposes a periodicity λ to the solution according to

$$\lambda = nB \qquad n = 1, 2, \ldots \tag{5.5}$$

Thus, multiple solutions, each one corresponding to a particular n, may theoretically occur for a given set of governing parameters. Such a behavior has already been discussed by Robillard et al. [46] for Re=0 (no forced flow). They arise from the fact that there is a conflicting situation between the base flow of arbitrary wave length B occurring at low Ra and the natural wavelength ($\lambda \simeq 2$) of the Bénard cells. However, there is no such relationship as equation (5.5) for the limit case $A = B$. In practice, experiments [91] reveal that the wavelength takes a value in the neighborhood of 2, for which the Nusselt number reaches a maximum.

In this study, we consider only the case $B = 2$ and we assume that $\lambda = B$. Consequently the domain to be solved is restricted to the rectangular window shown in Fig. 5.2, with the requirement that periodicity conditions are used for the vertical boundaries. The thermal and dynamical boundary conditions are

Lower Boundary ($Y = 0$):

$$\begin{aligned} &\text{for all X,} \quad \Psi = 0, \quad U = V = 0 \\ &\text{for } 0.5 < \mathrm{X} < 1.5, \quad \theta = 1, \text{ or } \frac{\partial \theta}{\partial Y} = -1; \quad \text{elsewhere } \frac{\partial \theta}{\partial Y} = 0 \end{aligned} \tag{5.6}$$

Upper Boundary ($Y = 1$):

$$\text{for all } X, \quad \Psi = 1, \quad \theta = 0, \quad U = V = 0 \tag{5.7}$$

Vertical Boundaries ($X = 0,\ \lambda$):

$$\left.\begin{aligned} \theta(0,Y,\tau) &= \theta(\lambda,Y,\tau) \\ \Psi(0,Y,\tau) &= \Psi(\lambda,Y,\tau) \\ \Omega(0,Y,\tau) &= \Omega(\lambda,Y,\tau) \\ U(0,Y,\tau) &= U(\lambda,Y,\tau) \\ V(0,Y,\tau) &= V(\lambda,Y,\tau) \end{aligned}\right\} \quad \text{periodicity conditions} \tag{5.8}$$

5.2 NUMERICAL METHOD

Finite difference techniques with uniform mesh size (40×40) are used in the

numerical approach to discretize the entire domain. Detail procedure is described in chapter 3.

Numerical computations are carried out with time increments varying from 0.0001 to 0.001, until the flow and temperature fields reach the steady (or stationary periodic) state.

In order to verify the accuracy of the numerical code, some of the cases considered by Ouazzani et al. [91] and Fukui et al. [93] for pure natural convection between horizontal parallel plates isothermally heated from bottom were reproduced. The results show a nice agreement with the maximum difference of about 2% between the two studies for Ra ranging from 2×10^3 to 5×10^5.

5.3 RESULTS AND DISCUSSION

In the present investigation, all computations are done at a Prandtl number equal to 0.71, which is the value for air at standard conditions.

5.3.1 Entirely Heated Wall With Uniform Temperature ($A = B$)

By using the reference scales of h, h^2/α, α/h, $\Delta T = T_h - T_c$, α/h^2 and α for length, time, velocity, temperature, vorticity and stream function, the dimensionless governing equations (5.1) to (5.4) is modified by substituting $1/Pr$ to Re, and the dynamical boundaries conditions on bottom and top walls become $\Psi_b = -Pe/2$ and $\Psi_t = Pe/2$, where $Pe = u_0 h/\alpha$ is the Péclet number. For this limit case, a galilean transformation may be used which moves the window at a predetermined velocity V_a. Being considered a reference frame $(\hat{X}, \hat{Y})$ moving at an arbitrary horizontal velocity V_a relative to the boundaries, the following

relationships hold:

$$\begin{cases} \hat{X} = X - V_a\tau \\ \hat{U} = U - V_a \\ \hat{\Psi} = \Psi - V_a Y \end{cases} \tag{5.9}$$

Other variables such as Ω, θ, V have the same spatial distribution in both fixed and moving frame. However their time dependence is modified as follows. Let

$$f(X, Y, \tau) = \hat{f}(\hat{X} + V_a\tau, \hat{Y}, \tau) \tag{5.10}$$

where f stands for such physical variable, we have

$$\left.\frac{\partial \hat{f}}{\partial \tau}\right|_{\text{moving frame}} = \left.\frac{\partial f}{\partial \tau}\right|_{\text{fixed frame}} + V_a \frac{\partial f}{\partial X} \tag{5.11}$$

Governing equations remain unchanged when expressed in the moving reference frame, except the boundary conditions are modified as below:

Lower Boundary ($Y = 0$):

$$\text{for all X,} \qquad \Psi = -\frac{(Pe - V_a)}{2}, \qquad U = -V_a \tag{5.12}$$

Upper Boundary ($Y = 1$):

$$\text{for all X,} \qquad \Psi = \frac{(Pe - V_a)}{2}, \qquad U = -V_a \tag{5.13}$$

Figure 5.3 shows a typical result in terms of flow and temperature fields, streamline at left and isotherms at right. As mentioned earlier the value of the wavelength λ was found experimentally [91] to be in the neighborhood of 2. The

result shown in Fig. 5.3 was obtained with the assumption that $\lambda = 2$. In Fig. 5.3a, the window is fixed and the solution obtained is of the same type as in [91] and [103]. In Fig. 5.3b, V_a has been chosen in such a way that the window moves at the velocity of the transverse rolls (V_c) and therefore a steady state is represented. Since V_c is large than Pe, a net flow between the two boundaries equal to $Pe - V_c$ is imposed in the direction at which the upper and lower boundaries are moving with respect to the window Eqs. (5.12) and (5.13). The steady state was obtained by a successive approximation procedure incorporated to the numerical approach. In the steady state representation of the flow field, the streamlines correspond to the paths of the fluid particles. The temperature pattern of Fig. 5.3a is time dependent and moves with the rolls in the positive X direction, while in Fig. 5.3b, it demonstrates a time independent pattern in X direction.

The velocity of the transverse rolls ($V_c = 10.723$) in Fig. 5.3a is the result of the proper estimate of the time dependent terms in governing equations. The galilean transformation Eqs. (5.12) and (5.13) relocates the computation of this velocity into the convective terms of the same equations. Comparison between V_c of Fig. 5.3a and V_a of Fig. 5.3b shows a good agreement between the two types of computation.

In Fig. 5.4, the ratio V_c/Pe is shown as a function of Ra. Our results (table 5.1) indicate that this ratio is practically independent of Pe. This fact was already reported in [91]. The curve corresponding to the present investigation is slightly above unity and corresponds roughly to the value reported in [103].

Table 5.1 The ratio V_c/Pe

Ra	Pe	V_c/Pe
2000	5	1.1126
4000	5	1.0939
	8	1.0946
6000	5	1.0817
	10	1.0823
8000	5	1.0730
	10	1.0735
	13	1.0734
10000	5	1.0656
	10	1.0662
15000	5	1.0521
	10	1.0526
	20	1.0523

5.3.2 Partially Heated Wall With Uniform Temperature

For the case when the lower boundary is partially heated, all computations were done at values $A = 1$ and $B = 2$, with an imposed wavelength $\lambda = B$. This particular choice for B avoids the conflicting situation already mentioned between the base flow and the Bénard cells. With the same consideration of the 5.3.1, the

dimensionless governing equations are based on Péclet number and its related dynamical boundary conditions. For the ranges of Rayleigh and Péclet numbers investigated ($0 < Ra < 15000$; $0 < Pe < 20$), it was found that the resulting flow and temperature fields may be either steady or unsteady (time periodic), with or without convective cells. Figure 5.5, based on the numerical results obtained in the present investigation defines the regions corresponding to those characteristics. From Fig. 5.5, one may note that there exists for a given $Ra > \sim 2500$ a critical Pe (Pe_{cr}) beyond which the cells are carried downstream. If $Pe < Pe_{cr}$, the cells remain attached to the heating elements (steady state regime). Figures 5.6 and 5.7 show the flow and temperature fields given by streamlines (left) and isotherms (right) respectively. Figure 5.6a and 5.6b correspond to steady state regimes. Figure 5.7 corresponds to a time periodic regime. At $Pe = 0$, a nonzero flow field always exists for $Ra > 0$. A typical result corresponding to $Ra = 10000$ is shown in Fig. 6a. The presence of an imposed flow between the two boundaries ($Pe > 0$) destroys the symmetric characteristic in Fig. 6a. However a steady state might still be reached, as shown in Fig. 6b, provided that the imposed flow is not too strong, i.e., provided that Pe remains below a threshold value. The convective cells remain then attached to the heating elements with their center displaced downstream. Beyond the threshold value, the resulting flow and temperature fields are comparable to those obtained by Prasad et al. [104] for the case of an individual heating element at lower boundary of a horizontal porous layer. the convective cells are carried downstream in an irregular (time periodic) motion.

Figure 5.7 shows the sequence of flow and temperature fields occurring over one full cycle, for the case $Ra = 10000$ and $Pe = 5$. For each one of the seven flow

fields shown, it is observed that the convective cells alternate from top to bottom, being respectively in the clockwise and counterclockwise direction. Moreover it is observed that these cells are reinforced when moving over the heating elements and weakened elsewhere. The cell motion is quite irregular, with a nonuniform (periodic) velocity V_c in the downstream direction, as shown in Fig. 5.8. It is therefore impossible, by a galilean transformation, to reduce the actual problem of a layer partially heated from bottom to a steady state.

Figure 5.9 gives $\overline{V_c}$, the time averaged velocity of the cells, as a function of Pe. Extrapolation of the curves corresponding to different Ra toward the abscissa provides the critical Péclet number (Pe_{cr}) which separates steady state from unsteady behavior. $\overline{V_c}$ drops sharply when Pe approaches Pe_{cr}. It may also be observed from Fig. 5.9 that the ratio $\overline{V_c}/Pe \approx 1.1$ for $Pe \gg Pe_{cr}$ i.e., the cells tend to move on the average in a way comparable to the motion observed for the limit case $A = B$. Also the order of the curves corresponding to different Ra in Fig. 5.9 reproduces the tendency of the ratio V_c/Pe shown in Fig. 5.4 decreasing with the increment of Ra.

A particular feature of the mixed convection within a layer having regularly spaced heating elements along its lower boundary is the irregular (cyclic) way by which heat is transported to the top boundary. We consider the following definitions 1^0 of the Nusselt number relative to the top boundary:

$$Nu = \frac{\int_0^\lambda \left.\frac{\partial \theta}{\partial Y}\right|_{Y=1} dX}{\int_0^\lambda \left.\frac{\partial \theta^*}{\partial Y}\right|_{Y=1} dX} \tag{5.14}$$

and 2^0 of the parameter θ_{av}:

$$\theta_{av} = \frac{1}{\lambda}\int_0^{\lambda}\int_0^1 \theta dY dX \tag{5.15}$$

θ_{av} is a measure of the heat energy by unit volume contained within the layer. Figure 5.10 shows the time dependence of Nu and θ_{av}. It indicates clearly that heat is released by bursts from the fluid layer to the top boundary.

The time averaged Nusselt number $\overline{Nu}$ is shown in Fig. 5.11 as a function of Pe. There is a tendency for $\overline{Nu}$ to decrease with Pe. Also each of the curves corresponding to different Ra shows a discontinuity at $Pe = Pe_{cr}$.

5.3.3 Partially Heated Wall With Uniform Heat Flux

All computations were done at values $A = 1$ and $B = 2$ with imposed wavelength $\lambda = B$.

For the range of Ra and Re considered ($0 < Ra < 50000$; $0 < Re < 12$), it was found that the resulting flow and temperature fields may be either steady or unsteady (time periodic) with or without cells. Regions corresponding to those different types of solutions can be identified in the $Ra - Re$ graph of Fig. 5.12. One may note in Fig. 5.12 that there exists, for a given $Ra > 3000$, a critical Re (Re_{cr}), beyond which the cells are carried downstream, while when $Re < Re_{cr}$, the cells remain attached to the heating elements (steady state regime).

Figures 5.13 and 5.14 show the flow and temperature fields given by streamlines (left) and isotherms (right) respectively. Figures 5.13a and 5.13b represent steady state regimes. Figure 5.14 represents a periodic regime at different times during one period. At $Re = 0$, the pure free convection produces symmetric type

of flow and temperature fields, as shown in Fig. 5.13a. The limit case $Re \rightarrow 0$ was obtained numerically by setting $Re = 1/Pr$ in governing equations (5.1) and (5.2) and $\Psi(Y = 1) = 0$ in boundary condition (5.7). For $Re > 0$, a net flow is imposed between the two boundaries and the symmetric characteristic in Fig. 5.13a is destroyed. However a steady state may still be reached, as shown in Fig. 5.13b, provided that Re remains below the threshold value. The two convective cells remain then attached to the heating elements, but their centers are displaced downstream, with the imposed flow circulating between them. If the imposed flow is too strong, i.e., if $Re > Re_{cr}$, the convective cells are carried downstream in an irregular periodic motion. A sequence of flow and temperature fields covering one full cycle is shown in Figs. 5.14a to 5.14g. The convective cells shown in those figures alternate from top to bottom, being respectively in the counterclockwise and clockwise directions. It may be observed also that these cells are reinforced when they move over the heating elements and weakened elsewhere. The cell motion is quite irregular with a nonuniform periodic velocity V_c in the downstream direction, as shown in Fig. 5.15. It is noticed on this figure that for $Re = 2.5$, which is just above the threshold value ($2.25 < Re_{cr} < 2.5$ from Fig. 5.12), V_c is characterized by strong peaks separated by long time intervals where it is barely above zero. This corresponds to a jerky motion of the cells from one heating element to the others. This behavior is attenuated with increasing Re, as shown, by the curve corresponding to $Re = 8$ on the same figure. This irregular motion of the cells gives rise to a periodic time dependence for other physical variables such as ones appearing in Fig. 5.16, where Nu_A is the Nusselt number based on

the temperature averaged over the heating element defined by

$$Nu_A = \frac{\theta_A^*}{\theta_A} \tag{5.16}$$

where $\theta_A = \frac{1}{A}\int_0^A \theta(X,0)dX$, and the superscript $(*)$ refers to pure conduction temperature field at $Re = 0$. Ψ_{max} and Ψ_{min} correspond respectively to the counterclockwise and clockwise cells.

It is important for the equipment designer to predict the distribution of air temperature in order to hold the temperature of modules below a tolerable level near the channel exit, as well as to constrain the temperature variation among the modules within a permissible range. Figure 5.17 shows the time dependence of this maximum temperature and its position X_{max} along the surface element. The physical quantities of Figs. 5.15 and 5.16, time-averaged over one period and denoted by $\overline{V_c}$, $\overline{Nu_A}$, $\overline{\Psi_{max}}$ and $\overline{\Psi_{min}}$ are given in Figs. 5.18, 5.19 and 5.20 as functions of Re, for three different values of Ra.

$\overline{V_c}$ is observed to drop sharply when Re is decreased toward Re_{cr}. Also with increasing Re, $\overline{V_c}$ is seen to reach an asymptotic value slightly above unity. Thus, on the average, the cells tend to move slower than the imposed flow with increasing Re. This particular behavior in cell motion contrasts sharply with the one observed in past literature for the case of a uniformly heated channel as investigated by Ouazzani et al. [91] and also different with the case of partially heated wall with uniform temperature discussed in section 5.3.2. For those cases, the ratio of the cell velocity $\overline{V_c}$ to the imposed mean flow velocity is above unity for any Re (or Pe), with a tendency to decrease toward unity, when Re is increased.

The time dependence of the Nusselt number Nu_A appearing in Fig. 5.16a

indicates that the heat is released by bursts from the fluid layer to the top boundary. Since the heat is supplied at a steady rate from the heating elements, θ_{av}, the temperature averaged over the entire domain and Nu_t, the Nusselt number relative to the top boundary, must be time dependent and satisfy the following relationship:

$$Nu_t - 1 = \lambda RePr \frac{\partial \theta_{av}}{\partial \tau} \tag{5.17}$$

with

$$Nu_t = \int_0^\lambda \left. \frac{\partial \theta}{\partial Y} \right|_{Y=1} dX \tag{5.18}$$

$$\theta_{av} = \frac{1}{\lambda} \int_0^\lambda \int_0^1 \theta dX dY \tag{5.19}$$

The energy conservation at each time step is illustrated by the agreement between the two curves of Fig. 5.21, which correspond to each side of equation (5.17). This particular behavior in heat transfer from the bottom to the top boundary is accompanied by a maximum temperature on the surface of the heating elements that varies strongly with time, as it was shown on Fig. 5.17. This feature is of important practical consequence in the design of cooling systems of electronic packages. The convective patterns may be unsteady, giving rise to temperature peaks at the surface of individual heat generating elements.

5.4 SUMMARY

The mixed convection taking place within a horizontal fluid layer with regularly spaced heating elements on its lower boundary has been numerically studied. For the limit case of a uniformly heated lower boundary ($A = B$), a galilean transformation has been successfully applied to reduce the problem to a steady state.

By comparison to a uniformly heated channel for which the cells are carried downstream with a constant velocity for any Reynolds number (or Pélect number), the case with localized heating is more complex. For low enough Reynolds numbers (or Pélect number), the cells remain attached to the heating elements and a steady state is achieved. Beyond a given threshold value of the Reynolds number (or Pélect number), the cells are carried downstream with a time dependent periodic velocity.

Due to the irregular motion of the convective pattern in the downstream direction, all other physical variables are characterized by a periodic time dependence. In particular, the overall Nusselt number relative to the top boundary and the temperature averaged over the fluid layer (which is a measure of the heat energy contained in the fluid) are not in phase and show a strong periodic time dependence. Physically this indicates that the heat produced at a steady state by the heating elements accumulates within the fluid layer before being released through the upper boundary.

The present study has been restricted to an imposed wavelength of the heated elements along the bottom equal to twice the channel height, i.e., equal to the natural wavelength that was found to occur in the case of a uniformly heated bottom.

Chapter 6

EFFECTS OF A MOVING THERMAL WAVE ON BÉNARD CONVECTION IN A HORIZONTAL FLUID LAYER

Since Schubert and Whitehead [105] proposed that the traveling thermal wave caused by solar radiation is responsible for the fact that the upper atmosphere of the planet Venus rotates approximately 60 times faster than the planet itself, the study of natural convection with a periodically changing surface temperature has received an increasing interest. A comprehensive review of this subject may be found in the article by Hinch and Schubert [106]. Whitehead [107] performed a moving-flame experiment with liquid mercury and observed that the mean surface flow was up to four times greater than the heater speed. His experimental data were also confirmed by a theoretical analysis of flows driven by buoyancy and surface tension. To determine whether the thermal wave is capable of producing mean flows which exceed the phase velocity by a few orders of magnitude, Busse [108] studied analytically the effects of a thermal wave propagating in a horizontal fluid layer on the flow behavior. His results show that the generation of a mean flow depends on the existence of harmonics in the fluctuating velocity field. The presence of a thermal wave represents in fact the possibility of producing the appropriate harmonics in the velocity fields that are responsible for nonvanishing Reynolds stresses. Young et al. [109] solved a similar problem numerically under

three sets of boundary conditions: rigid upper and lower boundaries with symmetrical heating; free upper boundary and rigid lower boundary with heating at the top; free upper and lower boundaries with symmetrical heating. Their analyses also showed the possibility of producing large mean flows when the thermal forcing becomes large but the fluid viscosity is not necessarily small.

The works mentioned above are limited to cases in which the flow is generated exclusively by thermal wave, with the mean velocity of the fluid much smaller or much larger than the source speed. However, the effect of a moving thermal wave on Bénard convection has not been discussed so far, although the mechanism of interaction between a thermal wave and Bénard cells is of considerable interest.

In the case of a stationary thermal wave, the problem has been treated by the stability theory by many investigators (see, for example, Kelly and Pal [110], Kelly and Pal [97], Kelly and Pearlstein [111]). Their analyses have, in part, been motivated by the desire to model experimental imperfections such as thermal noise, and boundary misalignment or roughness. The results obtained are also of great interest in the context of bifurcation theory and in the study of nonlinear systems in general. Yet, very few numerical investigations have been devoted to these problems.

The purpose of the present numerical study is to investigate the effect of a moving thermal wave on Bénard convection. Also, in the limit case of a stationary wave, attention will be focused on the effects of the spatially periodic boundary condition on the amplitude of convection, and the stability of the multiple solutions in the supercritical regime. Here, the thermal wave takes the form of a

sinusoidal perturbation superposed on the hot temperature of the lower boundary, with a wavenumber K equal to the critical wavenumber K_{cr} of the classical Bénard problem. Moreover, we assume that the solution will be periodic in the x direction, with a wavelength corresponding to the imposed perturbation. This may appear a bold assumption in the context of finite amplitude Bénard cells. On one hand, the linear stability analysis alone admits a whole band of wavenumbers at a given supercritical Rayleigh number Ra. On the other hand, experimental observation indicates that a single wavenumber, function of the Rayleigh and Prandtl numbers (Ra, Pr), is selectively amplified (see, for instance, Chen and Whitehead [112], Pocheau and Croquette [113]). One may therefore question the periodicity resulting from the interaction between an imposed periodic disturbance and a finite amplitude Rayleigh-Bénard convection of potentially different wavelength. There is however some ground for the above assumption. Firstly, past experiments by Chen and Whitehead [112] for the range of $Ra_{cr} < Ra < 2.5Ra_{cr}$ indicate that a disturbance with an arbitrary wavenumber (not too far from k_{cr}) imposed as a boundary condition will promote a convective pattern corresponding to that wavenumber. Secondly, nonlinear analyses for finite amplitude convection, with Ra slightly above Ra_{cr} (see, for instance, Segel [114]), precludes the possibility of a mixed equilibrium containing both disturbances, i.e., only one will survive. It also appears from these studies that initial conditions strongly determine the precise wavenumber selected. In the present study, the disturbance is maintained indefinitely. Also the problem is solved in a reference frame moving at the same velocity of the thermal wave. From that point of view, the problem is to some extent similar to the mixed convection in a horizontal layer with heating elements regularly spaced on the lower boundary, as considered by Hasnaoui et al. [96].

Their results show that at low Reynolds numbers (Re), a steady state is possible for which the convective cells remain attached to the heating elements. Beyond a critical Reynolds number (Re_{cr}), the cells are carried downstream, reinforced and weakened periodically.

As mentioned earlier, the wavelength of finite amplitude convection is affected by the Prandtl number. Experiments have shown that the wavelength increases with Ra at low Pr. The opposite behavior occurs at high Pr. There is an abundant literature on the problem of wavenumber selection. In most of the theoretical articles on the subject, specific geometric or thermal boundary conditions are considered. Among those articles, the works by Buell and Catton [115] and [116] are respectively for axisymmetric and ramped convection. In both cases, results indicate that the wavenumber for finite amplitude convection would remain close to K_{cr} with increasing Ra, if the Prandtl number remains in the neighborhood of 0.7. Thus, in an effort to minimize the discrepancy between the imposed periodicity at the boundary and the natural periodicity of finite amplitude Bénard cells for the range $Ra_{cr} < Ra < 4.6Ra_{cr}$, we solve the problem numerically by choosing Prandtl number equal to 0.71.

6.1 MATHEMATICAL FORMULATION

The problem considered here consists of a fluid layer of infinite extent, bounded by two horizontal impermeable walls, as shown in Fig. 6.1. The upper boundary is uniformly cooled with a temperature T_t. The lower boundary is heated at a temperature $T_b = \widetilde{T_b} + \sigma \sin(K'x - \gamma t)$, where $\sigma < \widetilde{T_b} - \widetilde{T_t} = \Delta T$, is the amplitude of the thermal wave. The wavenumber K' is set equal to the critical

wavenumber $K'_{cr} \simeq \pi/h$.

Assuming that the Boussinesq approximation holds and that all fluid properties are constant, except for density in the buoyancy term, the 2-D flow considered here can be formulated in terms of stream function ψ and the vorticity ω with respect to fixed coordinates $(x,\ y)$ as

$$\frac{\partial T}{\partial t} + \frac{\partial uT}{\partial x} + \frac{\partial vT}{\partial y} = \alpha \nabla^2 T \tag{6.1}$$

$$\frac{\partial \omega}{\partial t} + \frac{\partial u\omega}{\partial x} + \frac{\partial v\omega}{\partial y} = \nu \nabla^2 \omega + \beta g \frac{\partial T}{\partial x} \tag{6.2}$$

$$\nabla^2 \psi = -\omega \tag{6.3}$$

$$u = \frac{\partial \psi}{\partial y}, \quad v = -\frac{\partial \psi}{\partial x} \tag{6.4}$$

With the boundary condition $\psi_b = \psi_t = 0$, we assume there is no main flow generated between the plates.

Here, a coordinate system $(\hat{x},\ \hat{y})$ which moves with the imposed thermal wave may be used in which the governing equations can be written as

$$\frac{\partial \hat{T}}{\partial t} + \frac{\partial \hat{u}\hat{T}}{\partial \hat{x}} + \frac{\partial \hat{v}\hat{T}}{\partial \hat{y}} = \alpha \nabla^2 \hat{T} \tag{6.5}$$

$$\frac{\partial \hat{\omega}}{\partial t} + \frac{\partial \hat{u}\hat{\omega}}{\partial \hat{x}} + \frac{\partial \hat{v}\hat{\omega}}{\partial \hat{y}} = \nu \nabla^2 \hat{\omega} + \beta g \frac{\partial \hat{T}}{\partial \hat{x}} \tag{6.6}$$

$$\nabla^2 \hat{\psi} = -\hat{\omega} \tag{6.7}$$

$$\hat{u} = \frac{\partial \hat{\psi}}{\partial \hat{y}}, \quad \hat{v} = -\frac{\partial \hat{\psi}}{\partial \hat{x}} \tag{6.8}$$

The relationship between variables in the fixed coordinate system (x, y) and those in the moving system $(\hat{x}, \hat{y})$ are

$$\begin{cases} x = \hat{x} + v_w t \\ y = \hat{y} \\ u = \hat{u} + v_w \\ v = \hat{v} \\ T = \hat{T} \\ \omega = \hat{\omega} \\ \psi = \hat{\psi} + v_w y \end{cases} \tag{6.9}$$

Moreover, the time derivative is transformed from one coordinate system to the other according to

$$\left.\frac{\partial \hat{f}}{\partial t}\right|_{\text{moving frame}} = \left.\frac{\partial f}{\partial t}\right|_{\text{fixed frame}} + v_w \frac{\partial f}{\partial x} \tag{6.10}$$

with $\dfrac{\partial f}{\partial x} = \dfrac{\partial \hat{f}}{\partial \hat{x}}$

where f stands for any physical variable and $v_w = \gamma/K'$ is the velocity of the imposed thermal wave.

Introducing the scales h, α/h, h^2/α, α, α/h^2 and ΔT for length, velocity, time, stream function, vorticity and temperature, respectively, Eqs. (6.5) – (6.8) take the following dimensionless form

$$\frac{\partial \hat{\theta}}{\partial \tau} + \frac{\partial \hat{U}\hat{\theta}}{\partial \hat{X}} + \frac{\partial \hat{V}\hat{\theta}}{\partial \hat{Y}} = \nabla^2 \hat{\theta} \tag{6.11}$$

$$\frac{\partial \hat{\Omega}}{\partial \tau} + \frac{\partial \hat{U}\hat{\Omega}}{\partial \hat{X}} + \frac{\partial \hat{V}\hat{\Omega}}{\partial \hat{Y}} = Pr\nabla^2\hat{\Omega} + PrRa\frac{\partial \hat{\theta}}{\partial \hat{X}} \tag{6.12}$$

$$\nabla^2\hat{\Psi} = -\hat{\Omega} \tag{6.13}$$

$$\hat{U} = \frac{\partial \hat{\Psi}}{\partial \hat{Y}}, \quad \hat{V} = -\frac{\partial \hat{\Psi}}{\partial \hat{X}} \tag{6.14}$$

where $Pr = \nu/\alpha$ (Prandtl number) and $Ra = g\beta\Delta T h^3/\nu\alpha$ (Rayleigh number). The governing parameters are Pr, Ra, K and V_w, with $K = K_{cr} = \pi$.

The boundary conditions in the moving system then become

At the lower boundary ($\hat{Y} = 0$)

$$\begin{cases} \hat{\theta} = 1 + \delta \sin(K\hat{X}) \\ \hat{\Psi} = 0 \\ \hat{V} = 0, \qquad \hat{U} = -V_w \end{cases} \tag{6.15}$$

At the upper boundary ($\hat{Y} = 1$)

$$\begin{cases} \hat{\theta} = 0 \\ \hat{\Psi} = -V_w \\ \hat{V} = 0, \qquad \hat{U} = -V_w \end{cases} \tag{6.16}$$

where $V_w = \Gamma/K$ is the dimensionless velocity of the thermal wave, or equivalently, the imposed velocity in the negative X direction.

The solution is assumed to be periodic in $\hat{X}$, based on the wavenumber K_{cr}. Consequently, the domain to be solved numerically may be restricted to a

rectangular "window" shown in Fig. 6.2, with the periodic condition imposed on the vertical boundaries for any appropriate flow quantity $\hat{F}$

$$\hat{F}(\hat{X}, \hat{Y}, \tau) = \hat{F}(\hat{X} + \hat{\lambda}, \hat{Y}, \tau) \tag{6.17}$$

The overall Nusselt numbers at the upper and lower boundaries are defined respectively as

$$\begin{aligned} \widetilde{Nu_t} &= -\frac{1}{\lambda}\int_0^{\lambda} \left.\frac{\partial\theta}{\partial Y}\right|_{Y=1} dX \\ &= -\frac{1}{\hat{\lambda}}\int_0^{\hat{\lambda}} \left.\frac{\partial\hat{\theta}}{\partial\hat{Y}}\right|_{\hat{Y}=1} d\hat{X} \end{aligned} \tag{6.18}$$

$$\begin{aligned} \widetilde{Nu_b} &= -\frac{1}{\lambda}\int_0^{\lambda} \left.\frac{\partial\theta}{\partial Y}\right|_{Y=0} dx \\ &= -\frac{1}{\hat{\lambda}}\int_0^{\hat{\lambda}} \left.\frac{\partial\hat{\theta}}{\partial\hat{Y}}\right|_{\hat{Y}=0} d\hat{X} \end{aligned} \tag{6.19}$$

Note that $\widetilde{Nu_t}$ and $\widetilde{Nu_b}$ must satisfy the energy balance

$$\widetilde{Nu_b} - \widetilde{Nu_t} = \frac{\partial\theta_{av}}{\partial\tau} \tag{6.20}$$

where θ_{av} is the average temperature of the fluid layer, defined by

$$\begin{aligned} \theta_{av} &= \frac{1}{\lambda}\int_0^1\int_0^{\lambda} \theta dX dY \\ &= \frac{1}{\hat{\lambda}}\int_0^1\int_0^{\hat{\lambda}} \hat{\theta} d\hat{X} d\hat{Y} \end{aligned} \tag{6.21}$$

Another quantity of interest, the pressure decrement in one wavelength, ΔP, can be determined from the shear stress at the boundaries according to the relationship [109]

$$\Delta P = \int_0^{\hat{\lambda}} \left(\left.\frac{\partial\hat{U}}{\partial\hat{Y}}\right|_{\hat{Y}=0} - \left.\frac{\partial\hat{U}}{\partial\hat{Y}}\right|_{\hat{Y}=1}\right) d\hat{X} \tag{6.22}$$

6.2 NUMERICAL METHOD

The numerical method used here is based on finite difference techniques, which has been discussed in the chapter 3.

A uniform mesh size was used for both x and y directions, and a grid of 40×40 for $\lambda = 2$ was found to model accurately the flows described in this work. The time increment ranged from 0.0001 to 0.001.

With δ set to zero (classical Bénard cells), the numerical program was checked to reproduce satisfactorily the Nu vs Ra dependence (see, for instance, Ostrach and Kamotani [117], Fukui et al. [93], Ouazzani et al. [91]. Those results were practically unaffected in a moving frame of reference with $V_w \leq 15$. For $\delta = 0$ and $0 < V_w \leq 15$, the solution was of course time periodic when observed from the moving frame. The time-averaged cell velocity $\overline{V_c}$ was deduced from the time period Υ characterizing the unsteady solution ($\overline{V_c} = \lambda/\Upsilon$), and $\overline{V_c}$ was equal to $-V_w$ within 1%. The determination of V_c, the "instantaneous" velocity of cells has limitations inherent to the time and space discretization.

6.3 RESULTS AND DISCUSSION

For all the cases investigated in the present study, the Prandtl number Pr was set equal to 0.71 which is the value for air at standard conditions.

6.3.1 Stationary Thermal Wave

In the absence of a thermal wave ($\delta = 0$), convection is possible only when the Rayleigh number Ra is greater than a critical value $Ra_{cr} = 1707.8$, and occurs as a supercritical bifurcation from the conduction state. This phenomenon is depicted

in Fig. 6.3 by a solid line, which is determined by a well-known supercritical amplitude relation given by Malkus and Veronis [118].

$$C_1\Psi_{ext} = \pm(\frac{Ra - Ra_{cr}}{Ra_{cr}})^{\frac{1}{2}} \tag{6.23}$$

where Ψ_{ext} is the extreme value of the stream function and is taken as a measure of the convection amplitude; C_1 is a constant, determined from numerical results by the least square fit method, and was found to be 0.2396. At $Ra > Ra_{cr}$, the two stable convection states correspond to counterclockwise and clockwise cells respectively. Note that with the periodic boundary conditions (Eq. 6.17), the cells have no preferred location along the x direction in the solution domain.

When a stationary thermal wave ($\delta = 0.1$ in Fig. 6.3) is imposed on the lower boundary, convection occurs at all values of Ra. Kelly and Pal [97] have shown that the amplitude of convection is then governed by a cubic equation of the form

$$(C_1\Psi_{ext})^3 = (\frac{Ra - Ra_{cr}}{Ra_{cr}})(C_1\Psi_{ext}) + C_2\delta \tag{6.24}$$

In the range $0 < Ra < Ra_{cr}$, convective cells can be observed along the layer, alternating from clockwise to counterclockwise motion. The cells are always in phase (curve with solid squares) with the thermal wave, the upward flow being located above the maximum temperature of the lower wall. As Ra is increased beyond Ra_{cr}, no abrupt change occurs near the Ra_{cr}, although Ψ_{ext} increases more rapidly and remains above the curve corresponding to classical Bénard cells. This solution branch is called "preferred branch" according to Ehrhard and Muller [119] and "natural branch" according to Nield and Bejan [120]. In fact, numerical computations starting from the rest state always converge toward this branch.

As discussed by Kelly and Pals [97], there are three theoretical possible solutions for Ra well above Ra_{cr}. However, only the one in phase with the thermal wave is stable with respect to a phase shift. This is confirmed by the present numerical results. A search for a second solution was done by starting the computations from initial conditions corresponding to the solution of the preferred branch. Figures 6.4a and 6.4b show the time evolution of Ψ_{ext}, and of its position along the X coordinate, from the initial conditions ($Ra = 8000$ and $\Psi_{ext} = 8.416$). At time $\tau = 2$, by changing δ to $-\delta$, the thermal wave is phase-shifted suddenly by 180^0. After a relatively short transient period, the system reaches an almost time-independent state (quasi-steady state, $\Psi_{ext} = 7.987$), which corresponds to the isolated branch of Fig. 6.3. However, as time passes, the cells gradually move by half a wavelength to a final location where they are in phase with the imposed thermal wave and Ψ_{ext} goes back to the preferred value. This behavior may be clearly seen in Figs. 6.4a and 6.4b. The imposed thermal wave is symmetrically located with its maximum temperature at center on the ordinate of Fig. 6.4b. After a short period of initial transient starting at $\tau = 2$, the quasi-steady state is reached at $\tau \simeq 2.25$. At $\tau \simeq 11$, Ψ_{ext} disappears at the left of the flow domain and reappears at the right.

From the numerical results of the preferred and isolated branches obtained in this way, the constant C_2 in equation (6.24) was found to be 0.582.

6.3.2 Moving Thermal Wave

As mentioned in the previous section, the problem may be considered in a reference frame moving with velocity V_w (Fig. 6.2), in which the thermal wave

becomes stationary and a net flow V_w is seen in the opposite direction. For small V_w, stationary cells are observed in this reference frame as if they are attached to (and travel with) the thermal wave.

As V_w is gradually increased, it was found that there exists a critical V_w for a given pair of values Ra and δ, below which the cells remain attached to the thermal wave, but beyond which they are carried downstream. Figures 6.5 and 6.6 show the effect of V_w on the fluid flow and heat transfer in terms of streamlines (left) and isotherms (right). Note that in these figures, the maximum temperature is located at the center of the lower boundary.

When $V_w = 0$, a symmetric pattern is obtained for both temperature and flow fields, as shown in Fig. 6.5a. It corresponds to the preferred branch described earlier, and consists of two counter-rotating cells with an upward flow above the "hot " point. As V_w is increased, the symmetry is destroyed, such that the convective cells become skewed and displaced downstream, as can be seen in Fig. 6.5b ($V_w = 1$). However, the flow is still steady as the convective cells remain attached to the thermal wave.

When $V_w = 2$, a steady state no longer exists, and the cells are carried downstream with V_w in a periodic fashion. Figure 6.6 for the flow and temperature fields at different times during one full period $\Upsilon = 1.2834$ clearly shows how the shape and intensity of the cells changes as they move.

The time-averaged velocities of the cells, $\overline{V_c}$ and $\overline{\hat{V}_c}$ for $Ra = 8000$ and $\delta = 0.3$, are plotted as functions of V_w in Figs. 6.7a and 6.7b. The threshold value $V_{w_{cr}} \simeq 1.2489$ is obtained by extrapolation of the numerical results. Figure 6.7b

shows that $\overline{V_c}/V_w$ tends asymptotically toward zero as $V_w \to \infty$. Thus, for an observer in the fixed frame, the entrainment of the convective cells by the moving thermal wave is gradually reduced to zero with increasing V_w.

Figure 6.8 shows the variations of $V_{w_{cr}}$ with Rayleigh number ($2000 < Ra < 8000$) for two values of δ (0.1 and 0.3). In this figure, the lower limit $Ra_{cr} = 1707.8$ corresponds to the critical Rayleigh number for Bénard cells. One can remark that the amplitude δ is a parameter that influences strongly the value of $V_{w_{cr}}$ such that the ratio $V_{w_{cr}}/\delta$ only increases slightly as δ is decreased from 0.3 to 0.1. These curves also show that $V_{w_{cr}}/\delta$ attains a minimum value at $Ra \simeq 3500$ Thus as Ra is decreased from 3500 to Ra_{cr}, the convective cells are carried more easily with the thermal wave. This behavior might be explained by the fact that the convective cells depend more and more upon the thermal wave itself when $Ra \to Ra_{cr}$. However, when Ra is increased from 3500, it is rather difficult to see why the Bénard cells remain attached for higher values of V_w

The unsteady state obtained for $V_w > V_{w_{cr}}$ is characterized by a periodic motion relatively to the thermal wave, as shown in Fig. 6.9a where $\hat{V}_c$ is given as a function of time. Other quantities of interest, such as the extreme stream function (Fig. 6.9b), the overall Nusselt number $\widetilde{Nu_t}$ and $\widetilde{Nu_b}$ (Fig. 6.9c).

It is of practical interest to predict ΔP, the pressure decrement in one wavelength. As discussed by Busse [108] and Young et al. [109], a mean flow can be generated by a moving thermal wave under the condition of zero pressure drop. Conversely, we can calculate the pressure decrement necessary to maintain a zero mean flow in the presence of a thermal wave. From the time-averaged pressure

decrement $\overline{\Delta P}$, shown in Fig. 10a as a function of the thermal wave velocity, it appears that as V_w is increased from 0 to $V_{w_{cr}}$, the pressure decrement $\overline{\Delta P}$ linearly increases from 0 to attain a maximum value at $V_w = V_{w_{cr}}$. At this point, $\overline{\Delta P}$ suffers from a sudden drop in the same manner as $\overline{\widetilde{Nu}}$ (Fig. 6.10b), before it continues to increase with V_w, but at a much slower rate.

The time-averaged $\overline{\widetilde{Nu}}$ and $\overline{\hat{\psi}_{ext}}$ are given in Figs. 6.10b and 6.10c as functions of V_w. A discontinuity is also observed for these quantities at $V_{w_{cr}}$. A particular feature of the periodic state is the way by which heat is transferred from the lower boundary to the upper. It may be noticed in Fig. 6.9c that $\widetilde{Nu_t}$ and $\widetilde{Nu_b}$ are out of phase in their cyclic variations. Thus the heat content in the fluid media must also be time-dependent. During one cycle, part of the heat coming from the lower boundary is at first stored within the layer before being released though the upper boundary. It should be noted that the energy balance expressed by Eq. (6.20) at each time step is satisfied to a high degree of accuracy by the present numerical code, as it can be seen in Fig. 6.11 where the left and right hand side terms of Eq. (6.20) have been calculated separately, and shown by a dotted line and a solid line, respectively.

The effect of a moving thermal wave on Bénard cells in a fluid layer with a zero pressure decrement has also been investigated. Following the procedure of Young et al. [109], we set the stream function to zero at the lower boundary and vary the stream function at the upper boundary in order to satisfy $\Delta P = 0$. The numerical calculations are performed in the moving coordinate system $(\hat{X}, \hat{Y})$.

In accordance with the momentum conservation in the horizontal direction,

we have

$$\frac{\partial \hat{\Psi}(1)}{\partial \tau} = -Pr[\tilde{\Omega}(1) - \tilde{\Omega}(0)] \tag{6.25}$$

where $\tilde{\Omega} = \frac{1}{\hat{\lambda}} \int_0^{\hat{\lambda}} \Omega d\hat{X}$.

Figure 6.12 gives the time-averaged net flow $\overline{\Psi_t}$ (based on the fixed coordinate system) as a function of the wave velocity. This clearly shows that a moving thermal wave always generates a net flow in the opposite direction of the thermal wave for all $V_w \neq 0$. A similar behavior was observed experimentally by Whitehead [107]. Figure 6.12 is qualitatively similar to Fig. 6.10a. In fact, by comparison with the case of imposed zero net flow discussed previously, there exists also a critical wave velocity for given values of Ra and δ (for instance, $V_{w_{cr}} = 0.776$ for $Ra = 8000$ and $\delta = 0.3$), below which a steady state is obtained with cells attached to the thermal wave. Above that threshold, the cells are carried downstream and the net flow oscillates with a time-averaged value increasing linearly with V_w, as shown in Fig. 6.12.

6.4 Summary

The effect of a moving thermal wave imposed as a boundary condition on Bénard cells in a horizontal layer of infinite extent has been studied numerically for the range of $Ra_{cr} < Ra < 4.6Ra_{cr}$ and for a constant Prandtl number of 0.71. The wavelength of the modulation has been set equal to the critical wavelength of the incipient Bénard cells and we have assumed that the resulting periodicity of the solution would correspond to the imposed disturbance, thus reducing our solution domain to one wavelength.

The main finding is the occurrence of a threshold for the velocity of the thermal wave, below which the Bénard cells are carried along with the disturbance. That threshold depends upon the amplitude δ and upon the Rayleigh number Ra. Below the threshold, the convective cells are attached to the imposed thermal wave so that a steady state may be observed in a reference frame moving with the thermal wave. Above this threshold, no steady state can be obtained and the cells move with a time-averaged velocity lower than the thermal wave. In fact, the flow exhibits an unsteady periodic behavior in which all flow quantities are characterized by a cyclic time dependence. In particular, heat is released by bursts from the fluid layer through the upper boundary.

Chapter 7

MIXED CONVECTION IN AN INCLINED CHANNEL WITH LOCALIZED HEAT SOURCES

Channels formed by parallel plates or fins are a frequently encountered configuration in natural and forced convection cooling by air of electronic equipment. Many scientists are involved in the research subject of heat transfer in channels. However, just a few studies have been reported thus far in the literature for channels with arbitrary inclination angles. Tomimura et al. [95] have explored the aiding mixed convection flow and heat transfer between inclined parallel plates with localized heat flux over their length. Their results demonstrate that the temperature field is considerably affected by the inclination angle and much affected by the discrete heating because of the intermittent development of thermal boundary layer. Lavine [121] [122] has derived a one-dimensional analytical model for fully developed aiding and opposing mixed convection between inclined parallel plates, where a flow reversal regime is observed that strongly affects temperature distribution, wall friction and velocity profile. The analytical solution is then confirmed by experimental results [123].

The purpose of this chapter is to investigate numerically the idealized case of a two-dimensional laminar flow in a channel of infinite extent and arbitrary inclination angle with one of the walls isolated while discrete heating elements with uniform heat flux are regularly spaced along the other wall that is elsewhere

adiabatic. A forced flow of arbitrary intensity is imposed between the walls. The heat from each heating element is conveyed downstream and a steady state is achieved for which the temperature field is characterized by a spatial increment which repeats at each heating element in the downstream direction. Consequently, the flow field and temperature gradients are assumed to repeat periodically along the channel according to the imposed periodicity of the heating elements on the lower boundary. The numerical flow domain used for most of the results is thus restricted to one wavelength of the imposed periodicity with periodic conditions applied at the two end boundaries. Some numerical results were also obtained from a whole channel configuration with a few heating elements and specified entrance and outlet conditions. This last configuration requires a large mesh size and much more CPU time. Its main purpose is to validate the one-wavelength configuration by showing 1^0 that the flow field tends to repeat along the channel according to the imposed periodicity of the heating elements and 2^0 that the velocity profiles at a distance far enough from the entrance and outlet, do agree with those of the one-wavelength configuration. Finally an analytical solution is given in appendix B for the limit case where the entire boundary is heated. The approach for this solution is based on a parallel flow hypothesis. The developments are similar to those by Bejan and Tien [124], Vasseur, Robillard and Sen [125] and follow closely the work by Lavine [122], [122].

7.1 MATHEMATICAL FORMULATION

The problem considered here is illustrated in Fig. 7.1. It consists of a two-dimensional fluid layer of infinite extent in the x direction, bounded by two inclined parallel plates at an angle φ with the horizontal direction. The upper wall

is insulated and the bottom is heated with uniform heat flux q generated from heating elements of length a which are regularly spaced at a distance b, while the remaining surface is adiabatic. Moreover, an external flow with downward mean velocity (opposing flow) u_0 is imposed. Assuming that the laminar flow is incompressible with constant properties, that the usual Boussinesq approximation holds, $\rho = \rho_0[1-\beta(T-T_r)]$, and that the heat generated from the heating elements is totally carried downstream by the forced flow, we obtain the following set of dimensionless equations expressing the conservation of energy, momentum and mass:

$$\frac{\partial\theta}{\partial\tau} + \frac{\partial U\theta}{\partial X} + \frac{\partial V\theta}{\partial Y} = \frac{1}{PrRe}\nabla^2\theta \tag{7.1}$$

$$\frac{\partial\Omega}{\partial\tau} + \frac{\partial U\Omega}{\partial X} + \frac{\partial V\Omega}{\partial Y} = \frac{1}{Re}\nabla^2\Omega + \frac{Ra}{PrRe^2}[\frac{\partial\theta}{\partial X}\cos\varphi + \frac{\partial\theta}{\partial Y}\sin\varphi] \tag{7.2}$$

$$\Omega = -\nabla^2\Psi \tag{7.3}$$

$$U = \frac{\partial\Psi}{\partial Y}, \qquad v = -\frac{\partial\Psi}{\partial X} \tag{7.4}$$

Equations (7.1-7.4) have been nondimensionalized by defining X, Y, U, V, θ, Ω and Ψ as

$$X = \frac{x}{h}, \qquad Y = \frac{y}{h} \tag{7.5}$$

$$U = \frac{u}{u_0}, \qquad V = \frac{v}{u_0} \tag{7.6}$$

$$\theta = \frac{T-T_r}{\Delta T}, \qquad \Delta T = \frac{qh}{k} \tag{7.7}$$

$$\Omega = \frac{\omega h}{u_0}, \qquad \Psi = \frac{\psi}{h u_0} \tag{7.8}$$

The intensity of the natural convection and the strength of the forced convection are characterized by the Rayleigh number, $Ra = \frac{g\beta\Delta T h^3}{\alpha\nu}$, and the Reynolds number $Re = \frac{u_0 h}{\nu}$, respectively. The other parameters $A = a/h$, $B = b/h$, φ and $Pr = \nu/\alpha$ are the dimensionless length of heating elements, the dimensionless periodicity of the heating elements, the inclination angle and the Prandtl number respectively. The numerical approach solves the time-dependent form of the energy and vorticity equations as given by Eqs. (7.1) and (7.2) with initial conditions corresponding to static states of both velocity and temperature fields.

Two flow domains are considered for the solution of Eqs. (7.1 - 7.4): the whole channel configuration with entrance and outlet sections, shown in Fig. 7.2a and the one-wavelength configuration shown in Fig. 7.2b. This last flow domain is based on the assumption that the solution is periodic in x direction according to the periodic spacing of the heating elements. Consequently, it is aimed at reproducing the flow conditions in a channel of infinite extent. Both flow domains have the same thermal and dynamical boundary conditions for the lower and upper walls. Those conditions are:

Lower Boundary ($Y = 0$):

$$\begin{aligned} &\text{for all } X, && \Psi = 0, \quad U = V = 0 \\ &\text{for each heating element,} && \frac{\partial\theta}{\partial Y} = -1 \\ &\text{elsewhere,} && \frac{\partial\theta}{\partial Y} = 0 \end{aligned} \tag{7.9}$$

Upper Boundary ($Y = 1$):

$$\text{for all } X, \quad \Psi = 1, \quad \frac{\partial \theta}{\partial Y} = 0, \quad U = V = 0 \tag{7.10}$$

The boundary conditions for the vertical boundaries are different for the two flow domains. For the whole channel configuration, they are

$$\begin{aligned} &\text{at } X = 0, \quad \theta = 0, \quad U = -6(Y^2 - Y), \quad V = 0 \\ &\text{at } X = L, \quad \frac{\partial^2 F}{\partial X^2} = 0 \end{aligned} \tag{7.11}$$

where F stands for any physical variable. The conditions at the outlet correspond to those used by Tomimura et al. [95] and Yücel et al. [126].

For the one-wavelength configuration, we assume that B, the regular spacing of the heating elements imposes its periodicity to the solution. Every physical quantity F, including the temperature gradient, satisfies the following periodic condition on the two vertical boundaries.

$$F(X + B, Y, \tau) = F(X, Y, \tau) \tag{7.12}$$

However, the temperature itself does not satisfy this condition. In fact, at each wavelength B, the temperature must be increased by a factor c such that

$$T(X + B, Y, \tau) = T(X, Y, \tau) + C \tag{7.13}$$

where $C = A/(RePr)$ is defined on the basis of energy balance. The increment C implies of course the existence of a conductive heat flux in the upstream direction that the convective heat flux must compensate.

The present problem contains six governing parameters, namely, the Rayleigh number Ra, the Reynolds number Re, the Prandtl number Pr, the spacing of the

heating elements B, the individual length of the heating elements A, and the inclination angle φ. As shown in the appendix B, for the limit case of an entirely heated wall ($A = B$), the number of governing parameters is reduced to two, P_1 and P_2.

7.2 NUMERICAL METHOD

The numerical procedure used here is based on finite difference techniques. The procedure has been discussed in chapter 3.

The uniform mesh size were used for both X and Y directions, and a grid of 40×40 for $B = 2$ was found to be an acceptable compromise between accuracy and computer time, while for the whole channel configuration with five heating elements, a grid of 20×150 was used. Spot checks of accuracy, however, were made using more refined grids. The time increment ranged from 0.0001 to 0.001. The temperature was set to zero as a reference value at a suitable location of the grid (either at the entrance of the whole channel configuration or at $X = 0$, $Y = 0$ for the one-wavelength configuration). Also the computation was started from $\theta = 0$ everywhere as an initial condition.

Results from the present numerical code are compared with the analytical solution given in appendix B for the limit case $A = B$ (entirely heated bottom wall). Figure 7.3 shows velocity profiles obtained from both approaches for $P_1 = 100$ and $P_2 = -70$, 70 and 140.

7.3 RESULTS AND DISCUSSION

For all the cases investigated numerically in the present study, the length

A of the heating elements and the spacing B were maintained equal to 1.0 and 2.0 respectively. Also, the Prandtl number Pr was set equal to 0.71, which is the value of air at standard conditions. The ranges of Rayleigh and Reynolds numbers were respectively $0 < Ra < 10000$ and $0 < Re < 10$. The inclination angle φ was varied between 0^0 and 90^0 so that the forced flow was downward with the heating elements on the bottom wall.

In Figs. 7.4 and 7.5, a comparison is done between numerical results obtained from the one-wavelength configuration and those from the whole channel configuration for a typical case of $Ra = 500$, $Re = 1$ and $\varphi = 75^0$. Flow and temperature fields are shown respectively by streamlines and isotherms in Figs 7.4a and 7.4b. Heating elements correspond to the shown by heavy line segments regularly spaced on the bottom wall. The whole channel configuration includes five heating elements with entrance and outlet conditions given by Eq. (7.11). With those boundary conditions, a definite recurrence, or periodicity of the flow field and temperature gradients is observed which corresponds to the spacing B of the heating elements. This periodicity could be improved by increasing the length of the channel and the number of heating elements. However, this would require prohibitive C.P.U. time. In Fig. 7.4a and 7.4b, one can notice the great similarity of flow and temperature fields for both configurations. Figures 7.5a and 7.5b show velocity and temperature profiles taken at locations D and E identified in Figs. 7.4a and 7.4b. It is seen that profiles from both configurations are quite similar. Such a similarity was also found for the other values of the parameters Ra, Re and φ (results are omitted for brevity), and it was concluded that results from one-wavelength configuration could adequately represent the flow behavior

in a long channel, away from the entrance and outlet regions.

Flow and temperature fields, as functions of the Rayleigh number, for a fixed Reynolds number $Re = 1$, are shown in Fig. 7.6, with streamlines (left) and isotherms (right). When the Rayleigh number is zero (Fig. 7.6a), a parabolic velocity profile is produced with the maximum velocity midway between the walls. The temperature field of that figure is the one obtained for pure forced convection, without any buoyancy effect. With Ra increasing from zero, the velocity is reduced near the top wall and increased near the bottom wall in order to maintain the mass conservation. This change in flow behavior corresponds to the occurrence of a convective cell of infinite extent superposed to the forced flow. Such phenomenon also exists for the case of entirely heated wall for which an analytical solution is given in appendix. The first term on the right hand side of Eq. (B.28) corresponds to that convective cell. This convective cell grows with Ra, and beyond a critical value, an upstream flow is produced near the top wall (Fig. 7.6c). For such conditions, results obtained from the whole channel configuration indicate that a clockwise recirculating flow occurs which extends over the whole channel length from entrance to outlet. Consequently, the upstream flow appearing in Fig. 6c, corresponds to a recirculating flow extending to infinity in both x directions (overall recirculating flow). This overall recirculating flow becomes more pronounced as Ra is increased beyond 250 (Figs. 7.6c to 7.6g). In Fig. 7.6g, the upstream flow is almost equivalent to the downstream flow near the bottom wall and the forced convection contributes in a negligible way to the velocity profile. The effect of localized heating is apparent in Fig. 7.6c to 7.6f, where two-dimensional features are caused by a recirculating flow which does not

extend beyond one wavelength (local recirculating flow).

As it can be expected, the above behavior in the flow field strongly influences the temperature gradients. For the whole set of Figs. 7.6a to 7.6g, the isotherms always intersect the adiabatic boundaries at right angle as they should and the heating elements at an angle that insures the constant heat flux boundary condition. However, it is noticed from the shape of isotherms that, with increasing Ra, the fluid near the top wall become hotter than the fluid near the bottom wall.

The effect of the inclination angle is shown in Fig. 7.7 with Fig. 7.7a corresponding to Fig. 7.6d. It is noticed in Figs 7.7a to 7.7d that the overall recirculating flow remains clockwise (flow reversal near the top wall) but decreases with increasing inclination angle up to $\varphi \simeq 70^0$, while the local recirculating flow remains relatively strong up to $\varphi \simeq 60^0$. At 70^0, the overall recirculating flow is zero. However there exists a local recirculating flow just above the heating element in the counterclockwise direction (Fig. 7.7e). For inclination angles above 70^0, local and overall recirculating flows occur in the counterclockwise direction. This reversal in the direction of the recirculating flows modifies the temperature field, the fluid near the top wall becoming colder than the fluid near the bottom wall.

The overall and local recirculating flows are defined from the following parameter (flow reversal parameter)

$$q_r(X) = -[1 - \Psi_{max} + \Psi_{min}] \qquad (7.14)$$

where Ψ_{max} and Ψ_{min} are respectively the maximum and minimum value of the stream function at a given location X along the wavelength. The flow reversal

parameter is given in Fig. 8 as a function of X for $Ra = 500$, $Re = 1$ and $\varphi = 0^0$, 20^0, 60^0, 70^0, 80^0 and 90^0. Upstream flow near the top and near the bottom are identified by continuous and dashed lines respectively. The overall recirculating flow is given by the minimum value of the flow reversal parameter along the wavelength ($q_{r_{min}}$), whereas the local recirculating flow is given by the difference $q_{r_{max}} - q_{r_{min}}$, $q_{r_{max}}$ being the maximum value of the flow reversal parameter along the wavelength. The flow reversal parameter is X independent for the entirely heated bottom wall, the local recirculating flow being a feature of localized heating on the bottom wall.

Figure 7.9 defines the limit between flow reversal (either overall or local flow reversal) and no flow reversal. It is seen that for the case of entirely heated bottom wall, $A = B$, there is no separate influence of the Reynolds number and this limit corresponds to a fixed critical value of ~ 50 for the coefficient $Ra/(Re^2Pr)$ of Eq. (7.2). The coefficient $Ra/(Re^2Pr) = Fr^{-2}$ (where Fr is a Froude number) expresses the ratio of buoyancy forces to inertia forces. With discrete heating, for instance, with $A = B/2$, the critical value of the coefficient $Ra/(Re^2Pr)$, as obtained numerically, decreases first with Re increasing from zero. When Re increases further, it reaches an asymptotic value of ~ 62.

The variation of the total heat flux along the channel is known a *priori* as it must increases linearly over each heating element by the quantity A and remain constant elsewhere. This behavior can be used to check the local energy balance of the present numerical code. The local quantities Q^*, Q_c and Q, defined as

$$Q^*(X) = -\int_0^1 \frac{\partial T}{\partial X} dY$$

$$Q_c(X) = PrRe \int_0^1 U\theta dY \tag{7.15}$$

$$Q(X) = Q^*(X) + Q_c(X)$$

are the conductive, convective and total heat fluxes respectively. Here we compute Q^* and Q_c separately. When added up, these two quantities must reproduce the known function Q adequately. Also Q increases at each wavelength by the same increment $Q(B) - Q(0) = A$, so that only the difference $\Delta Q(X) = Q(X) - Q(0)$ is relevant within the present framework. Moreover, as the conductive heat flux based on the X derivative of θ repeats integrally at each wavelength, the convective heat flux is also an increasing function of X. Figure 7.10 provides the separate values $\Delta Q^* = Q^*(X) - Q^*(0)$ and $\Delta Q_c = Q_c(X) - Q_c(0)$ as obtained numerically, by solid and light marks respectively. In Fig 7.9a, the effect of Ra is shown from three sets of data corresponding to $Ra = 0$, 500 and 1000, for the same $Re = 1$ and inclination angle $\varphi = 0$. In Fig. 7.10b, the effect of the inclination angle is shown with three sets of data corresponding to $\varphi = 60^0$, 70^0, 80^0 for the same $Re = 1$ and $Ra = 500$. It may be verified in Figs. 7.10a and 7.10b that each pair of curves ΔQ^* and ΔQ_c adds up to reproduce faithfully ΔQ.

7.4 SUMMARY

Fully developed mixed convection taking place within an inclined fluid layer with regularly spaced heating elements on its lower boundary and insulated on its top boundary has been studied numerically. Both a one-wavelength configuration

and a whole channel configuration are explored from which we conclude that the results obtained from the one-wavelength configuration could represent adequately the flow behavior in a long channel, away from the extrance and outlet regions.

The numerical results reveal that the buoyancy effects produce an overall recirculating flow, i.e., a recirculating flow that extends over the whole channel length. This flow is comparable to the one obtained when the bottom wall is entirely heated. Its direction and intensity are related to the Rayleigh number and inclination angle of the channel. A particular feature of discrete heating is the occurrence of local recirculating flow. These local recirculating flows produce the two-dimensional features of the solution.

The heat generated from the heating elements must be carried downstream and the mechanism involved in this process is forced convection. For this process to occur, the temperature must increase at each wavelength by the same increment. As a consequence, the conductive heat transfer is in the upstream direction and must be compensated by the forced convection.

Chapter 8

CONCLUSIONS AND RECOMMENDATIONS

There is a widely accepted need for improved methods of designing efficient thermal packaging systems for electronic components. This need has been accentuated by the rising level of overall power dissipation and by the high packaging density of electronic components. The choice of thermal control technology and the particular decisions made in the course of evolving the thermal packaging design often have far-reaching effects on both the reliability and cost of the electronic system. Despite the availability of many different heat transfer models in electronic package design, direct air cooling of electronic components continues to receive considerable attention due to its lower cost and its environmentally friendly nature.

Irrespective of various configurations of electronic components used in commercial and military equipments, a smooth-walled with fully developed laminar flow channel, that is, the basic channel is paid great attention in the present work, from which the heat transfer problem is explored numerically. The 2-D governing equations expressing the conservation of mass, momentum and energy in such channels are derived with respect to fixed and moving frames. Also the periodicity conditions are applied on the vertical boundaries of the domain to be solved. This domain is then equivalent to a "window" that can be located anywhere along the channel.

The numerical simulation has been performed for several cases: 1^0 mixed convection in a horizontal channel with isothermal or isoflux segments regularly spaced, 2^0 mixed convection in inclined channels with localized heating sources, 3^0 convective heat transfer in channels with moving thermal wave on the boundary. From this comprehensive analytical study it is concluded that:

□ By comparison to a uniformly heated channel for which the cells are carried downstream with a constant velocity for any Reynolds number (or Péclet number), the case with localized heating is more complex. For low enough Péclet number (or Reynolds number), the cells remain attached to the heating elements and a steady state is achieved. Beyond a given threshold value of the Péclect number (or Reynolds number), the cells are carried downstream with a time dependent periodic velocity.

□ Due to the irregular motion of the convective pattern for the localized heating, all other physical variables are characterized by a periodic time dependence. In particular, the overall Nusselt number relative to the upper boundary and the temperature averaged over the fluid layer (which is a measure of the heat energy contained in the fluid) are not in phase and show a strong periodic time dependence. Physically this indicates that the heat produced at a steady rate by the heating elements accumulates within the fluid layer before being released through the upper boundary.

□ The effect of a moving thermal wave imposed as a boundary condition on Bénard cells in a horizontal layer of infinite extent shows that there exists a threshold for the velocity of the thermal wave, below which the Bénard cells

are carried along with the disturbance. The convective cells are attached to the imposed thermal wave so that a steady state may be observed in a reference frame moving with the thermal wave. The threshold depends upon the amplitude δ and upon the Rayleigh number Ra. Above this threshold, no steady state can be obtained and the cells move with a time-averaged velocity lower than the thermal wave. In fact, the flow exhibits an unsteady periodic behavior in which all flow quantities are characterized by a cyclic time dependence. In particular, heat is released by bursts from the fluid layer through the upper boundary.

□ In the case of fully developed opposing mixed convection taking place within an inclined fluid layer with regularly spaced heating elements on the lower boundary while the top boundary is insulated, local and overall recirculating flow are observed to occur in the channel either near the top wall or bottom wall. Those features are obtained both numerically and analytically. The flow reversal parameter is introduced to calculate the intensity of recirculating flow qualitatively. It is found that the recirculating flow is considerably affected by a number of parameters of Rayleigh number, Reynolds number and inclination angle, which is then strongly influence the flow and temperature profiles as well as heat flux distribution.

This kind of idealized channel studied in this work does not exists as much in the complex modules of electronic equipment. However, the present studies provide a broad view of natural and mixed convection in channels with boundary perturbed thermally which may in turn be helpful to understand the cooling mechanism in electronic devices and to manipulating the electronic package design.

Bibliography

[1] HANNEMANN, R., 1990 "Thermal Control for Mini-and Microcomputers: The Limits of Air Cooling", *Heat Transfer in Electronic and Microelectronic Equipment*, pp. 61–82.

[2] BAR-COHEN, A. and KRANS, A. D. 1983 "Thermal Analysis and Control of Electronic Equipment", *Hemisphere Publishing Corporation.*

[3] BAR-COHEN, A. 1979 "Fin Thickness for an Optimized Natural Convection Array of Rectangular Fins", *J. Heat Transfer*, vol. 101, pp. 564–566.

[4] KRAUS, A. D. 1965 "Cooling Electronic Equipment", *Prentice - Hall, Englewood Cliffs, N.J..*

[5] AUNG, W., KESSLER, T. J. and BEITIN, K. I., 1973 "Free Convection Cooling of Electronic Systems", *IEEE Trans. Parts, Hybrids and Packaging*, vol. PHP - 9, no. 2, pp. 75-86.

[6] ELENBAAS, W., 1942 "Heat Dissipation of Parallel Plates by Free Convection", *Physica*, vol. 9, no. 1, pp. 665 - 671.

[7] BODOIA, J. R. and OSTERLE, J. F., 1964 "The Development of Free Convection Between Heated Vertical Plates", *J. Heat Transfer*, vol. 84, pp. 45–44.

[8] AUNG, W., 1972 "Fully Developed Laminar Free Convection Between Vertical Plates Heated Asymmetrically", *Int. Journal of Heat and Mass Transfer*, vol. 15, pp. 1577 - 1580.

[9] AIHARA, T., 1973 "Effects of Inlet Boundary Conditions on Numerical Solutions of Free Convection Between Vertical Plates", *Report of the Institute of High Speed Mechanics, Tohoku Univ., Japan*, vol. 28, pp. 1 - 27.

[10] SIEGEL, R. and NORRIS, R. H., 1957 "Tests of Free Convection in a Partially Enclosed Space Between Two Heated Vertical Plates", *J. Heat Transfer*, vol. 79, pp. 663–673.

[11] AUNG, W., FLETCHER, L. S. and SERNAS, V., 1972 "Developing Laminar Free Convection Between Vertical Flats With Asymmetric Heating", *Int. Journal of Heat and Mass Transfer*, vol. 15, pp. 2293 – 2308.

[12] WIRTZ, R. A. and STUTZMAN, R. J., 1982 "Experiments on Free Convection Between Vertical Plates With Symmetric Heating", *J. Heat Transfer*, vol. 104, pp. 501–507.

[13] MIYATAKE, O. and FUJII, T., 1972 "Free Convective Heat Transfer Between Vertical Parallel Plates - One Plate Isothermally Heated and the Other Thermally Insulated", *Heat Transfer Jan. Res.*, vol. 3, pp. 30–38.

[14] MIYATAKE, O., M. FUJII, M. and TANAKA, H., 1973 "Natural Convection Heat Transfer Between Vertical Parallel Plates - One Plate With a Uniform

Heat Flux and the Other Thermally Insulated", *Heat Transfer Jan. Res.*, vol. 4, pp. 25–33.

[15] DALBERT, A. M., 1982 "Natural Mixed and Forced Convection in a Vertical Channel With Asymmetric Uniform Heating", *Proc. 7th Int. Heat Transfer Conf., Hemisphere Publishing Corp.*, Washington, D.C., vol. 3, pp. 431-434.

[16] SPARROW, E. M., CHRYSLER, G. M. and AZEVEDO, L. F., 1984b "Observed Flow Reversals and Measured-Predicted Nusselt Numbers for Natural Convection in a One-Sided Heated Vertical Channel", *ASME Journal of Heat Transfer*, vol. 106, pp. 325–332.

[17] MIYAMOTO, M., KATOH, Y., KURIMA, M. J. and SASAKI, H., 1986 "Turbulent Free Convection Heat Transfer from Vertical Parallel Plates", *Heat Transfer-1986, Proc. 8th Int. Heat Transfer Conf.*, Hemisphere Publishing Corp., Washington, vol. 4, pp. 1593-1598.

[18] SPARROW, E. M., RAMSEY, J. W. and ALTEMANI, C. A. C., 1980 "Experiments on In-line Pin Fin Arrays and Performance Comparisons With Staggered Arrays", *ASME Journal of Heat Transfer*, vol. 102, pp. 44–50.

[19] BURCH, R., RHODES, T. and ACHARYA, S., 1985 "Laminar Natural Convection Between Finitely Conducting Vertical Plates", *International Journal of Heat and Mass Transfer*, vol. 28, pp. 1173–1186.

[20] BIRNBRIER, H., 1981 "Experimental Investigations on the Temperature Rise of Printed Circuit Boards in Open Cabinets with Natural Ventilation", *Heat Transfer in Electronic Equipment*, M. D. Kelleher and M. M. Yovanovich, eds., ASME HTD-Vol. 20, pp. 19 - 23.

[21] ORTEGA, A. and MOFFAT, R. J., 1985 "Heat Transfer from an Array of Simulated Electronic Components: Experimental Results for Free Convection with and without a Shrouding Wall", *Heat Transfer in Electronic Equipment-1985*, S. Oktay and R. J. Moffat, eds., ASME HTD-Vol. 48, pp. 5-15.

[22] BAKER, E., 1972 "Liquid Cooling of Microelectronic Devices by Free and Forced Convection", *Microelectronics and Reliability*, vol. 11, pp. 213 – 222.

[23] BAKER, E., 1973 "Liquid Immersion Cooling of Small Electronic Devices", *Microelectronics and Reliability*, vol. 12, pp. 163–173.

[24] CAREY, V. P. and MOLLENDORF, J. C., 1977 "The Temperature Field above a Concentrated Heat Source on a Vertical Adiabatic Surface", *International Journal of Heat and Mass Transfer*, vol. 20, pp. 1059–1067.

[25] PARK, K. A. and BERGLES, A. E., 1987 "Natural Convection Heat Transfer Characteristics of Simulated Micrelectronic Chips", *ASME Journal of Heat Transfer*, vol. 109, pp. 90–96.

[26] SPARROW, E. M. and FAGHRI, M., 1980 "Natural Convection Heat from the Upper Plate of a Colinear, Separated Pair of Vertical Plates", *ASME Journal of Heat Transfer*, vol. 102, pp. 623–629.

[27] CHU, H. H. S., CHURCHILL, S. W. and PATTERSON, C. V. S., 1976 "The Effect of Heater Size, Location, Aspect Ratio, and Boundary Conditions on Two-Dimensional, Laminar Natural Convection in Rectangular Channels", *ASME Journal of Heat Transfer*, vol. 98, pp. 194–201.

[28] YAGHOUBI, M. A. and INCROPERA, F. P., 1980 "Analysis of Natural Convection Due to Localized Heating in a Shallow Water Layer", *Numerical Heat Transfer*, vol. 3, pp. 315–330.

[29] TURNER, B. L. and FLACK, R. D., 1980 "Experimental Measurement of Natural Convective Heat Transfer in Rectangular Enclosures with Concentrated Energy Sources", *ASME Journal of Heat Transfer*, vol. 102, pp. 236–241.

[30] FLACK, R. D. and TURNER, B. L., 1980 "Heat Transfer Correlations for Use in Naturally Cooled Enclosures with High-Power Integrated Circuits", *IEEE Trans. on Components, Hybrids and Manufacturing Technology*, CHMT-3, pp. 449–452.

[31] LEE, J. J., LIU, K. V., YANG, K. T. and KELLEHER, M. D., 1987a "Laminar Natural Convection in a Rectangular Enclosure Due to Heated Protrusion of One Vertical Wall – Part ii: Numerical Simulations", *Proceedings of the Second ASME-JSME Thermal Engineering Joint Conference*, P. J. Marto and I. Tranasawa, eds., vol. 2, pp. 179-185.

[32] KELLEHER, M. D., KNOCK, R. H. and YANG, K. T., 1987 "Laminar Natural Convection in a Rectangular Enclosure Due to a Heated Protrusion on One Vertical Wall – Part 1: Experimental Investigation", *Proceedings of the Second ASME - JSME Thermal Engineering Joint Conference*, P. J. Mario and I. Tanasawa, eds., vol. 2, pp. 169-177.

[33] LIU, K. V., YANG, K. T. and KELLEHER, M. D., 1987 "Three-Dimensional Natural Convection Cooling of an Array of Heated Protrusions in an Enclo-

sure Filled with a Dielectric Fluid", *Proceedings of the International Symposium on Cooling Technology for Electronic Equipment*, Honolulu, HI, Mar. 17-21, pp. 486-497.

[34] KENNEDY, K. J. and KANCHL, J., 1983 "Free Convection in Tilted Enclosures", *Heat transfer in Electronic Equipment–1983*, S. Oktay and A. Bar-Cohen, eds., ASME HTD-Vol. 28, pp. 43-47.

[35] AZEVEDO, L. F. A. and SPARROW, E. M., 1985 "Natural Convection in Open-Ended Inclined Channels", *ASME Journal of Heat Transfer*, vol. 107, vol. 893 – 901.

[36] BEJAN, A., 1984 "Convection Heat Transfer", A Wiley - Interscience Publication JOHN WILEY & SONS.

[37] MOHANTY, H. K., 1979 "Unsteady Natural Convection in Horizontal Channels with Arbitrary Wall Temperature", *International Journal of Heat and Mass Transfer*, vol. 22, pp. 383–388.

[38] BUSSE, F. H. and CLEVER, R. M., 1979 "Instabilities of Convection Rolls in a Fluid of Moderate Prandtl Number", *Journal of Fluid Mechanics*, vol. 91, pp. 319–335.

[39] BUSSE, F. H. and RIAHI, N., 1980 "Nonlinear Convection in a Layer with Nearly Insulating Boundaries", *Journal of Fluid Mechanics*, vol. 96, pp. 243–256.

[40] CHAPMAN, C. J. and PROCTOR, M. R. E., 1980 "Nonlinear Rayleigh-Bènard Convection Between Poorly Conducting Boundaries", *Journal of Fluid Mechanics*, vol. 101, pp. 759–782.

[41] SOROUR, M. M., HASSAB, M. A. and ELEWA, F. A., 1985 "Effect of Suction on the Stability of Fluid Between Horizontal Plates at Differing Temperatures", *Proceedings of the Inst. Mech. Engrs.*, Part C., Mech. Engr. Sci. 199(2), 145.

[42] KAVIANY, M., 1984 "Onset of Thermal Convection in a Fluid Layer Subjected to Transient Heating from Below", *Journal of Heat Transfer*, vol. 106, pp. 817.

[43] ROPPO, M., DAVIS, S. and ROSENBLAT, S., 1984 "Bénard Convection with Time-Periodic Heating", *Phys. Fluids*, vol. 27, pp. 796.

[44] CALTAGIRONE, J. P. and BORIES, B., 1985 "Solutions and Stability Criteria of Natural Convective Flow in an Inclined Porous Layer", *Journal of Fluid Mechanics*, vol. 108, pp. 764

[45] ACOSTA, R. and MANERO, E., 1984 "Theoretical and Experimental Study of One and Two-Phase Thermosyphons", *Bachelor's Thesis*, Faculty of Ingenira, U.N.A.M., Mexico.

[46] ROBILLARD, L., WANG, C. H. and VASSEUR, P., 1988 "Multiple Steady State in a Confined Porous Medium with Localized Heating from Below", *Numerical Heat Transfer*, vol. 13, pp. 91–110.

[47] OZISIK, M. N. and HASSAB, M. A., 1979 "Effects of Convective Boundary Conditions on the Stability of Conduction Regime in an Inclined Slender Slot", *Numerical Heat Transfer*, vol. 2, pp. 251.

[48] OZOE, H, YAMAMOTO, K. and CHURCHILL, S. W., 1979 "Three-Dimensional Numerical Analysis of Natural Convection in an Inclined Channel with a Square Cross Section", *A.I.Ch.E. J.*, vol. 25, pp. 709.

[49] INABA, H., 1986 "Natural Convection in an Inclined Rectangular Channel Heated from the Bottom Surface", *Journal of Heat Transfer*, vol. 108, vol. 764.

[50] MASUOKA, T. and SHIMIZU, G., 1986 "Effects of Lateral Walls on the Stability of Natural Convection in an Inclined Fluid Layer", *Nippon Kikai Gakkai Bonbunshu*, B. Hen, 52(475), pp. 1350.

[51] MOUROMTSEFF, I. E., 1942 "water and forced-air cooling of vacuum tubes", *Proc. IRE*, vol. 30, pp. 190-205.

[52] MCADAMS, W. H., 1933 "Heat Transmission", McGraw-Hill, New York.

[53] KRAUS, A. D., 1986 "An Appraisal of Gardner's Pioneering Extended Surface Effort", *Heat Transfer in Electronic Equipment*, ed. A. Bar-Cohen, ASME HTD-Vol. 57, pp. 35-39.

[54] GARDNER, K. A., 1945 "Efficiency of Extended Surfaces", *Trans. ASME*, vol. 67, pp. 621-631.

[55] LONDON, K. A., 1954 "Air-Coolers for High Power Vacuum Tubes", *Trans. IRE, Professional Group on Electron Devices*, vol. ED-1, pp. 9-26.

[56] KAYS, W. M. and LONDON, A. L., 1955 "Compact Heat Exchangers", *National Press, Palo Alto, Calif.*

[57] KOBAYASHI, F., MURATA, S., WATANABE, H., KAWASHIMA, S., ANZAI, A. MURAKAMI, K. and IKUZAKI, K., 1986 "Hardware Technology for m-680/682h", *Nikkei Electronics*, pp. 268-288.

[58] INCROPERA, F. P., KNOX, A. L. and SCHUTT, J. A., 1986 "Onset of Thermally Driven Secondary Flow in Horizontal Rectangular Channels", *Heat Transfer - 1986, C. L. Tien, V. P. Carey, and J. K. Ferrel, eds., Hemisphere, New York*, vol. 3, pp. 1395-1400.

[59] BULLER, M. L. and KILBURN, R. F., 1981 "Evaluation of Surface Heat Transfer Coefficients for Electronic Module Packages", *Heat Transfer in Electronic Equipment*, ASME HTD-Vol. 20, pp. 25 - 28.

[60] SPARROW, E. M., YANEZMORENO, A. A. and OTIS, D. R., 1984a "Convective Heat Transfer Response to Height Differences in an Array of Block-Like Electronic Components", *Int. Journal of Heat and Mass Transfer*, vol. 27, pp. 469–473.

[61] SPARROW, E. M. and OTIS, D. S., 1985 "Ducd Flow Heat Transfer at a Smooth Wall Which Faces a Wall Covered by Protuberances", *Int. Journal of Heat and Mass Transfer*, vol. 28, pp. 1317–1326.

[62] LEHMANN, G. L. and WIRTZ, R. A., 1985 "The Effect of Variations in Streamwise Spacing and Length on Convection from Surface Mounting Rectangular Components", *Heat Transfer in Electronic Equipment-1985*, S. Oktay and R. J. Moffat, eds., ASME HTD-Vol. 48, pp. 39-47.

[63] DAVALATH, J. and BAYAZITOGLU, 1987 "Forced Convection Cooling Across Rectangular Blocks", *ASME Journal of Heat Transfer*, vol. 109, pp. 321–328.

[64] ARVIZU, D. E. and MOFFAT, R. J., 1982 "The Use of Superposition in Calculating Cooling Requirements for Circuit Board Mounted Electronic Components", *IEEE Paper*, No. CH1781 - 4/82-0133.

[65] MOFFAT, R. J., ARVIZU, D. E. and ORTEGA, A., 1985 "Cooling Electronic Components: Forced Convection Experiments with an Air-Cooled Array", *Heat Transfer in Electronic Equipment–1985, S. Oktay and R. J. Moffat eds.*, ASME HTD-Vol. vol. 48, pp. 17-27.

[66] BIEBER, C. R. and SAMMAKIA, B. G., 1986 "Transport from Discrete Heated Components in a Turbulent Channel Flow", *ASME Paper*, No. 86-WA/HT-68.

[67] ASHIWAKE, N., NAKAYAMA, W., DAIKOKU, T. and KOBAYASHI, F., 1983 "Forced Convective Heat Transfer from lsi Packages in an Air-Cooled Wiring Card Array", *Heat Transfer in Electronic Equipment, S. Oktay and A. Bar-Cohen, eds.*, ASME HTD Vol. 28, pp. 35 - 42.

[68] WIRTZ, R. A. and DYKSHOORN, P., 1984 "Heat Transfer from Arrays of Flat Packs in a Channel Flow", *Proceedings Fourth Annual International Electronics Packaging Conference*, pp. 318-326.

[69] SPARROW, E. M. and RAMSEY, J. W., 1978 "Heat Transfer and Pressure Drop for a Staggered Wall-Attached Array of Cylinders with Tip Clearance", *International Journal of Heat and Mass Transfer*, vol. 21, pp. 1369–1377.

[70] VAN FOSSEN, G. J., 1981 "Heat Transfer Coefficients for Staggered Arrays of Short Pin Fins", *ASME Paper* No. 81-GT-75.

[71] SIMONEAU, R. J. and VAN FOSSEN, G. J., 1984 "Effect of Location in an Array on Heat Transfer to a Short Cylinder Crossflow", *ASME Journal of Heat Transfer*, vol. 106, pp. 42–48.

[72] STEUBER, G. D. and METZGER, D. E., 1986 "Heat Transfer and Pressure Loss Performance for Families of Partial Length Pin Fin Arrays in High Aspect Ratio Rectangular Ducts", *Heat Transfer–1986, Proceedings 8th Int. Heat Transfer Conf., Hemisphere Publishing Corp., Washington*, vol. 6, pp. 2915-2920.

[73] LAU, S. C., KIM, Y. S. and HAN, J. C., 1985 "Effects of Fin Configuration and Entrance Length on Local End Wall Heat/Mass Transfer in a Pin Fin Channel", *ASME Paper* No. 85-WA/HT-62.

[74] SPARROW, E. M. and HSU, C. F., 1981 "Analytically Determined Fin-Tip Heat Transfer Coefficients", *ASME Journal of Heat Transfer*, vol. 103, pp. 18–25.

[75] KISHIMOTO, T., SASAKI, E. and MORIYA, K., 1984 "Gas Cooling Enhancement Technology for Integrated Circuit Chips", *IEEE Transactions on Components, Hybrids and Manufacturing Technology*, vol. CHMT-7, pp. 286-293.

[76] YOKONO, Y., SASAKI, T. and ISHIZUKA, M., 1987 "Small Cooling Fin Performances for lsi Packages", *Proceedings of the International Symposium on Cooling Technology for Electronic Equipment*, Honolulu, HI, Mar. 17-21.

[77] SPARROW, E. M., NIETHAMMER, J. E. and CHRYSLER, G. M., 1982 "Heat Transfer and Pressure-Drop Characteristics of Arrays of Rectangular Modules Encountered in Electronic Equipment", *Int. Journal of Heat and Mass Transfer*, vol. 25, pp. 961–973.

[78] HWANG, U. P., 1984 "Thermal Design Turbulators for Air-Cooled Electronic Modules on a Card Package", *National Electronic and Packaging Production Conference, (NEPCON) Conference Proceedings*, pp. 441-449.

[79] GREINER, M., GHADDER, N. K., MIKIC, B. B. and PATERA, A. T., 1986 "Resonant Convective heat transfer in grooved channels", *Heat Transfer 1986, C. L. Tien, V. P. Carey and J. K. Ferrell eds., Hemisphere, New York*, vol. 6, pp. 2867-2872.

[80] KARNIADAKIS, G. E., MIKIC, B. B. and PATERA, A. T., 1987 "Heat Transfer Enhancement by Flow Destabilization: Application to the Cooling of Chips", *Proceedings of the International Symposium on Cooling Technology for Electronic Equipment*, Honolulu, HI, Mar. 17-21, pp. 498-521.

[81] AUNG, W. and WORKU, G., 1986a "Developing Flow and Flow Reversal in a Vertical Channel with Asymmetric Wall Temperatures", *ASME Journal of Heat Transfer*, vol. 108, pp. 299 – 304.

[82] HABCHI, S. and ACHARYA, S., 1986b "Laminar Mixed Convection in a Partially Blocked Vertical Channel", *Int. Journal of Heat and Mass Transfer*, vol. 29, pp. 1711–1722.

[83] AUNG, W. and WORKU, G., 1986b "Theory of Fully Developed Combined Convection Including Flow Reversal", *ASME Journal of Heat Transfer*, vol. 108, pp. 485 – 488.

[84] GILL, W. N. and DEL CASAL, E., 1962 "A Theoretical Investigation of Natural Convection Effects in Forced Horizontal Flows", *A.I.Ch.E. J.*, vol. 8, pp. 513-581.

[85] BECKETT, P. M. and FRIEND, I. E., 1984 "Combined Natural and Forced Convection Between Parallel Walls: Developing Flow at Higher Rayleigh Numbers", *Int. Journal of Heat and Mass Transfer*, vol. 27, pp. 611–621.

[86] OSBORNE, D. G. and INCROPERA, F. P., 1985a "Laminar Mixed Convection Heat Transfer for Flow Between Horizontal Parallel Plates with Asymmetric Heating", *Int. Journal of Heat and Mass Transfer*, vol. 28, pp. 207–217.

[87] OSBORNE, D. G. and INCROPERA, F. P., 1985b "Experimental Study of Mixed Convection Heat Transfer for Transitional and Turbulent Flow Between Horizontal Parallel Plates", *Int. Journal of Heat and Mass Transfer*, vol. 28, pp. 1337–1344.

[88] INCROPERA, F. P. and SCHUTT, J. A., 1985 "Numerical Simulation of Laminar Mixed Convection in the Entrance Region of Horizontal Rectangular Ducts", *Numerical Heat Transfer*, vol. 8, pp. 707–729.

[89] INCROPERA, F. P., KNOX, A. L. and MAUGHAN, J. R., 1987 "Mixed Convection Flow and Heat Transfer in the Entry Region of Horizontal Rectangular Duct", *ASME Journal of Heat Transfer*, vol. 109, pp. 434–439.

[90] MAUGHAN, J. R. and INCROPERA, F. P., 1987 "Experiments on Mixed Convection Heat Transfer for Air flow in a Horizontal Inclined Channel", *Int. Journal of Heat and Mass Transfer*, vol. 30, pp. 1307–1318.

[91] OUAZZANI, M. T., CALTAGIRONE, J. P., MEYER, G. and MOJTABI, A., 1981 "Étude Numérique et Expérimentale de la Convection Mixed Entre Deux Plans Horizontaux à Température Différentes", *Int. Journal of Heat and Mass Transfer*, vol. 32, pp. 261–269.

[92] PLATTEN et al. "On the Existence of Thermoconvective Rolls, Transverse to a Superimposed Mean Poiseuille Flow", *Int. Journal of Heat and Mass Transfer*, vol. 24, pp. 1287–1291.

[93] FUKUI, K., NAKAJIMA, N. and UEDA, H., 1983 "The Longitudinal Vortex and its Effects on the Transport Processes in Combined Free and Forced Laminar Convection Between Horizontal and Inclined Parallel Plates", *Int. Journal of Heat and Mass Transfer*, vol. 26, pp. 109–120.

[94] KENNEDY, K. J. and ZEBIB, A., 1982 "Combined Forced and Free Convection Between Parallel Plates", *Proc. 7th International Heat Transfer Conference, Hemisphere, New-York*, paper 82-IHTC-152.

[95] TOMIMURA, T. and FUJII, M., 1987 "Laminar Mixed Convection Heat Transfer Between Parallel Plates with Localized Heat Sources", *Proceedings of International Symposium of Cooling Technology for Electronic Equipment*, Honolulu, March 17-21, pp. 233-247.

[96] HASNAOUI, M., BILGEN, E., VASSEUR, P. and ROBILLARD, L., 1991 "Mixed Convective Heat Transfer in a Horizontal Channel Heated Periodically From Below", *Numerical Heat Transfer*, vol. 20, pp. 297–315.

[97] KELLY, R. E. and PAL, D., 1978 "Thermal Convection with Spatially Periodic Boundary Conditions: Resonant Wavelength Excitation", *J. of Fluid Mech.*, vol. 86, pp. 433–456.

[98] ROACHE, P. J., 1980 "Numerical Heat Transfer and Fluid Flow", *Hemisphere Publishing Corporation.*

[99] PHILLIPS, W. R. C., 1988 "The Generalized Lagrangian Mean Equations and Stream Wise Vortices, Near Wall Turbulence", *Ed. S. Kline, Hemisphere.*

[100] PATANKAR, S. V., 1980 "Numerical Heat Transfer and Fluid Flow", *Hemisphere, New York.*

[101] GHIA, U., GHIA, K. N. and SHIN, C. T., 1982 "High-Re Solutions for Incompressible Flow Using the Navier-Stokes Equations and a Multigrid Method", *Journal of Computational Physics*, vol. 48, pp. 387–411.

[102] DAVIS, G. DE. VAHL, 1983 "Natural Convection of Air in a Square Cavity: A Bench Mark Solution", *Int. Journal for Numerical Methods in Fluids*, vol. 3, pp. 249–264.

[103] EVANS, G. and GREIF, R., 1989 "A Study of Traveling Wave Instabilities in a Horizontal Channel Flow with Applications to Chemical Vapor Deposition", *Int. Journal of Heat and Mass Transfer*, vol. 52, pp. 895–911.

[104] PRASAD, V., LAI, F. C. and KULACKI, F. A., 1986 "Mixed Convection in Horizontal Porous Layers Heated from Below", *ASME 86-HT-16*, pp. 1-11.

[105] SCHUBERT, G. and WHITEHEAD, J. A., 1969 "The Moving Flame Experiment with Liquid Mercury: Possible Implications for the Venus Atmosphere", *Science*, vol. 163, pp. 71-72.

[106] HINCH, E. J. and SCHUBERT, G., 1971 "Strong Streaming Induced by a Moving Thermal Wave", *J. of Fluid Mechanics*, vol. 47, pp. 291–304.

[107] WHITEHEAD, J. A., 1972 "Observations of Rapid Mean Flow Produced in Mercury by a Moving Heater", *Geophysical Fluid Dynamics*, vol. 3, pp. 161-180.

[108] BUSSE, F. H., 1972 "On the Mean Flow Induced by a Thermal Wave", *Journal of Atmospheric Sciences*, vol. 29, pp. 1423–1429.

[109] YOUNG, R. E., SCHUKERT, G. and TORRANCE, K. E., 1972 "Nonlinear Motions Induced by Moving Thermal Waves", *J. Fluid Mechanics*, vol. 54, pp. 163–187.

[110] KELLY, R. E. and PAL, D., 1976 "Thermal Convection Induced Between Non-Uniformly Heated Horizontal Surfaces", *Proceedings of Heat Transfer and Fluid Mechanics Institute*, pp. 433-456.

[111] KELLY, R. E. and PEARLSTEIN, A. J., 1985 "Local Resonance in Thermal Convection", *ASME*, HTD-Vol. 54, pp. 77-90.

[112] CHEN, M. and WHITEHEAD, J. A., 1968 "Evolution of Two-Dimensional Periodic Rayleigh Convection Cells of Arbitrary Wave-Number", *J. of Fluid Mechanics*, vol. 31, pp. 1–15.

[113] POCHEAU, A. and CROQUETTE, V., 1984 "Dislocation Motion: A Wavenumbers Selection Mechanism in Rayleigh-Bénard Convection", *J. Phys. (Paris)*, vol. 45, pp. 35–48.

[114] SEGEL, L. A., 1964 "Non-linear Hydrodynamic Stability Theory and its Applications to Thermal Convection and Curved Flows, in Non-Equilibrium Thermodynamics Variational Techniques and Stability", *Ed. R. J. Donnelly, R. Herman and I. Prigogine, University of Chicago Press.*

[115] BUELL, J. C. and CATTON, Y., 1986b "Wavenumber Selection in Large-Amplitude Axisymmetric Convection", *Phys. Fluids*, vol. 29, pp. 23–30.

[116] BUELL, J. C. and CATTON, Y., 1986b "Wavenumber Selection in Ramped Rayleigh-Bénard Convection", *J. Fluid Mech.*, vol. 171, pp. 477–494.

[117] OSTRACH, S. and KAMOTANI, Y., 1975 "Heat Transfer Augmentation in Laminar Fully Developed Channel Flow by Means of Heating from Below", *J. of Heat Transfer*, vol. 1, pp. 220–225.

[118] MALKUS, W. V. R. and VERONIS, G., 1958 "Finite Amplitude Cellular Convection", *J. of Fluid Mechanics*, vol. 4, pp. 225–260.

[119] EHRHARD, P. and MULLER, V., 1990 "Dynamic Behavior of Natural Convection in a Single-Phase Loop", *J. Fluid Mech.*, vol. 217, pp. 487-518.

[120] NIELD, D. A. and BEJAN, A., 1992 "Internal Natural Convection: Heating from the Side", *Convection in Porous Media*, Chap. 7, pp. 251-258, Springer-Verlag.

[121] LAVINE, A. S., 1987 "Analysis of Fully Developed Opposing Mixed Convection Between Inclined Parallel Plates", *Mixed Convection Heat Transfer - 1987*, ASME HTD-Vol. 84, pp. 29-35.

[122] LAVINE, A. S., 1988 "Analysis of Fully Developed Aiding Mixed Convection Between Inclined Parallel Plates", *ASME Proceedings of the 1988 National Heat Transfer Conference*, ASME HTD-96, vol. 2, pp. 87-94.

[123] LAVINE, A. S. et al., 1989 "Flow Reversal in Opposing Mixed Convection Flow in Inclined Pipes", *Journal of Heat Transfer*, vol. 111, pp. 114-120.

[124] BEJAN, A. and TIEN, C. L., 1978 "Laminar Natural Convection Heat Transfer in a Horizontal Cavity With Different End Temperatures", *J. of Heat Transfer*, vol. 100, pp. 641–647.

[125] VASSEUR, P., ROBILLARD, L. and M., 1987 "Unicellular Convective Motion in an Inclined Fluid Layer with Uniform Heat Flux", *J. Heat Mass Transfer*, vol. 30, pp. 2096–2102.

[126] YÜCEL, C., HASNAOUI, M., ROBILLARD, L. and BILGEN, E., 1993 "Mixed Convection Heat Transfer in Open Ended Inclined Channels with Discrete Isothermal Heating", *Numerical Heat Transfer*, vol. 24, pp. 109–126.

[127] BERGLES, A. E., 1990 "Heat Transfer in Electronic and Microelectronic Equipment", *Hemisphere Publishing Corporation.*

Appendix A

MATRIX PARTITION PROCEDURE

Suppose we have a set of algebric equation presented by a matrix as

$$\begin{bmatrix} A & B \\ C & D \end{bmatrix}_{m\times m} \begin{bmatrix} E_1 \\ E_2 \end{bmatrix}_{m\times 1} = \begin{bmatrix} F_1 \\ F_2 \end{bmatrix}_{m\times 1} \tag{A.1}$$

where

$$[A] = \begin{bmatrix} a_{1,1} & a_{1,2} & \cdots & a_{1,m-1} \\ a_{2,1} & a_{2,2} & & \\ \vdots & & & \\ a_{m-1,1} & a_{m-2,1} & \cdots & a_{m-1,m-1} \end{bmatrix}_{m-1\times m-1}$$

$$[B] = [a_{1,m}\ a_{2,m}\ \cdots\ a_{m-1,m}]^T$$

$$[C] = [a_{m,1}\ a_{m,2}\ \cdots\ a_{m,m-1}]$$

$$[D] = [a_{m,m}]$$

$$[E_1] = [X_1\ X_2\ \cdots\ X_{m-1}]^T$$

$$[E_2] = [X_m]$$

$$[F_1] = [b_1\ b_2\ \cdots\ b_{m-1}]^T$$

$$[F_2] = [b_m]$$

Setting

$$\begin{cases} [E_1] = [E_1^+] + [E_1^-] \\ [E_2] = [E_2^+] + [E_2^-] \end{cases}$$

we obtain two equations described by

$$[A][E_1^+] + [A][E_1^-] + [B][E_2^+] + [B][E_2^-] = [F_1] \tag{A.2}$$

$$[C][E_1^+] + [C][E_1^-] + [D][E_2^+] + [D][E_2^-] = [F_2] \tag{A.3}$$

By setting $[E_2^-] = 0$ and $[A][E_1^+] = [F_1]$, from Eq. (A.2), we then have $[A][E_1^-] = -[B][E_2^+]$. Let $[E_1^*] = -[E_1^-][E_2^+]^{-1}$, we obtain the relationships $[A][E_1^*] = [B]$ and $[E_1^*] = [A]^{-1}[B]$. The Eq. (A.3) becomes

$$[C][E_1^+] - [C][E_1^*][E_2^+] + [D][E_2^+] = [F_2] \tag{A.4}$$

Setting $[D] - [C][E_1^*] = G$, we have $[E_2^+] = \frac{1}{G}([F_2] - [C][E_1^+])$ and $[E_1^-] = -[E_1^*][E_2^+]$, consequently

$$\begin{bmatrix} E_1 \\ \\ E_2 \end{bmatrix} = \begin{bmatrix} E_1^+ \\ \\ E_2^+ \end{bmatrix} + \begin{bmatrix} E_1^- \\ \\ 0 \end{bmatrix} \tag{A.5}$$

where

$$\begin{aligned} [E_1^+] &= [A]^{-1}[F_1] \\ [E_2^+] &= \frac{1}{G}([F_2] - [C][E_1^+]) \\ [E_1^-] &= -[A]^{-1}[B][E_2^+] \end{aligned}$$

Appendix B

ANALYTICAL PROCEDURE OF MIXED CONVECTION IN AN ENTIRELY HEATED CHANNEL

The mixed convection in an inclined channel entirely heated from the bottom wall and insulated on the top wall can be characterized by dimensionless governing equations expressing the conservation of mass, energy and momentum:

$$\frac{\partial \theta}{\partial \tau} + \frac{\partial U\theta}{\partial X} + \frac{\partial V\theta}{\partial Y} = \frac{1}{PrRe}\nabla^2\theta \tag{B.1}$$

$$\frac{\partial \Omega}{\partial \tau} + \frac{\partial U\Omega}{\partial X} + \frac{\partial V\Omega}{\partial Y} = \frac{1}{Re}\nabla^2\Omega + \frac{Ra}{PrRe^2}[\frac{\partial \theta}{\partial X}\cos\varphi + \frac{\partial \theta}{\partial Y}\sin\varphi] \tag{B.2}$$

$$\Omega = -\nabla^2\Psi \tag{B.3}$$

$$U = \frac{\partial \Psi}{\partial Y}, \qquad V = -\frac{\partial \Psi}{\partial X} \tag{B.4}$$

Assuming that the flow is characterized by parallel streamlines and by a constant temperature gradient in the X direction, we take

$$U = U(Y), \quad V = 0 \tag{B.5}$$

and

$$\theta = CX + \Phi(Y) + \theta_r \tag{B.6}$$

where C is a constant temperature gradient in X direction which is determined on the basis of energy balance, and θ_r is a reference temperature that can be set to zero without loss of generality. Similar approaches have been used by Bejan and Tien [124], Vasseur, Robillard and Sen [125] and Lavine [121], [122]. By these assumption, the dimensionless governing equations (B.1) - (B.4) become

$$CU = \frac{1}{PrRe}\Phi'' \tag{B.7}$$

$$U''' = \frac{Ra}{PrRe}(C\cos\varphi + \Phi'\sin\varphi) \tag{B.8}$$

$$\int_0^1 U dY = 1 \tag{B.9}$$

$$U(0) = U(1) = 0, \quad \Phi'(0) = -1, \quad \Phi'(1) = 0 \tag{B.10}$$

Integrating Eq. (B.7) over the channel cross-section, and making use of boundary condition Eqs. (B.9) and (B.10), it may be readily deduced that

$$C = \frac{1}{PrRe} \tag{B.11}$$

$$\Phi'' = U \tag{B.12}$$

Differentiating Eq. (B.8) with respect to Y and making use of Eq. (B.12) yields

$$\frac{d^4U}{dY^4} = (\frac{Ra}{PrRe}\sin\varphi)U \tag{B.13}$$

There exists two possible solutions for the above equation (B.13) corresponding to a specific range of the inclination angle.

1^0 $0 < \varphi < \pi$ (downward forced flow)

Setting $M = P_1^{1/4}$ and $P_1 = \dfrac{Ra}{PrRe}\sin\varphi$, the solution of Eq. (B.13) leads to

$$U = C_1\sinh(MY) + C_2\sin(MY) + C_3\cosh(MY) + C_4\cos(MY) \tag{B.14}$$

where C_1, C_2, C_3 and C_4 are constants to be determined by boundary conditions. Substituting Eq. (B.14) into Eq. (B.12), we have

$$\begin{aligned}\Phi = \ & \frac{C_1}{M_2}\sinh(MY) - \frac{C_2}{M^2}\cosh(MY) + \frac{C_3}{M^2}\cosh(MY) \\ & -\frac{C_4}{M^2}\cos(MY) + C_5 Y\end{aligned} \tag{B.15}$$

Defining parameter $P_2 = \dfrac{Ra}{Re^2Pr^2}\cos\varphi$, Eq. (B.8) becomes

$$U''' = P_2 + P_1\Phi \tag{B.16}$$

Substituting Eqs. (B.14) and (B.15) into Eq. (B.16), we have $C_5 = -\dfrac{P_2}{P_1}$. Using boundary conditions $U(0) = 0$ and $\Phi'(0) = -1$, we have $C_3 = -C_4$, and $C_2 = C_1 + (1 - \dfrac{P_2}{P_1})M$, consequently the velocity and temperature field become

$$\begin{aligned}U \ = \ & C_1[\sinh(MY) + \sin(MY)] + C_3[\cosh(MY) - \cos(MY)] \\ & + M(1 - \frac{P_2}{P_1})\sin(MY)\end{aligned} \tag{B.17}$$

$$\begin{aligned}\Phi \ = \ & \frac{1}{M^2}\{C_1[\sinh(MY) - \sin(MY)] + C_3[\cosh(MY) + \cos(MY)] \\ & - M(1 - \frac{P_2}{P_1})\sin(MY)\} - \frac{P_2}{P_1}Y\end{aligned} \tag{B.18}$$

The constants C_1 and C_3 can be determined by using boundary conditions $U(1) =$

0 and $\Phi'(1) = 0$

$$C_1 = \frac{\begin{vmatrix} -M(1-\frac{P_2}{P_1})\sin(M) & \cosh(M)-\cos(M) \\ \frac{P_2}{P_1}M + M(1-\frac{P_2}{P_1})\cos(M) & \sinh(M)-\sin(M) \end{vmatrix}}{\begin{vmatrix} \sinh(M)+\sin(M) & \cosh(M)-\cos(M) \\ \cosh(M)-\cos(M) & \sinh(M)-\sin(M) \end{vmatrix}} \tag{B.19}$$

$$C_3 = \frac{\begin{vmatrix} \sinh(M)+\sin(M) & -M(1-\frac{P_2}{P_1})\sin(M) \\ \cosh(M)-\cos(M) & \frac{P_2}{P_1}M + M(1-\frac{P_2}{P_1})\cos(M) \end{vmatrix}}{\begin{vmatrix} \sinh(M)+\sin(M) & \cosh(M)-\cos(M) \\ \cosh(M)-\cos(M) & \sinh(M)-\sin(M) \end{vmatrix}} \tag{B.20}$$

$2^0 \quad -\pi < \varphi < 0$ (upward forced flow)

In a similar procedure as the above specified inclination angle range, the velocity and temperature distribution in this case can readily be obtained as

$$\begin{aligned} U &= A_2[\cos(NY)\sinh(NY)+\sin(NY)\cosh(NY)] + A_4\sin(NY)\sinh(NY) \\ &\quad +2N(1-\frac{P_2}{P_1})\sin(NY)\cosh(NY) \end{aligned} \tag{B.21}$$

$$\Phi = \frac{1}{2N^2}A_2[\cosh(NY)\sin(NY) - \sinh(NY)\cos(NY)] - \frac{1}{2N^2}A_4\cosh(NY)\cos(NY) - \frac{1}{N}(1-\frac{P_2}{P_1})\sinh(NY)\cos(NY) - \frac{P_2}{P_1}Y \quad \text{(B.22)}$$

with $N = (-P_1/4)^{1/4}$

The constants A_2 and A_4 are specified according to boundary conditions, $U(1) = 0$ and $\Phi'(1) = 0$

$$A_2 = \frac{2N}{\sin^2 N - \sinh^2 N}[(1-\frac{P_2}{P_1})\sin^2 N + \frac{P_2}{P_1}\sin(N)\sinh(N)] \quad \text{(B.23)}$$

$$A_4 = \frac{2N}{\sin^2 N - \sinh^2 N}\{-(1-\frac{P_2}{P_1})[\sin(N)\cos(N) + \sinh(N)\cosh(N)] - \frac{P_2}{P_1}[\sin(N)\cosh(N) + \cos(N)\sinh(N)]\} \quad \text{(B.24)}$$

In the limit case of a horizontal channel, $\varphi = 0$, the dimensionless governing equations become

$$CU = \frac{1}{PrRe}\Phi'' \quad \text{(B.25)}$$

$$U''' = \frac{Ra}{PrRe}C \quad \text{(B.26)}$$

By making use of Eq. (B.11), the (B.27) then becomes

$$U''' = \frac{Ra}{Pr^2Re^2} \quad \text{(B.27)}$$

which leads to the following solution by exploying boundary conditions $U(0) = U(1) = 0$, $\int_0^1 UdY = 1$

$$U = \frac{Ra}{12Re^2Pr^2}(2Y^3 - 3Y^2 + Y) - 6(Y^2 - Y) \quad \text{(B.28)}$$

Also from Eq. (B.25) and related boundary contions $\Phi'(0) = -1$ and $\Phi'(1) = 0$, the temperature distribution can be easily obtained as

$$\Phi = \frac{Ra}{24Re^2Pr^2}\left(\frac{Y^5}{5} - \frac{Y^4}{2} + \frac{Y^3}{3}\right) - \frac{Y^4}{2} + Y^3 - Y \tag{B.29}$$

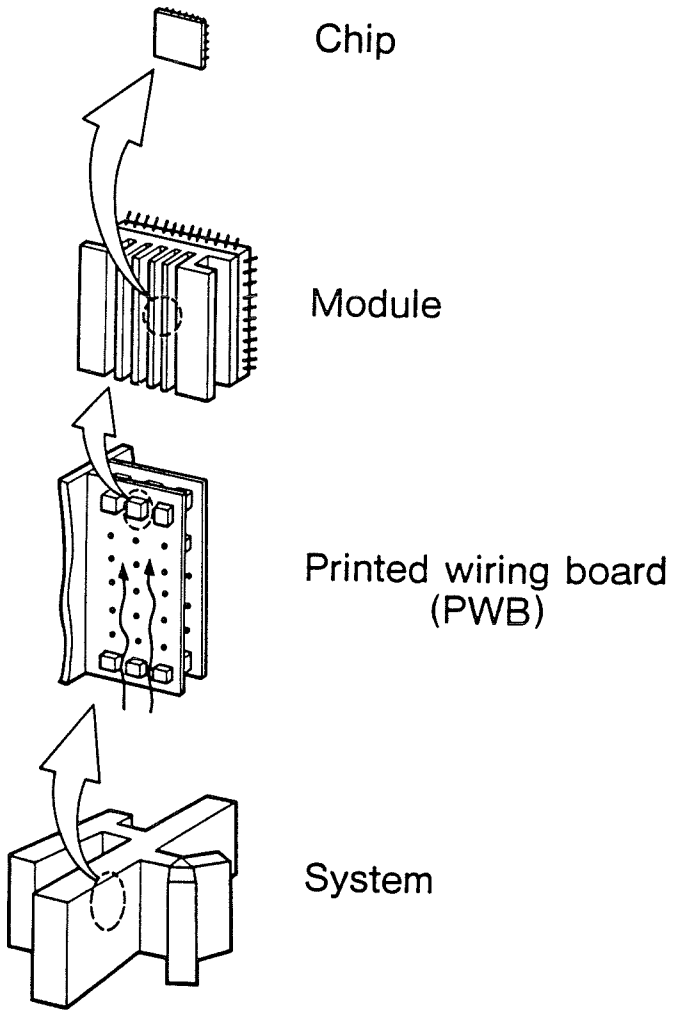

Fig. 1.1 Structural levels of an electronic computer [127]

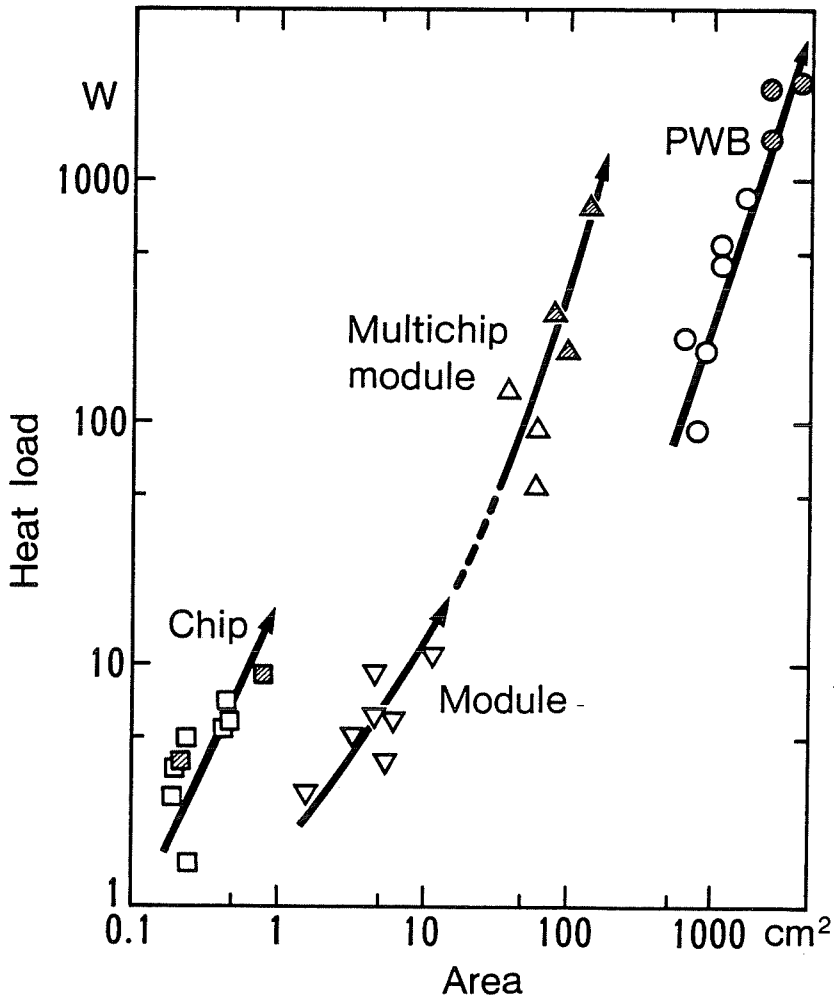

Fig. 1.2 Heat load on chips, modules and PWBs (printed wiring boards) levels of mainframe computers (shaded symbol=indirect water-cooled machine, open symbol=air-cooled machine) [127]

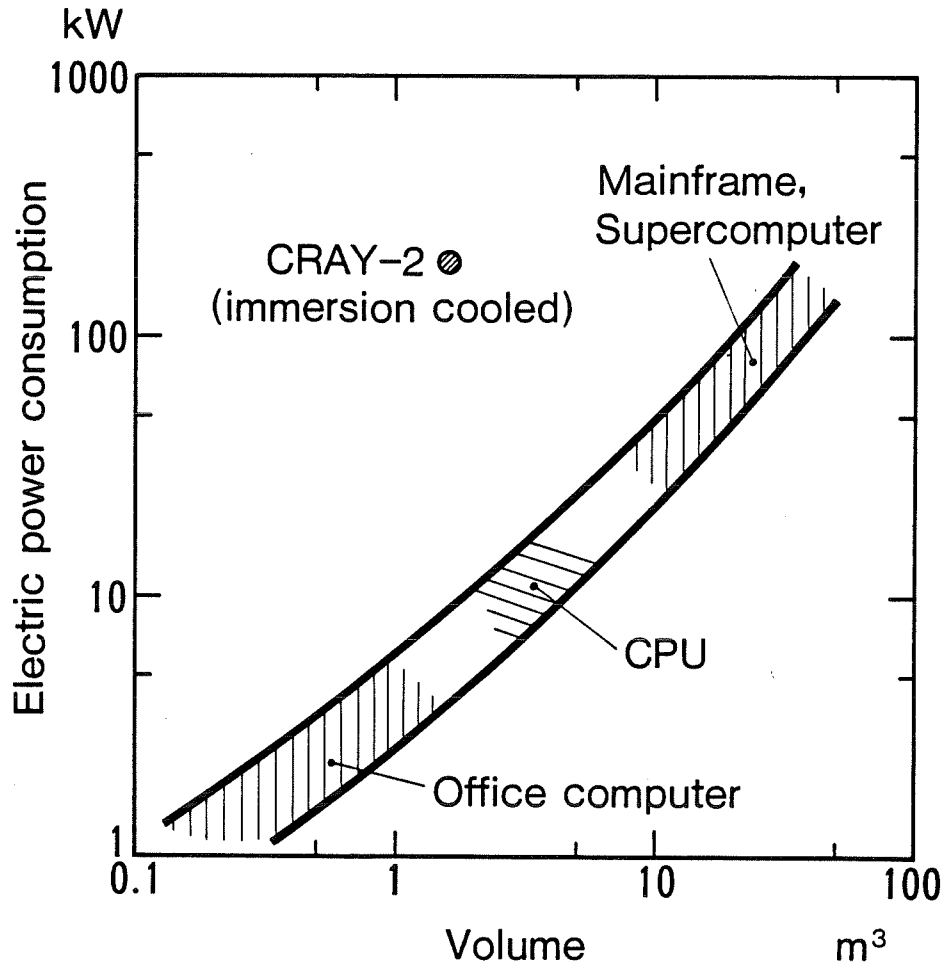

Fig. 1.3 Electric power consumption function of the computer volume [127]

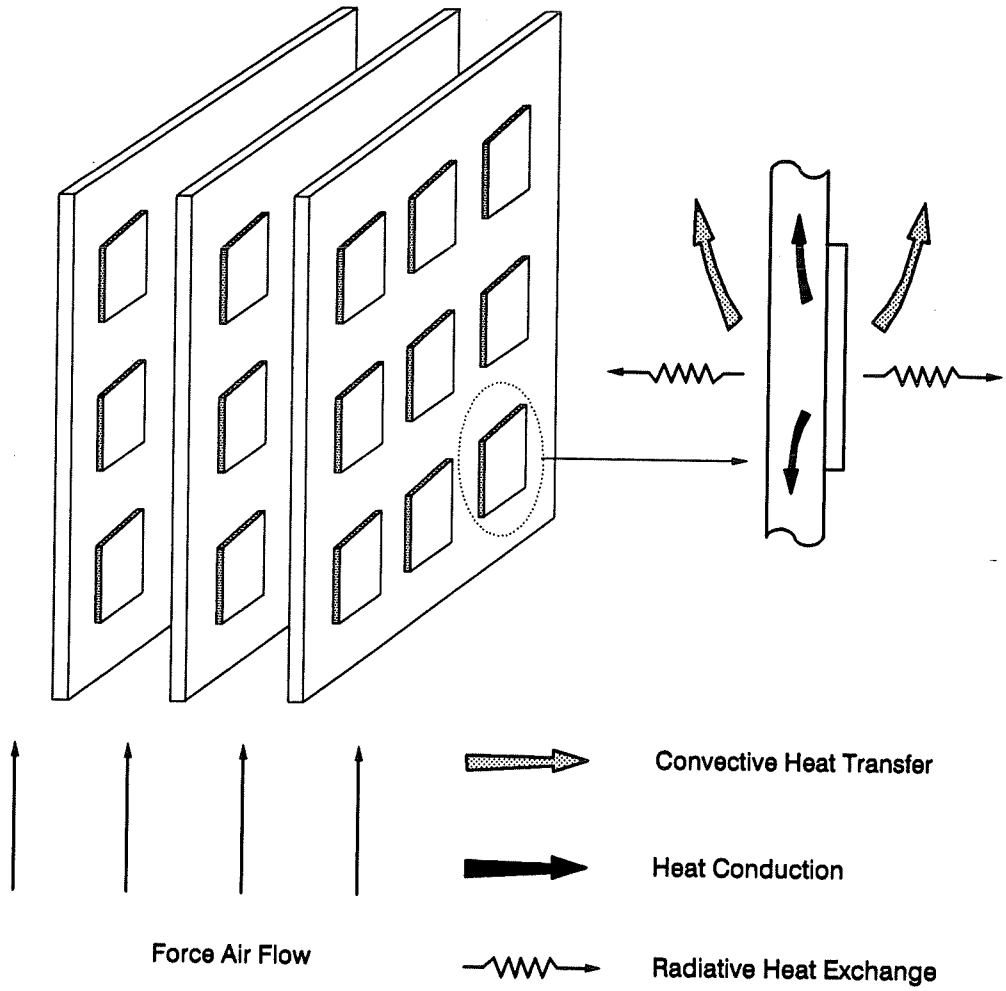

Fig. 1.4 Printed circuit board shown with schematic of thermal dissipation from heat sources

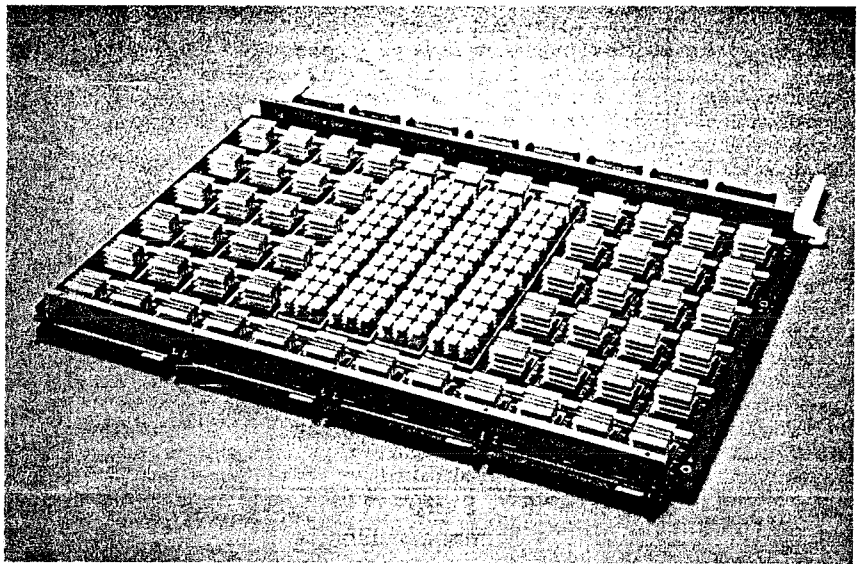

Fig. 1.5 Array of logic modules and memory modules on printed wiring board (PWB)

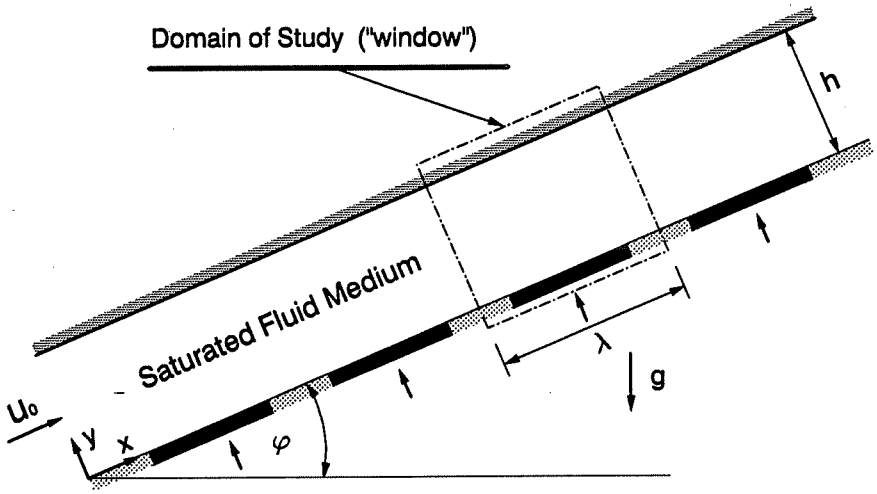

Fig. 2.1 Geometry of the problem

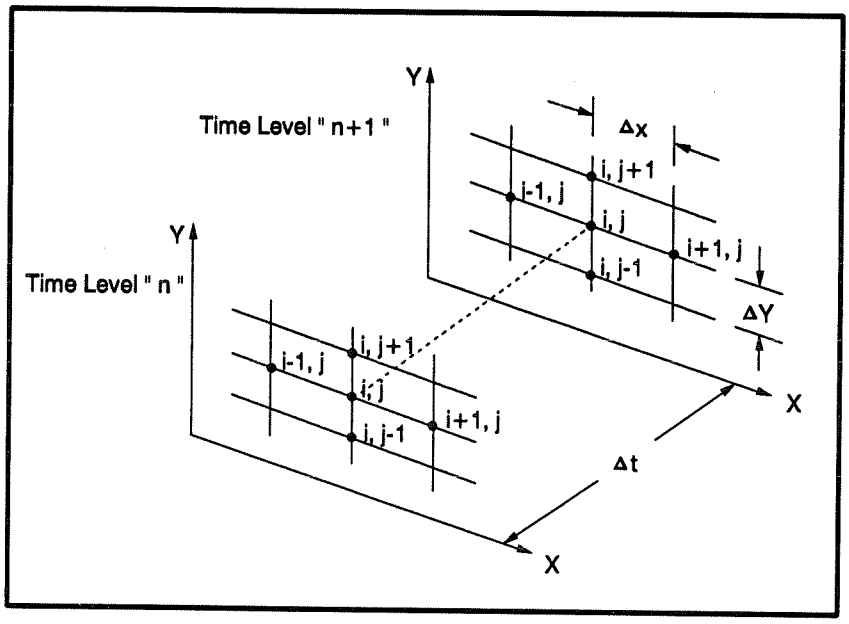

Fig. 3.1 Computational grid system

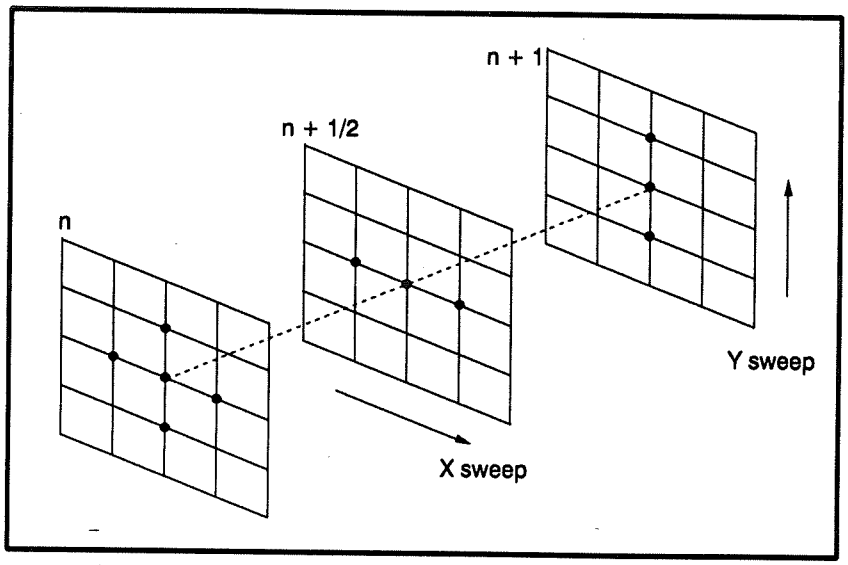

Fig. 3.2 Illustration of the grid system for the ADI method

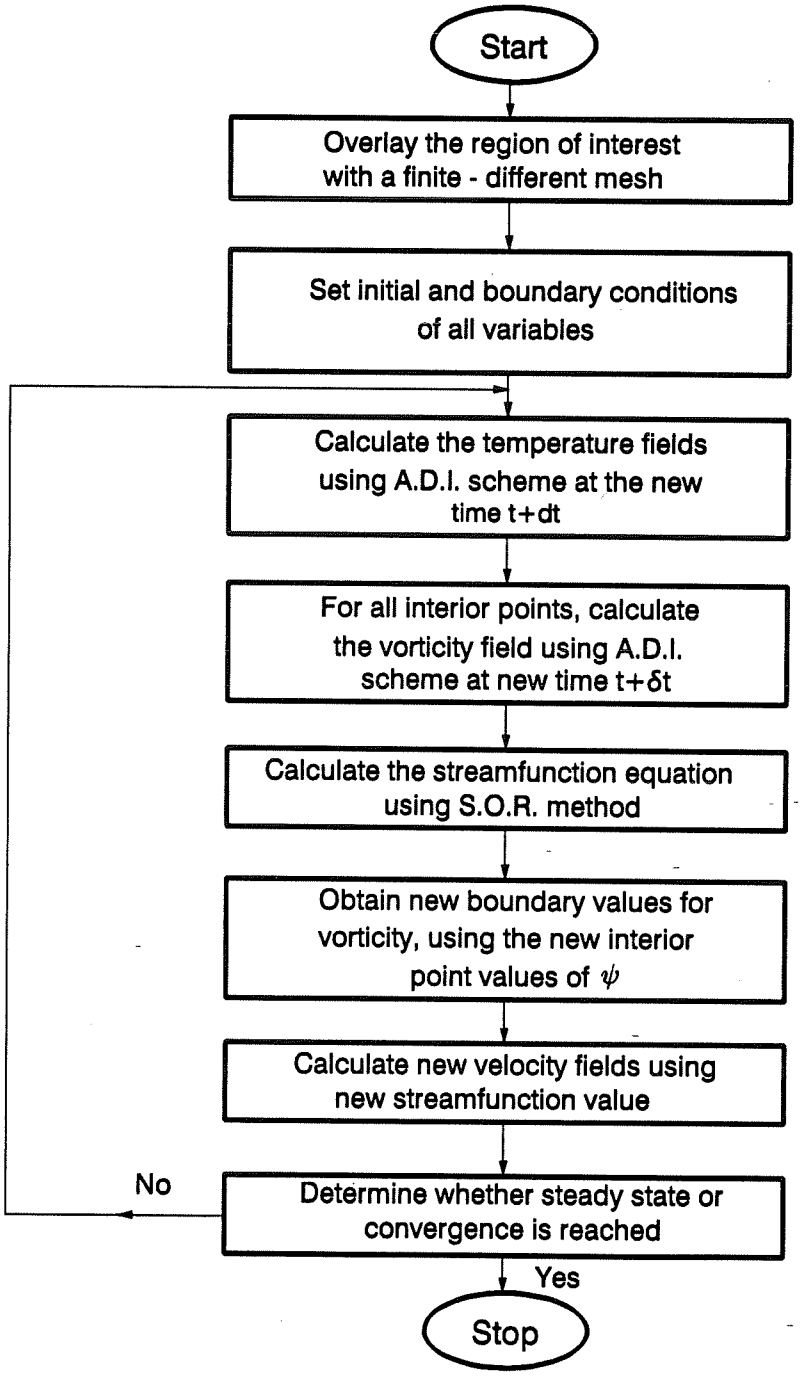

Fig. 3.3 Flow chart

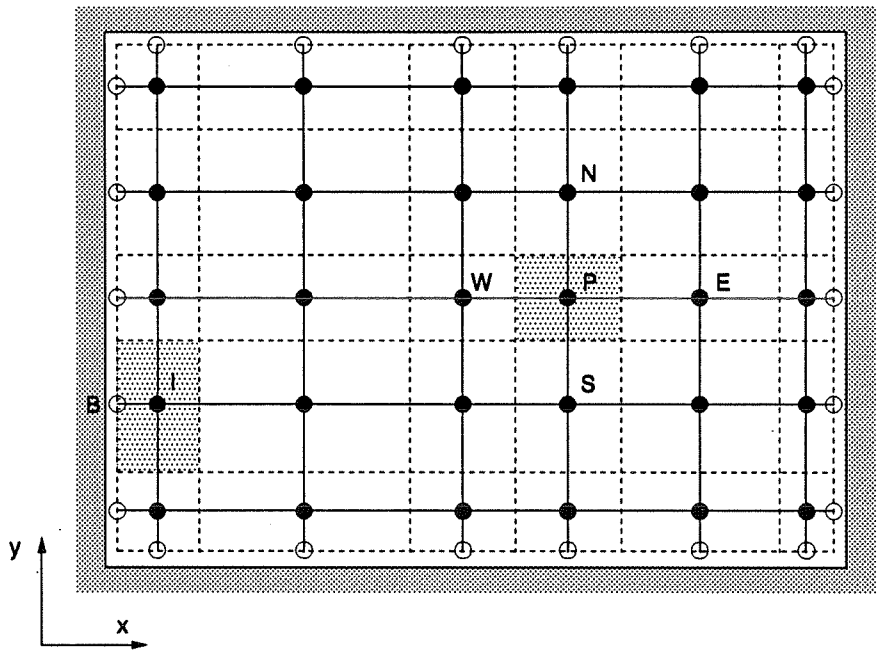

Fig. 3.4 Grids and control volumes

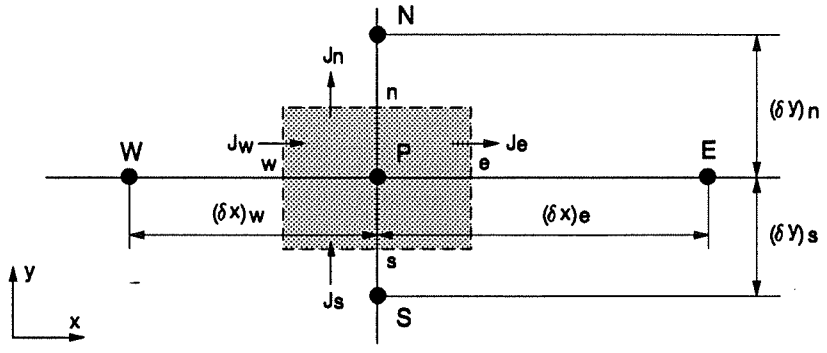

Fig. 3.5 A typical control volume

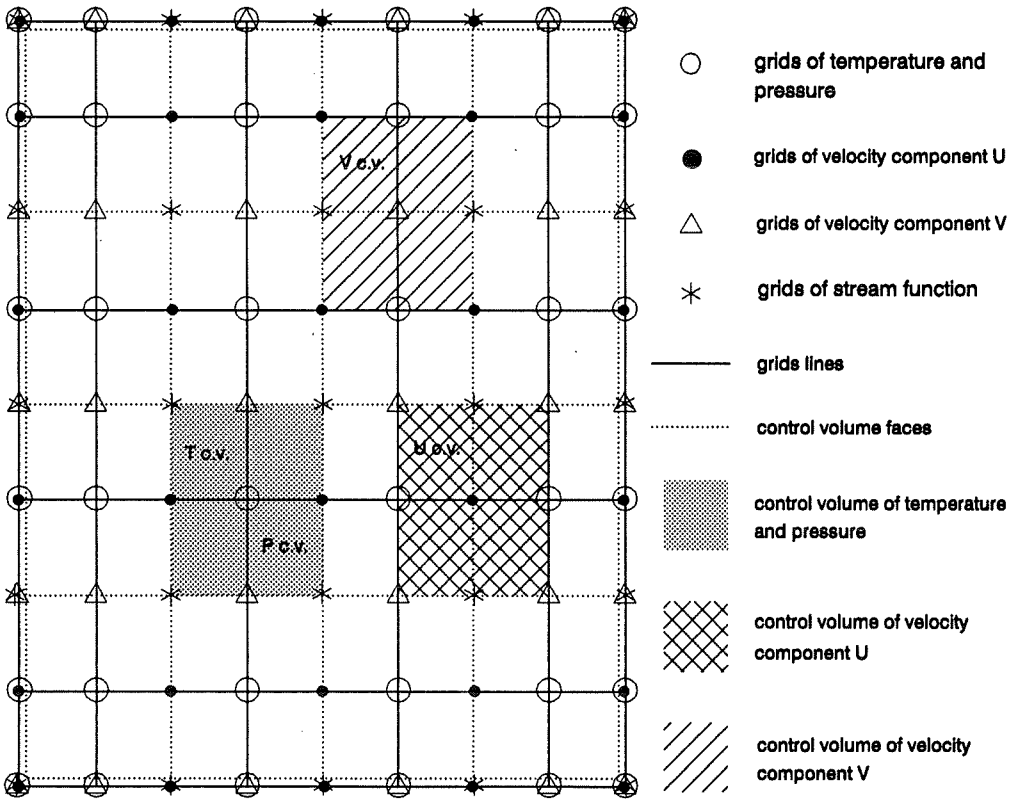

Fig. 3.6 Configuration of control volume and grid distribution

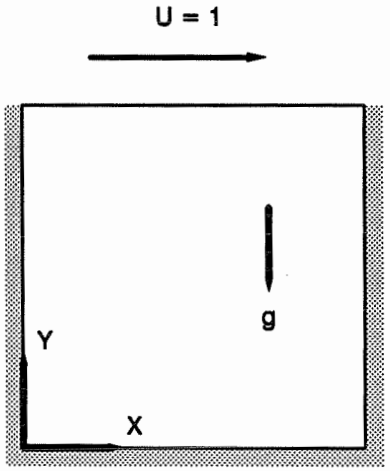

Fig. 4.1 Configuration of driven-cavity flow

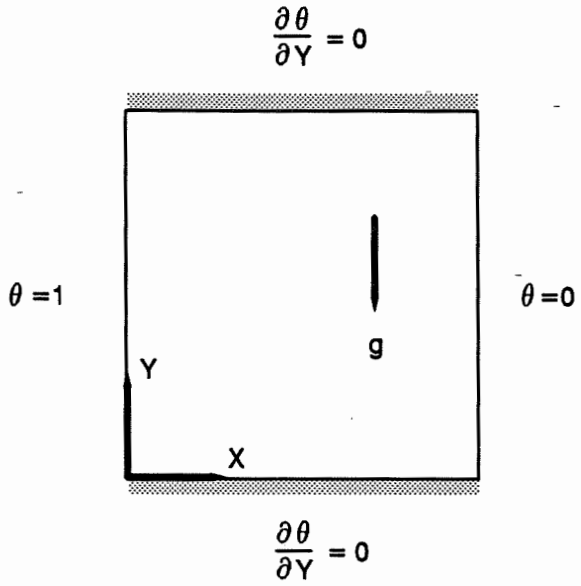

Fig. 4.4 Configuration of natural convection in a square cavity

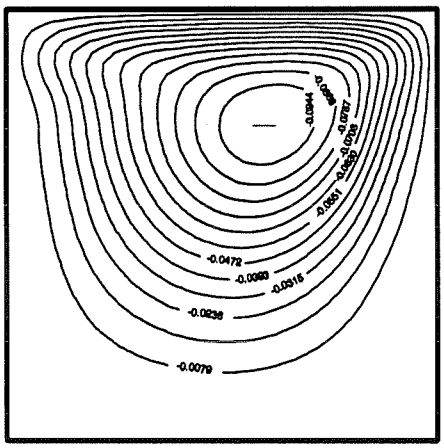

Re = 100

ψ_{min} =-0.1146

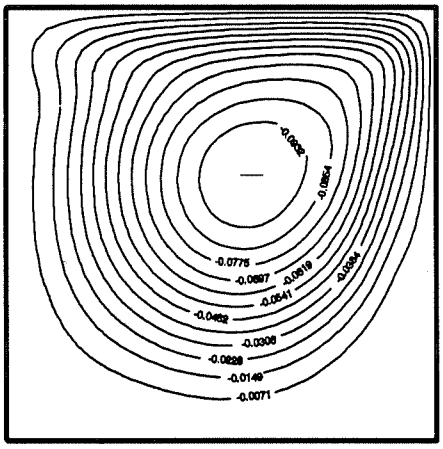

Re = 400

ψ_{min} =-0.1106

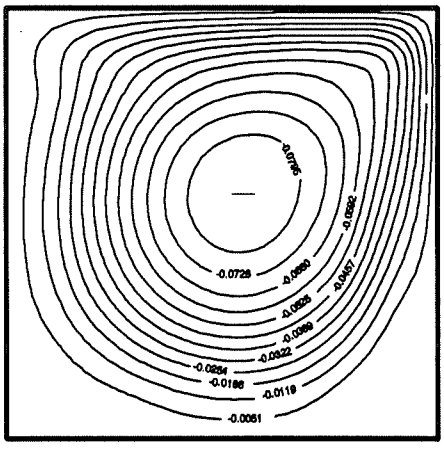

Re = 1000

ψ_{min} =-0.0951

Fig. 4.2 Streamline pattern of driven-cavity flow

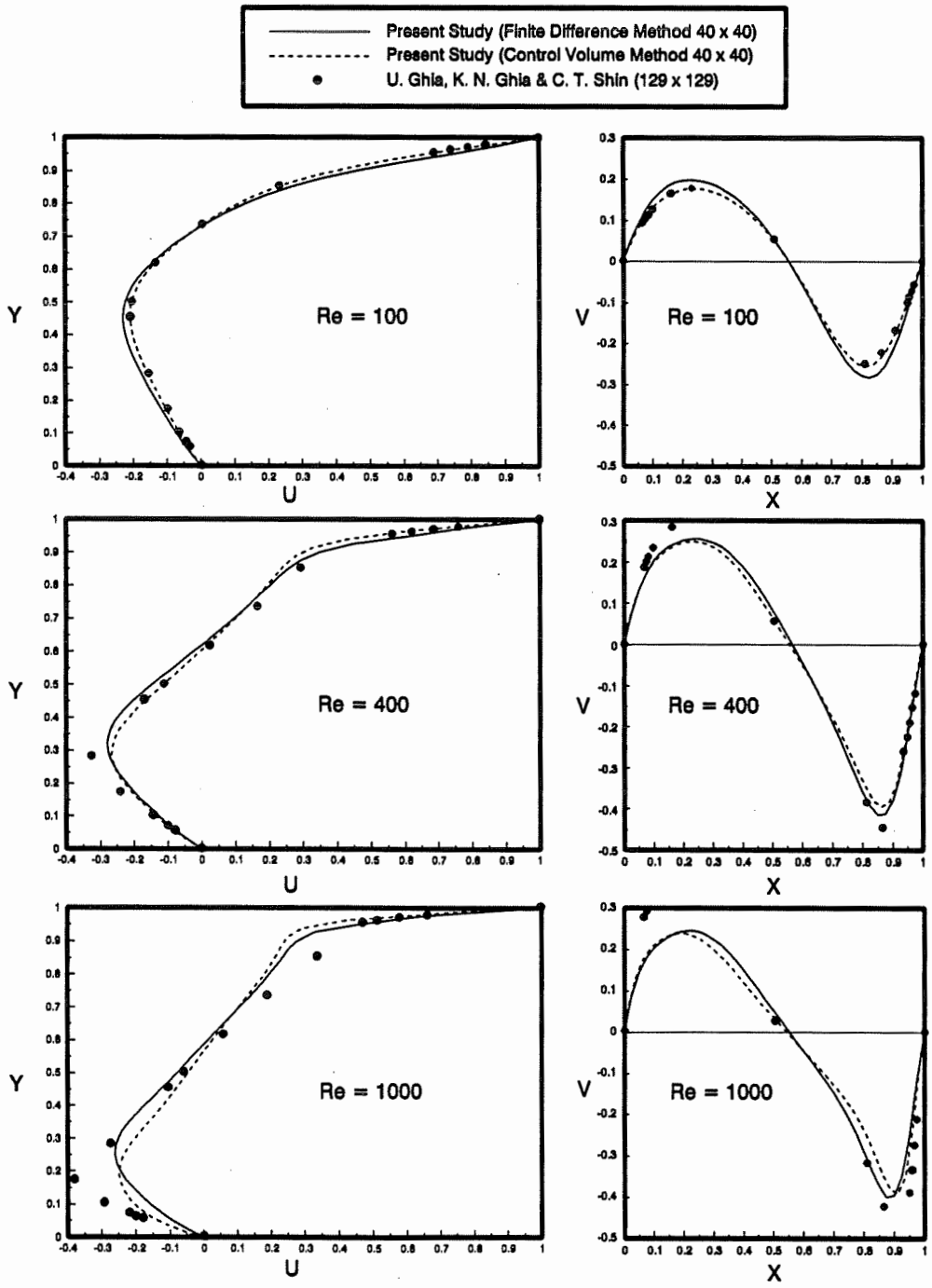

Fig. 4.3 Velocity profiles through geometric center of the cavity

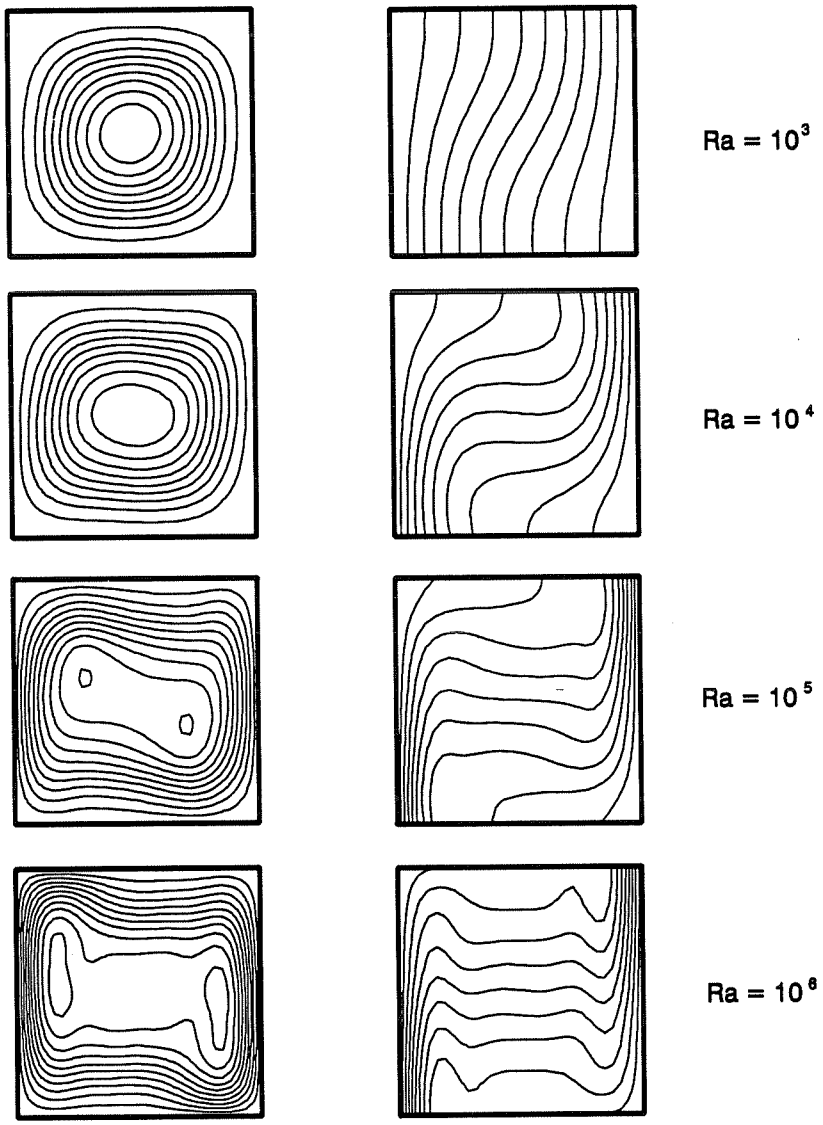

Fig. 4.5 The effect of Ra on natural convection in a square cavity

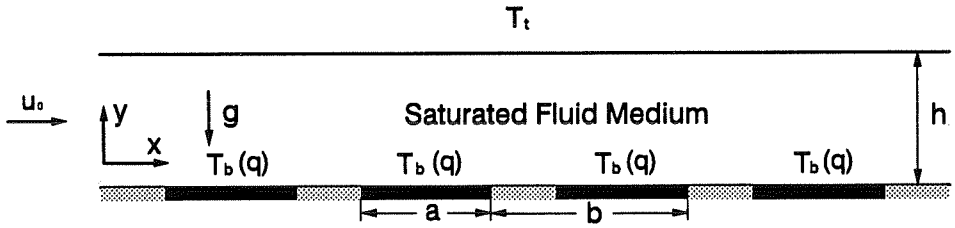

Fig. 5.1 Geometry of the problem

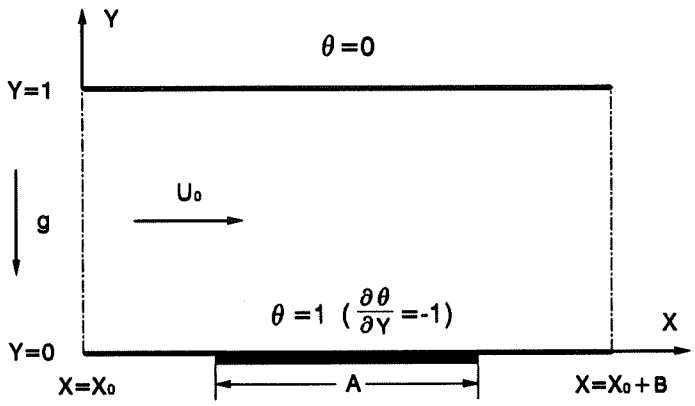

Fig. 5.2 Numerical domain

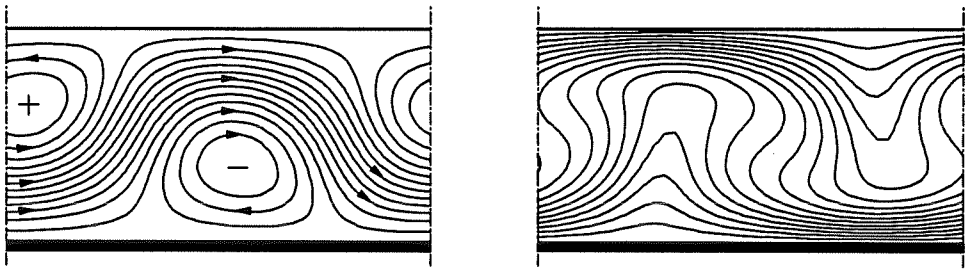

a) Ra=8000 Pe=10 $V_a = 0$ V_c=10.723

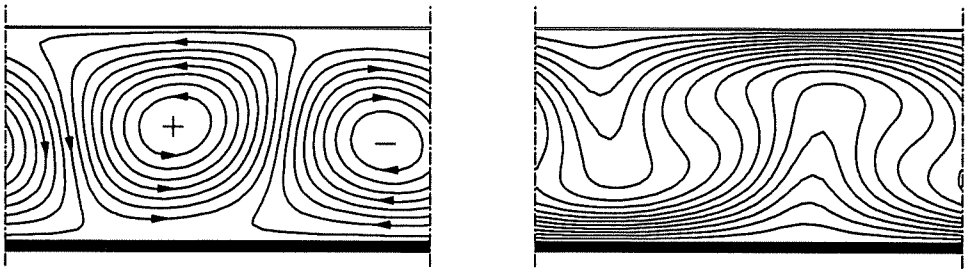

b) Ra=8000 Pe=10 $V_a = 10.728$ (Steady State)

Fig. 5.3 Velocity and temperature fields ($A = B$)

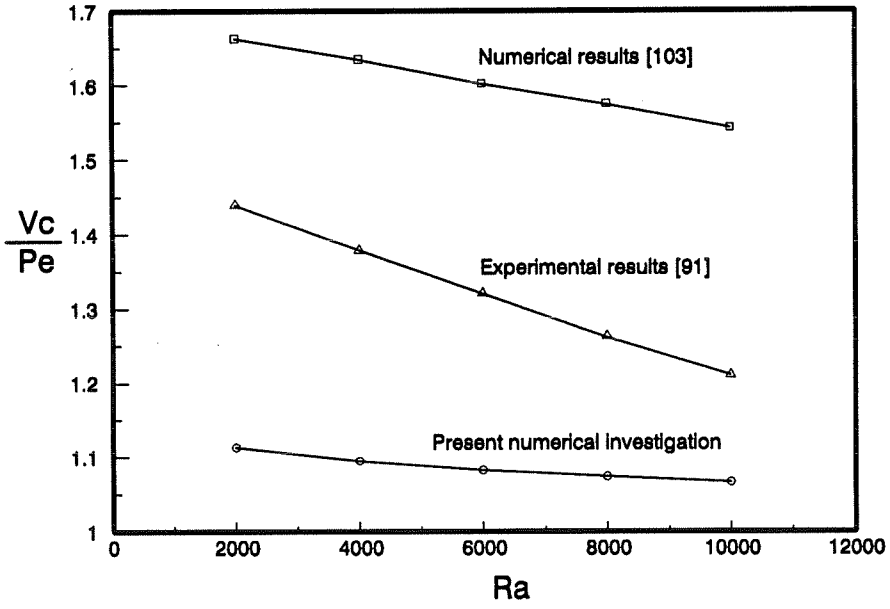

Fig. 5.4 Velocity of the transverse rolls

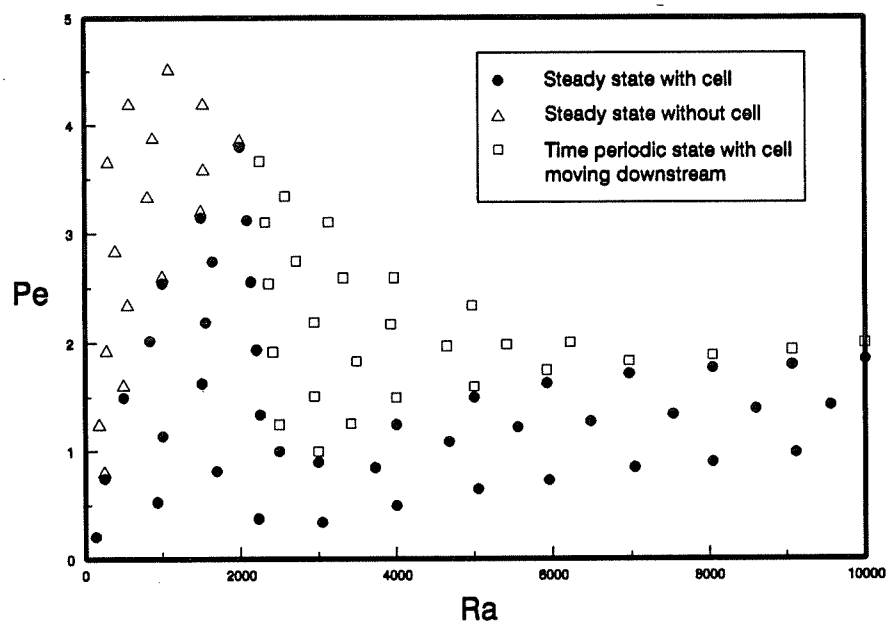

Fig. 5.5 Flow regimes function of Pe and $\bar{Ra}$

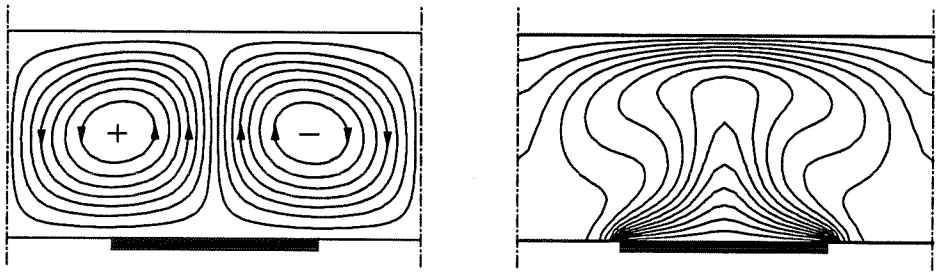

a) $Pe = 0$

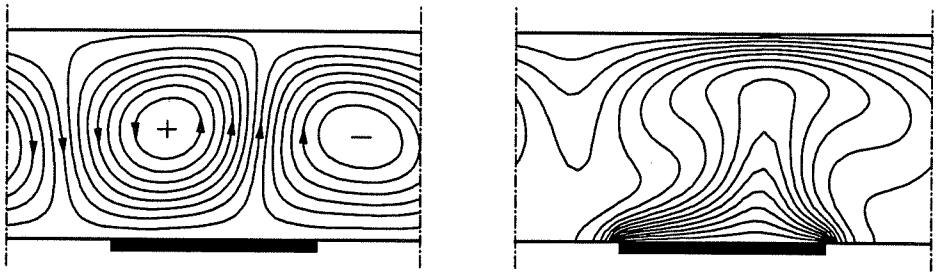

b) $Pe = 1.5$

Fig. 5.6 Steady state flow and temperature fields ($Ra = 10000$)

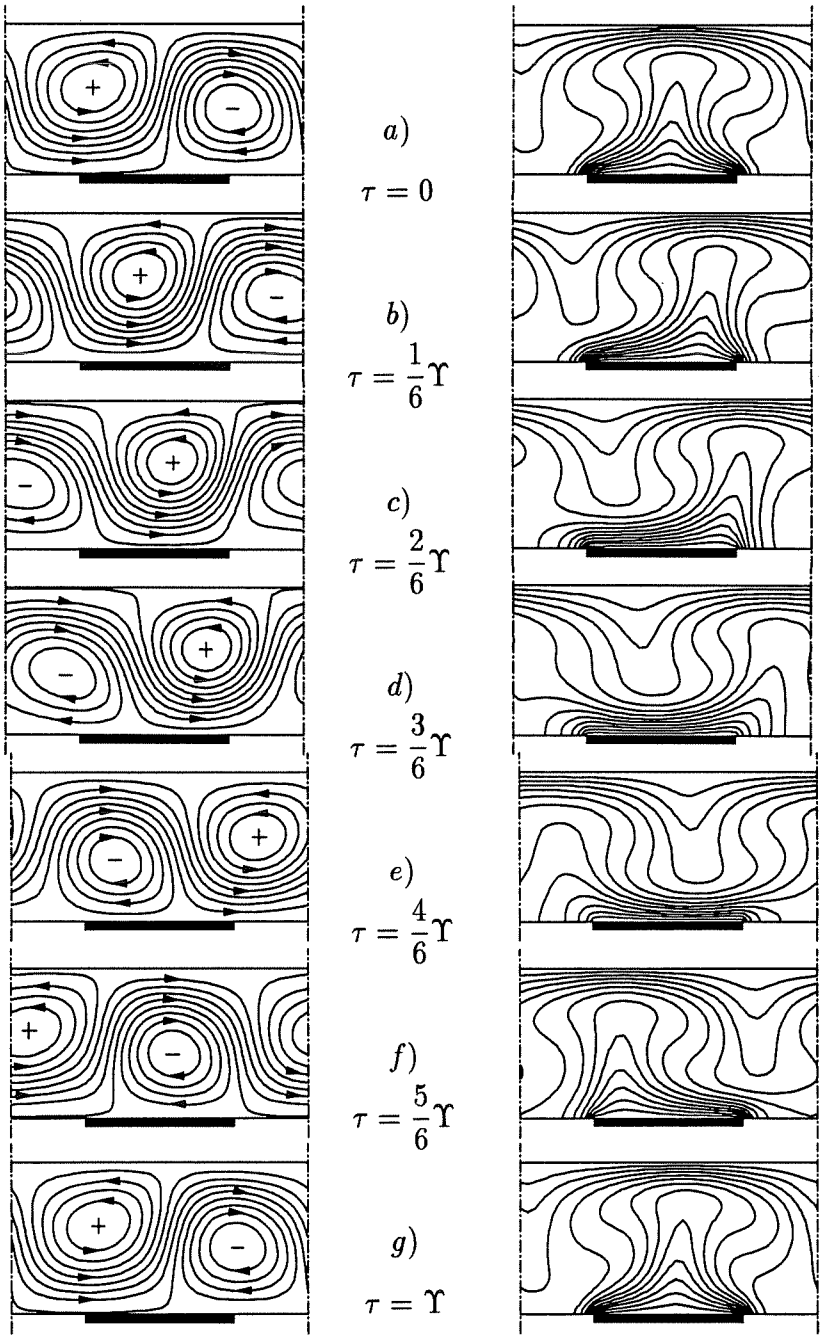

Fig. 5.7 Unsteady (periodic) flow and temperature fields at different times during one cycle ($Ra = 10000$, $Pe = 5$, $\Upsilon = 0.4026$)

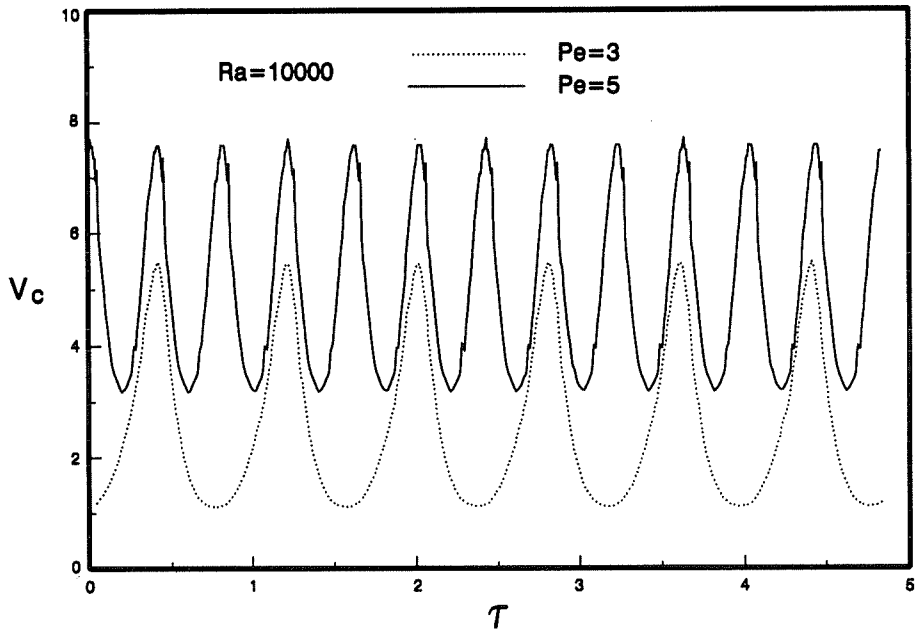

Fig. 5.8 Velocity of convective cells, function of time

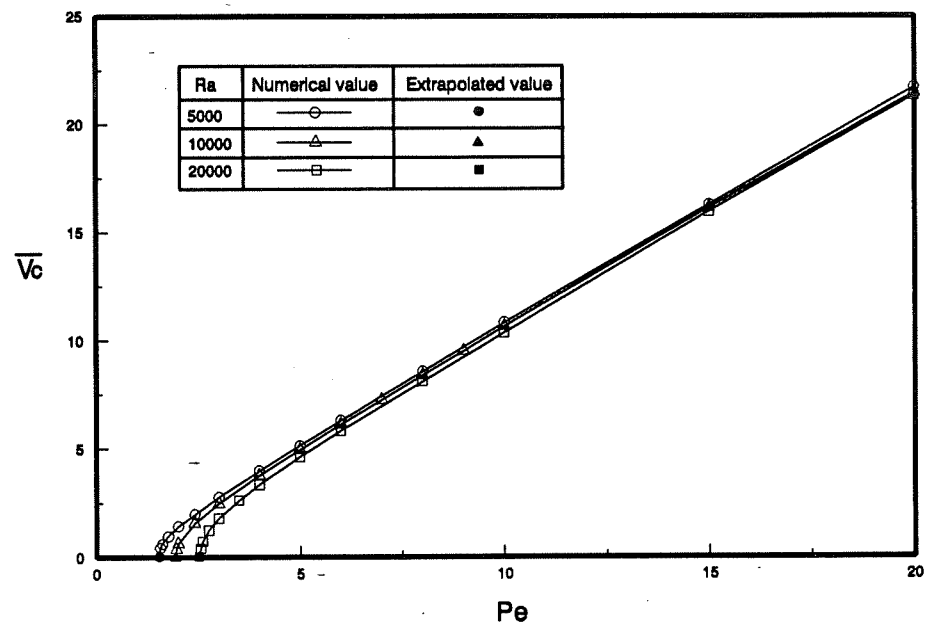

Fig. 5.9 Time average velocity of the convective cells

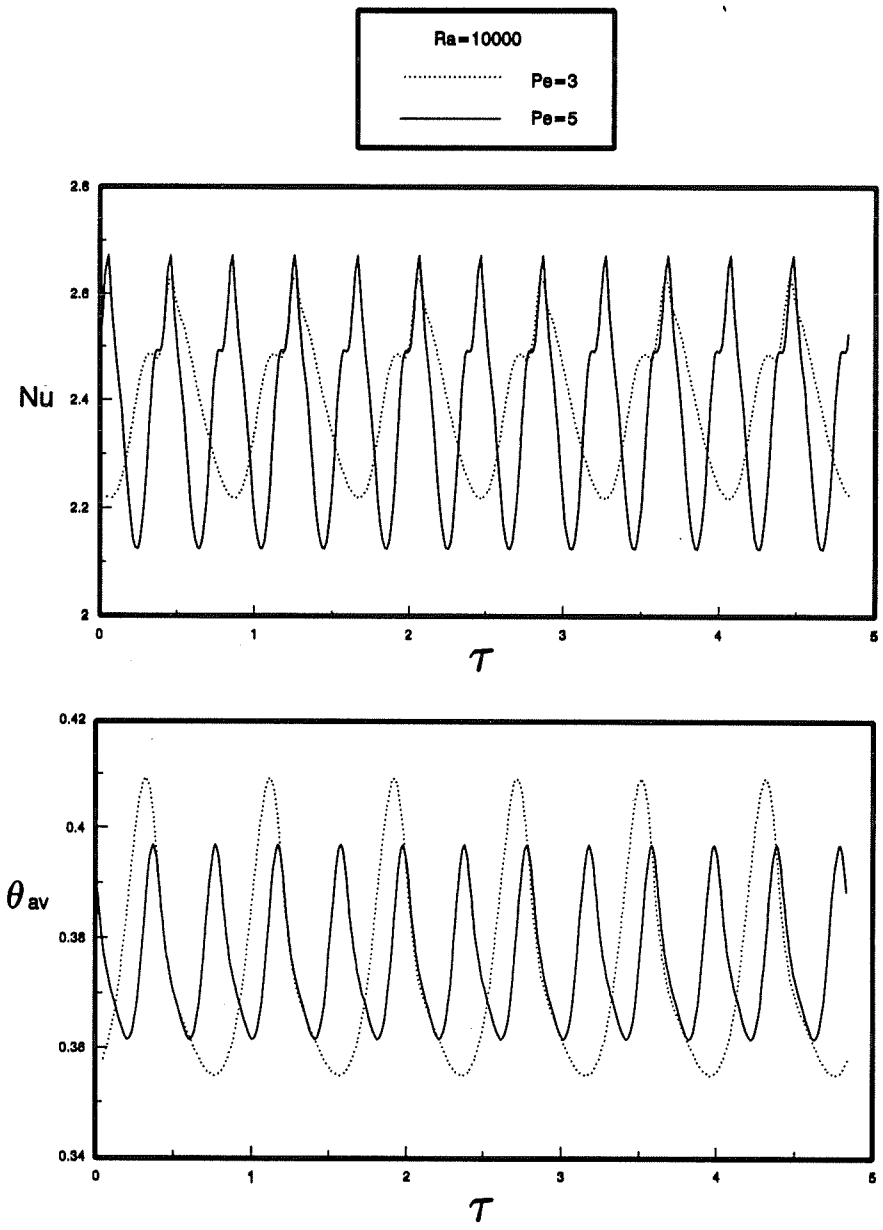

Fig. 5.10 Time dependence of Nu and θ_{av}

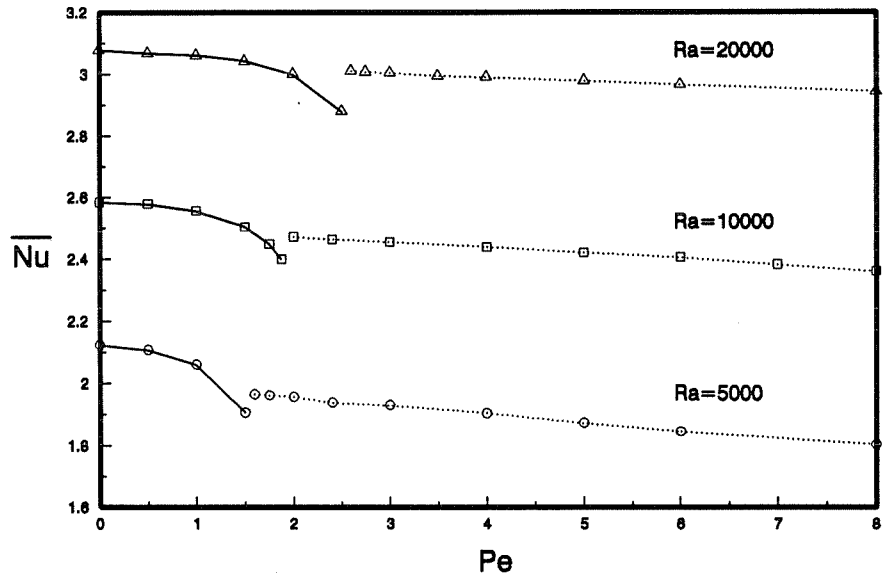

Fig. 5.11 Time average Nusselt number

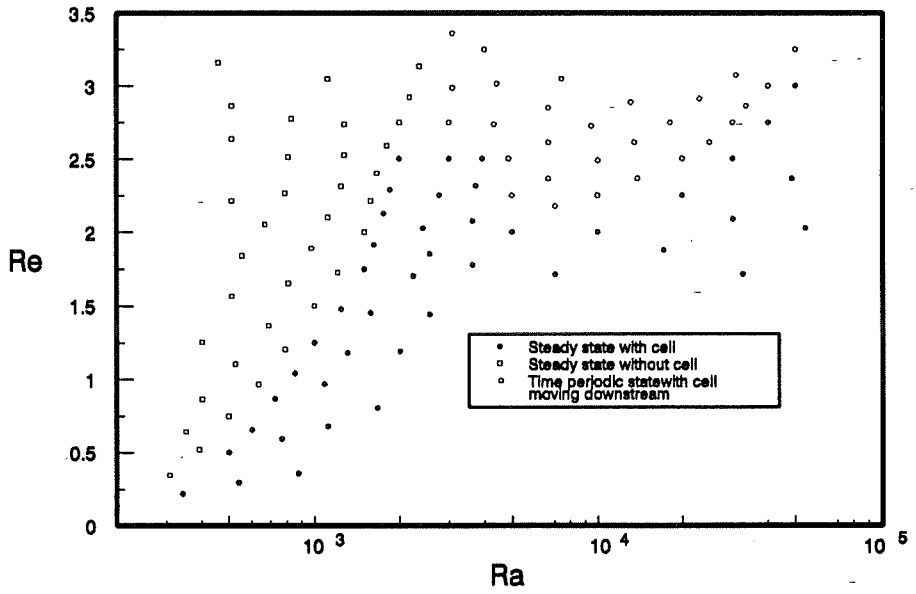

Fig. 5.12 Flow regimes functions of Re and Ra

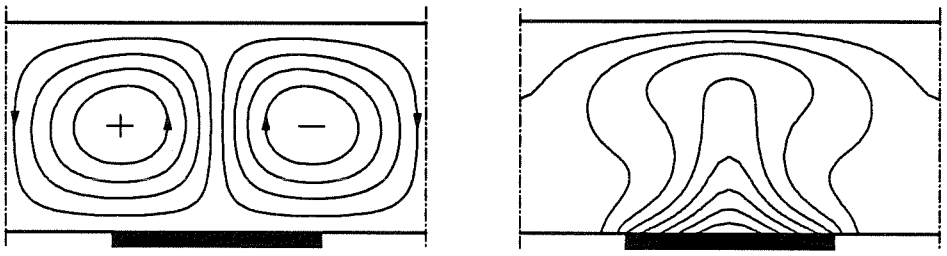

a) $Re = 0$

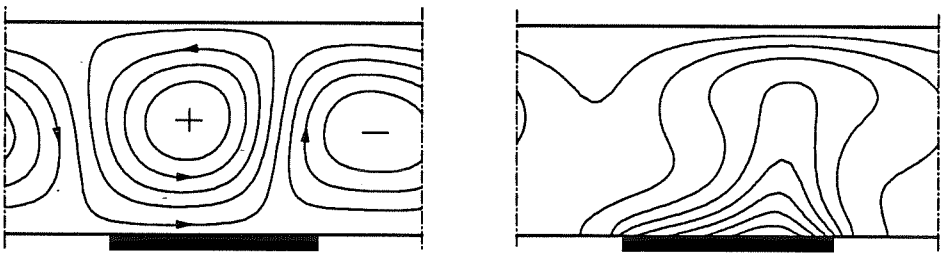

b) $Re = 2$

Fig. 5.13 Steady state flow and temperature fields ($Ra = 20000$)

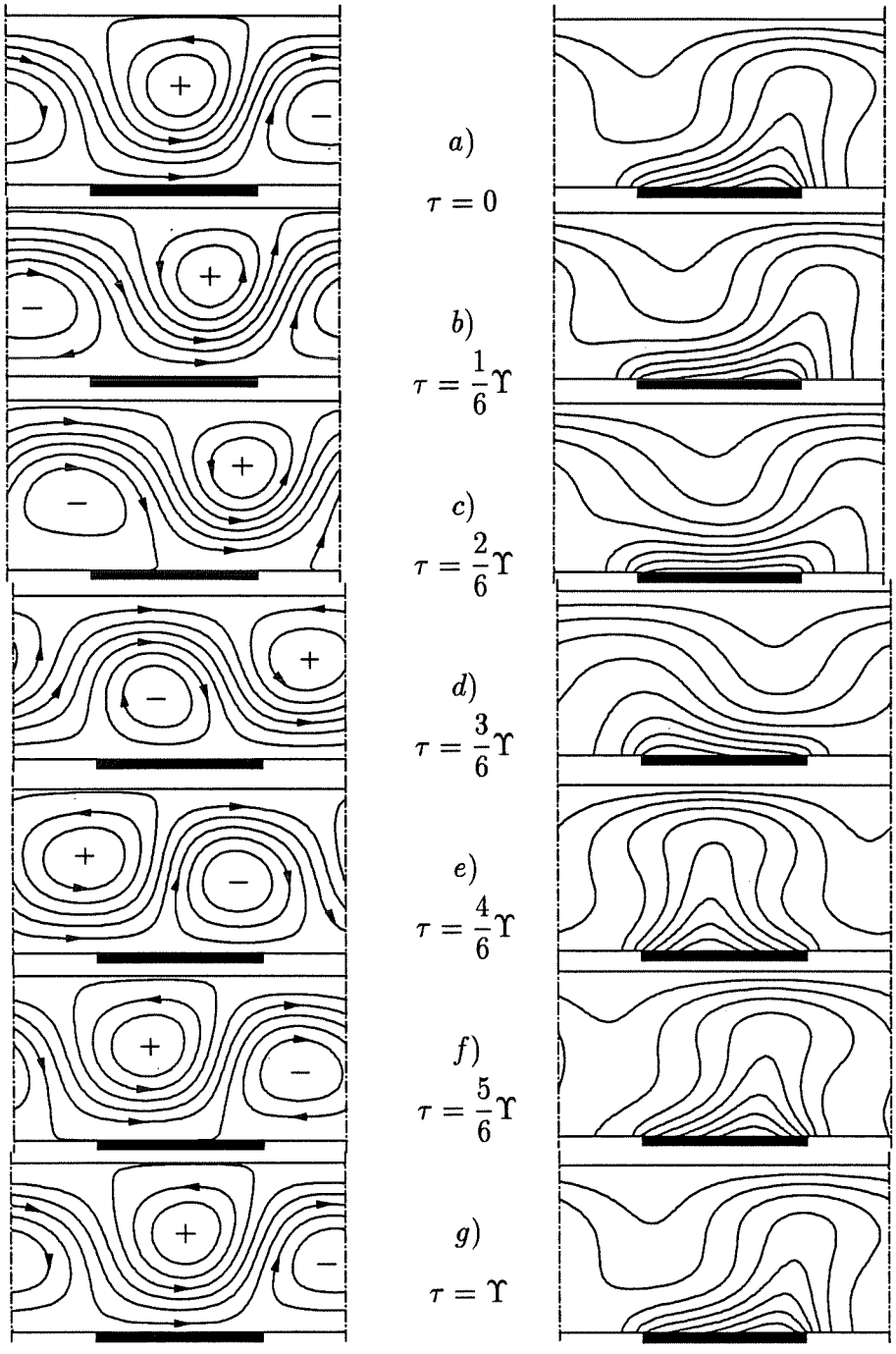

Fig. 5.14 Unsteady (periodic) flow and temperature fields at different times during one cycle ($Ra = 10000$, $Re = 4$, $\Upsilon = 2.1770$)

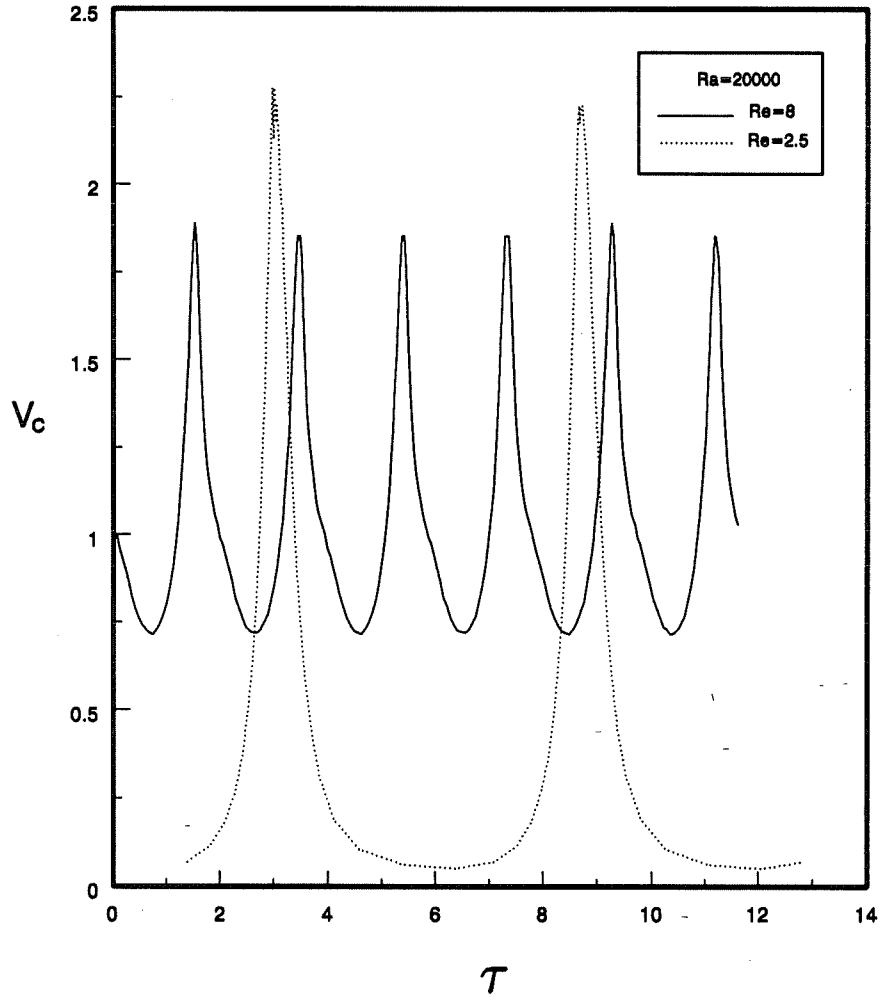

Fig. 5.15 Velocity of convective cells function of time

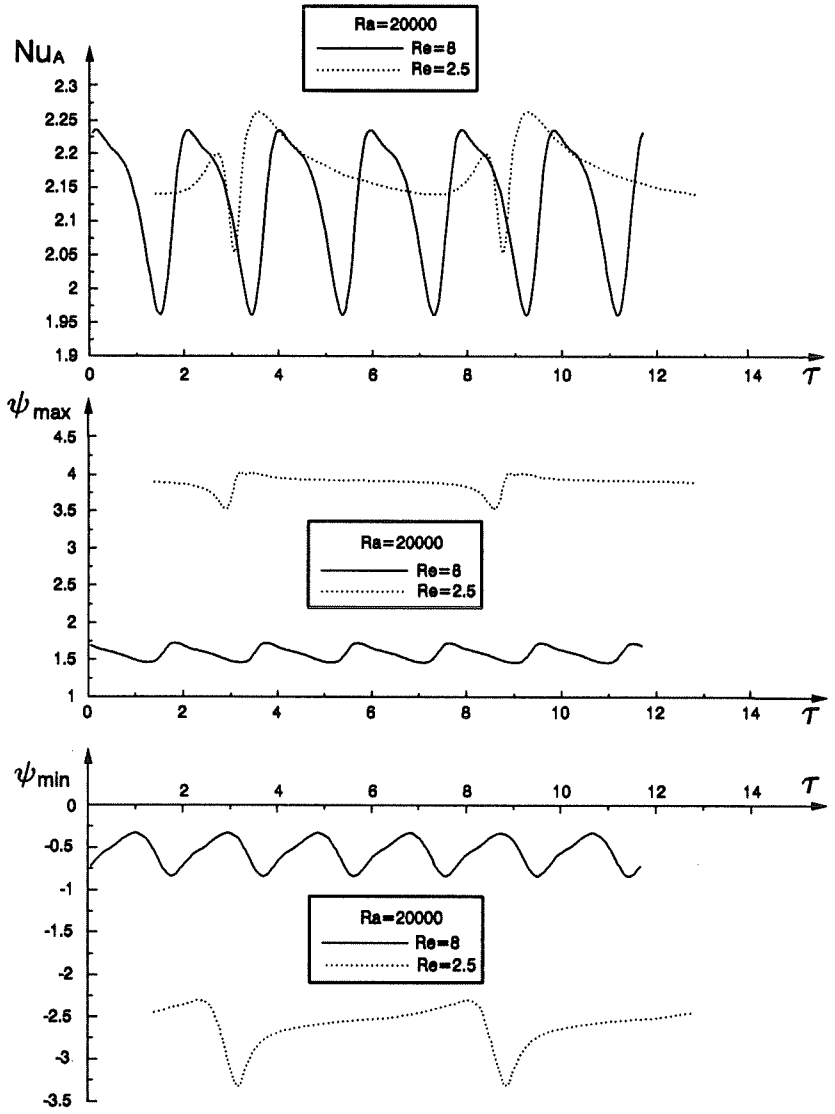

Fig. 5.16 Time dependence of Nu_A, Ψ_{max} and Ψ_{min}

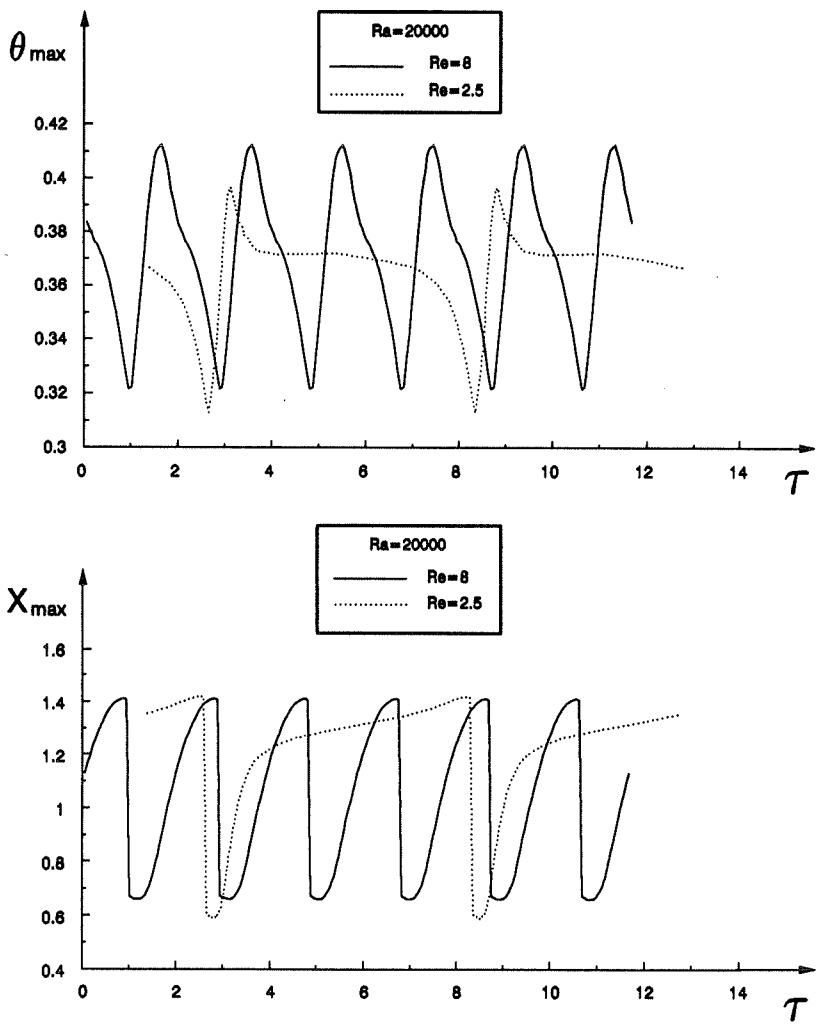

Fig. 5.17 Time dependence of θ_{max} and X_{max}

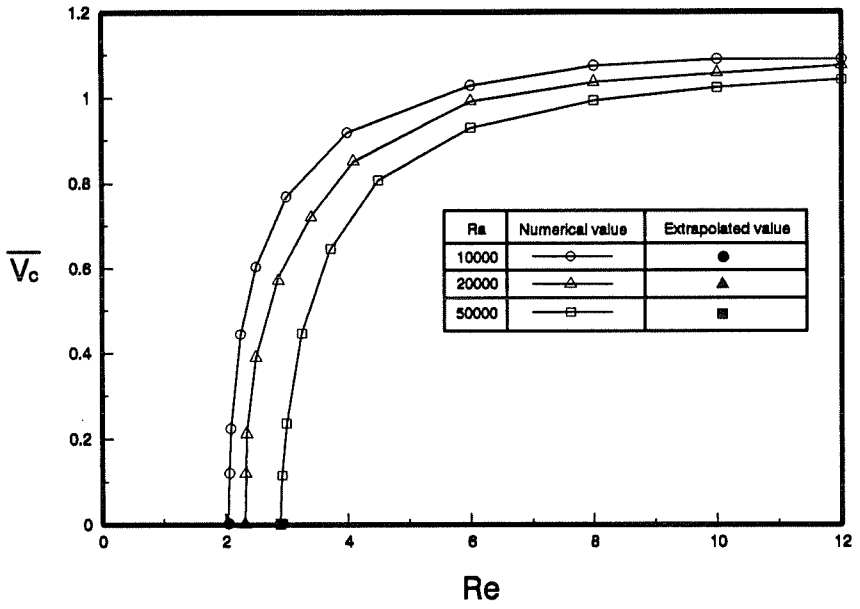

Fig. 5.18 Time average velocity of the convective cells

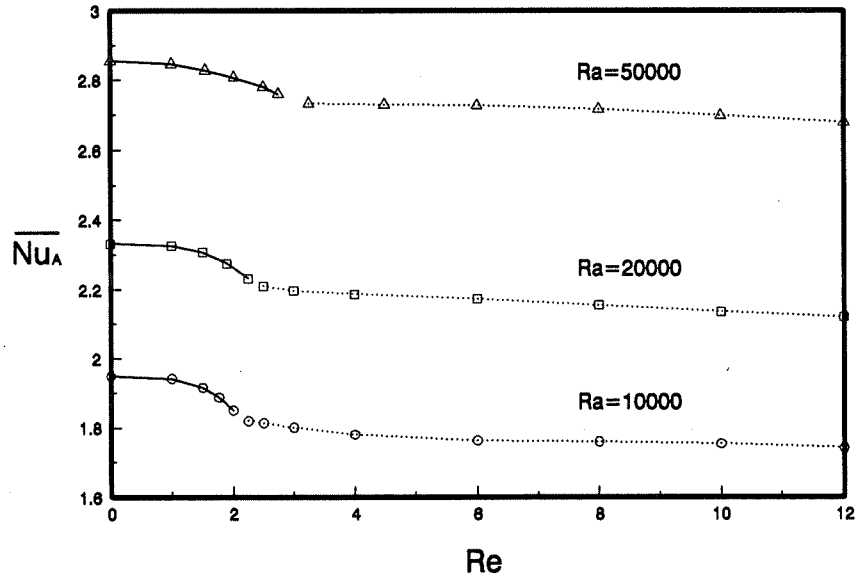

Fig. 5.19 Time average Nusselt number $\bar{Nu}_A$

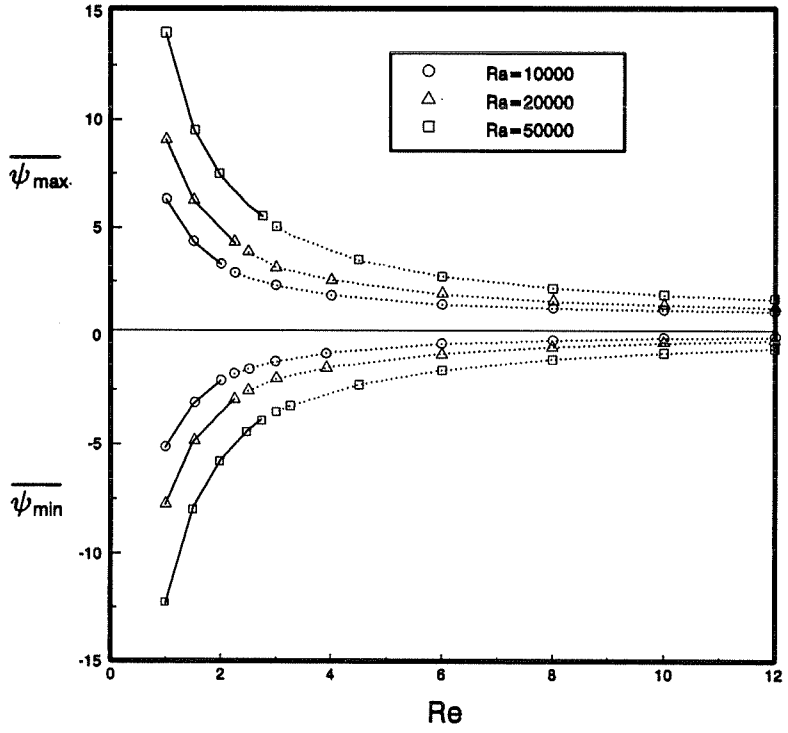

Fig. 5.20 Time average maximum and minimum stream function

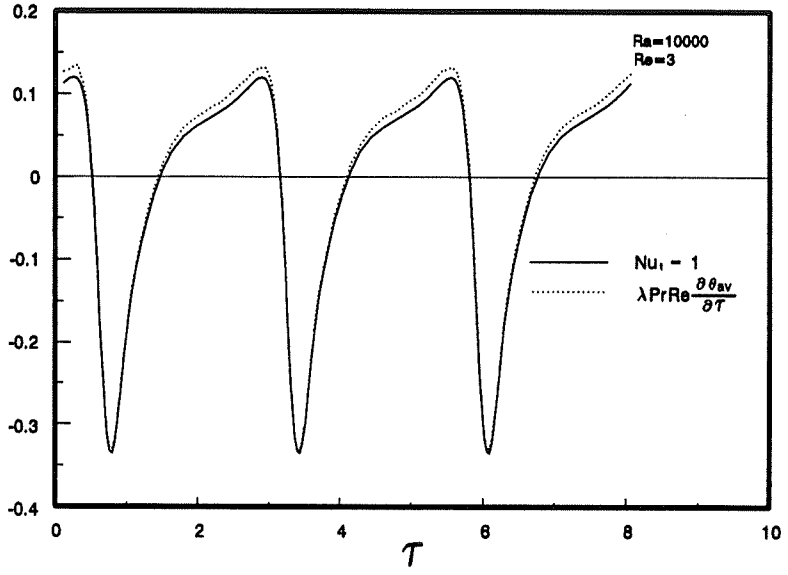

Fig. 5.21 Energy balance

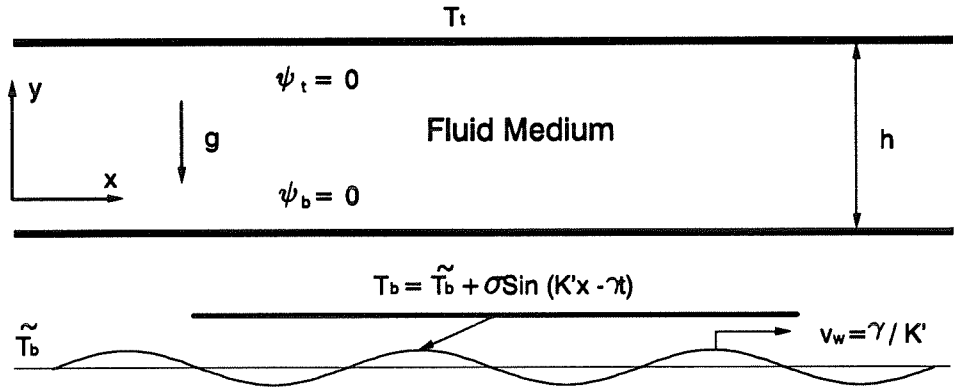

Fig. 6.1 Geometry of the problem

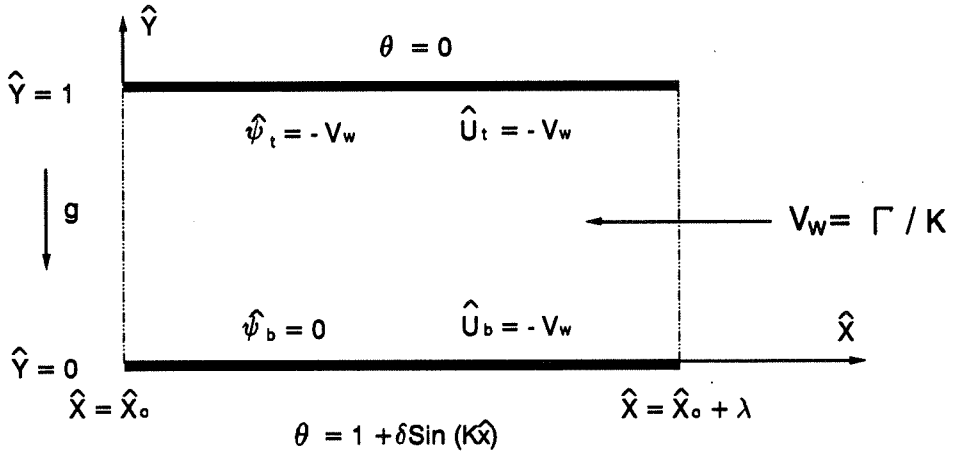

Fig. 6.2 Numerical domain

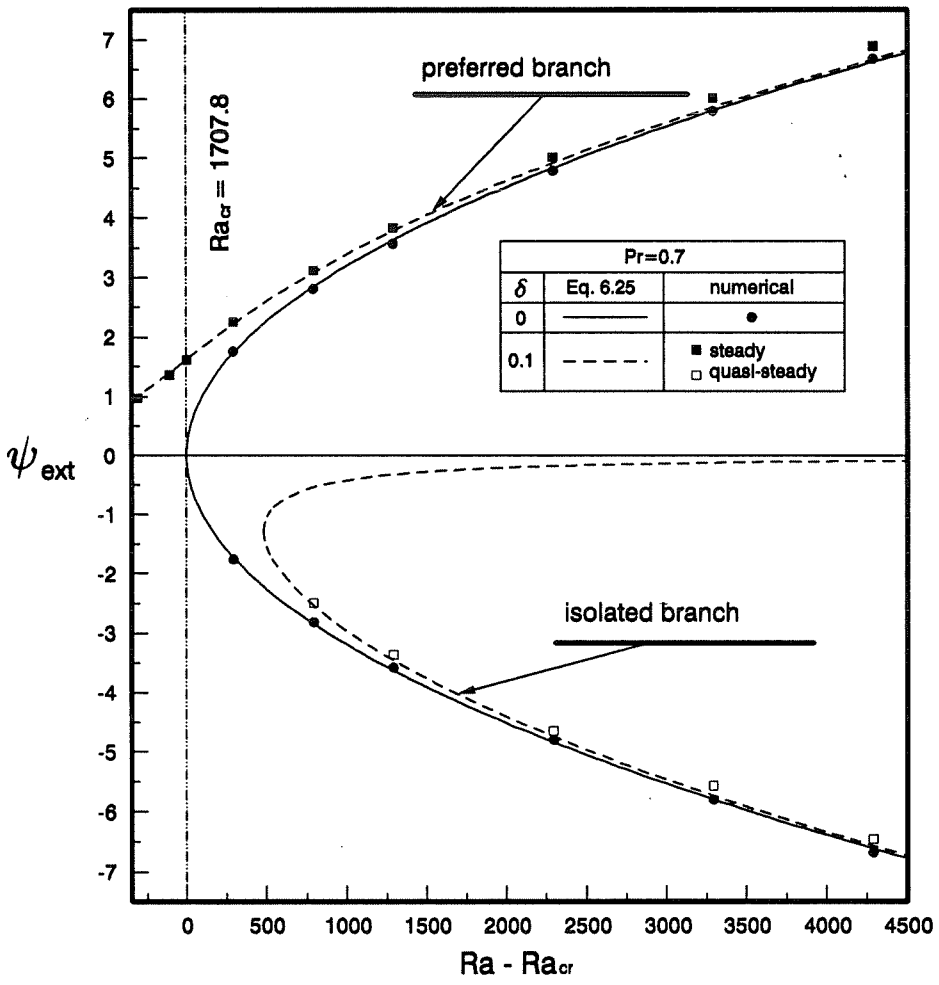

Fig. 6.3 Stationary thermal wave — multi-solution

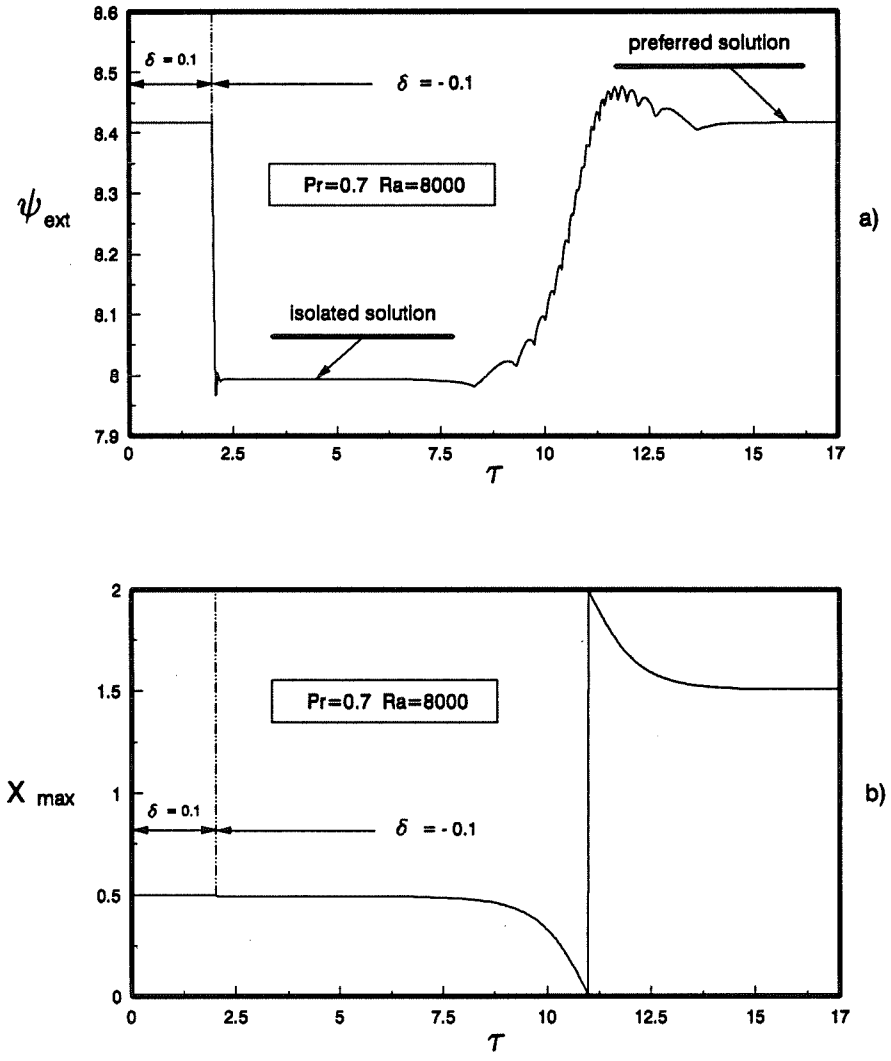

Fig. 6.4 - Extreme value of stream function and its location as a function of time

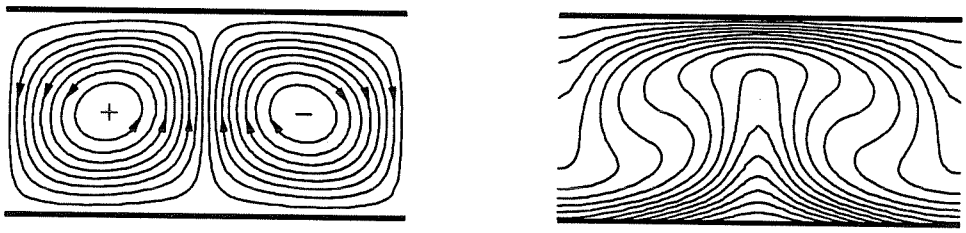

a) $V_w = 0$

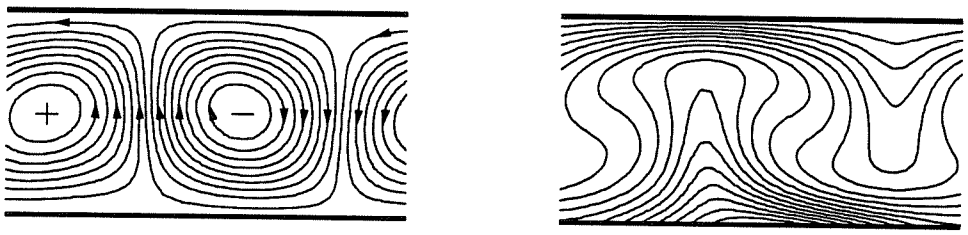

b) $V_w = 1$

Fig. 6.5 Steady state flow and temperature fields
($Ra = 8000$, $\delta = 0.3$)

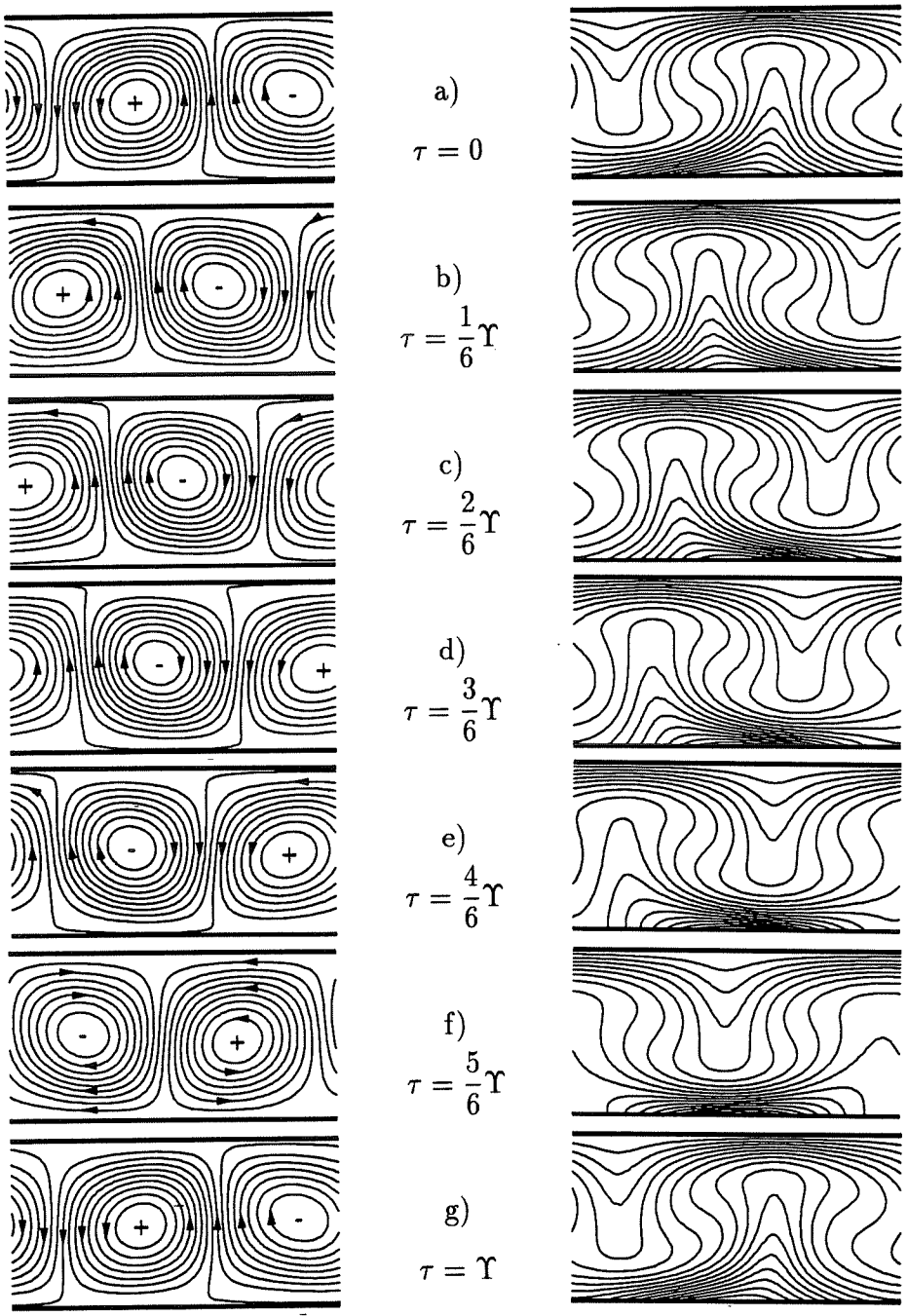

Fig. 6.6 Unsteady periodic flow and temperature fields at different times during one cycle ($Ra = 8000$, $V_w = 2$, $\delta = 0.3$ and $\Upsilon = 1.2834$)

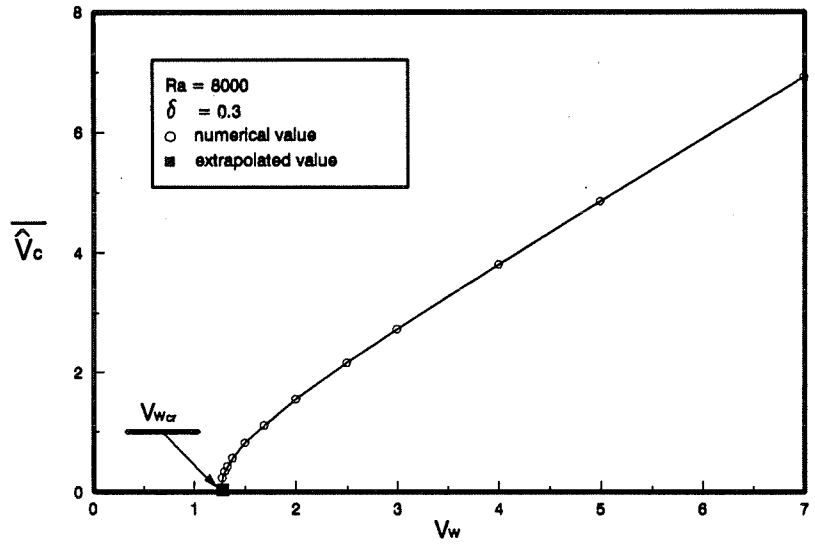

Fig. 6.7a Cell average velocity based on moving frame as a function of thermal wave velocity V_w

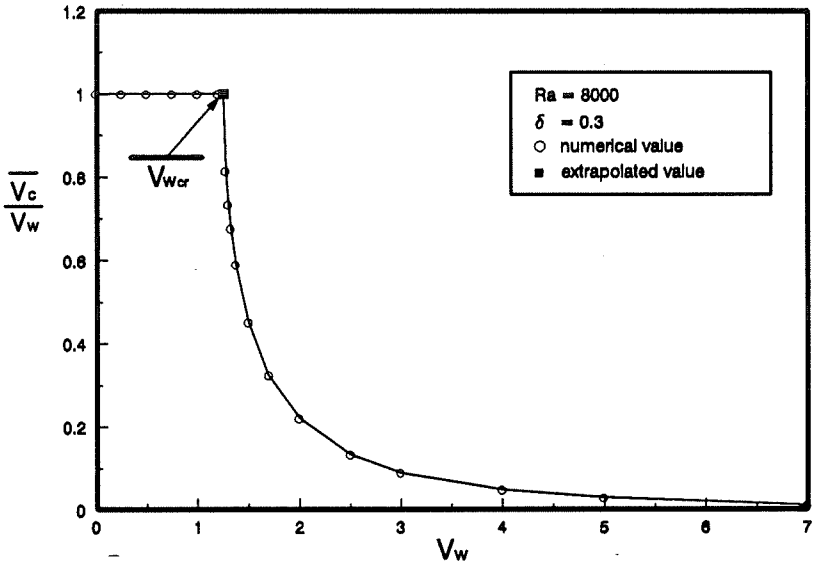

Fig. 6.7b Cell average velocity based on fixed frame as a function of thermal wave velocity V_w

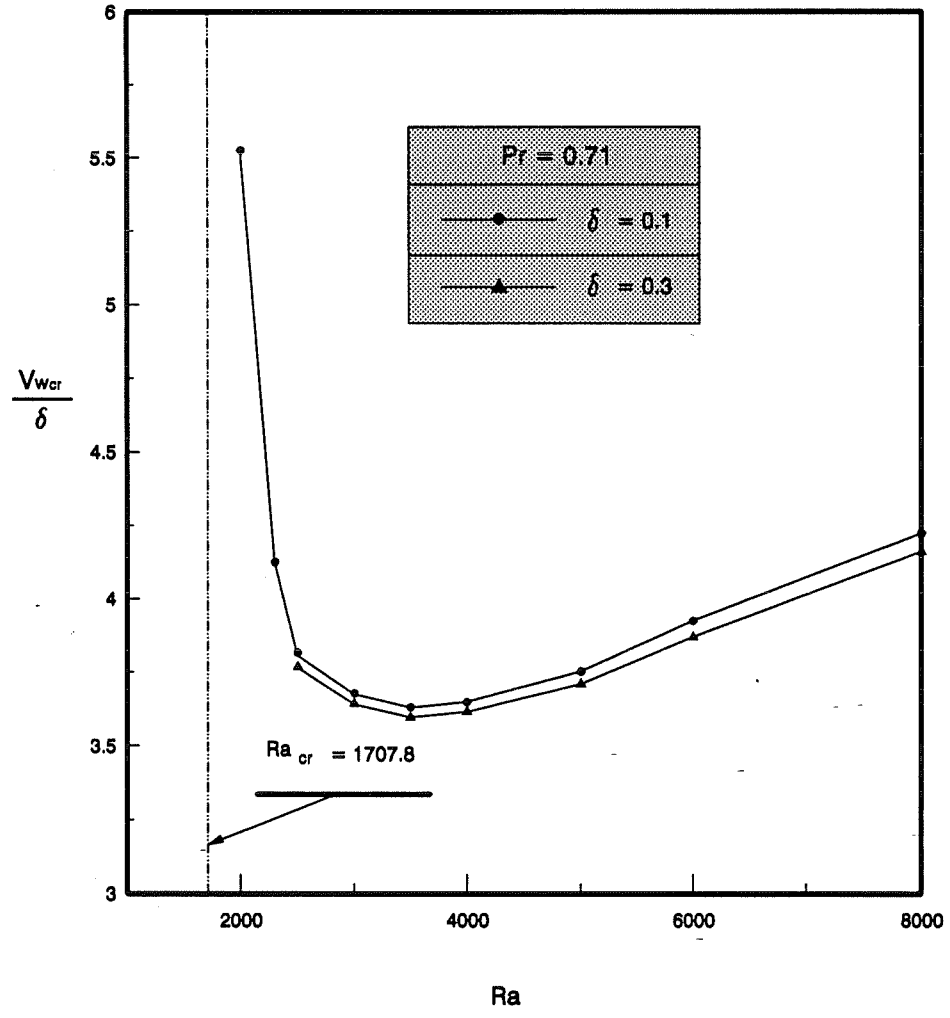

Fig. 6.8 Critical thermal wave velocity function of Ra

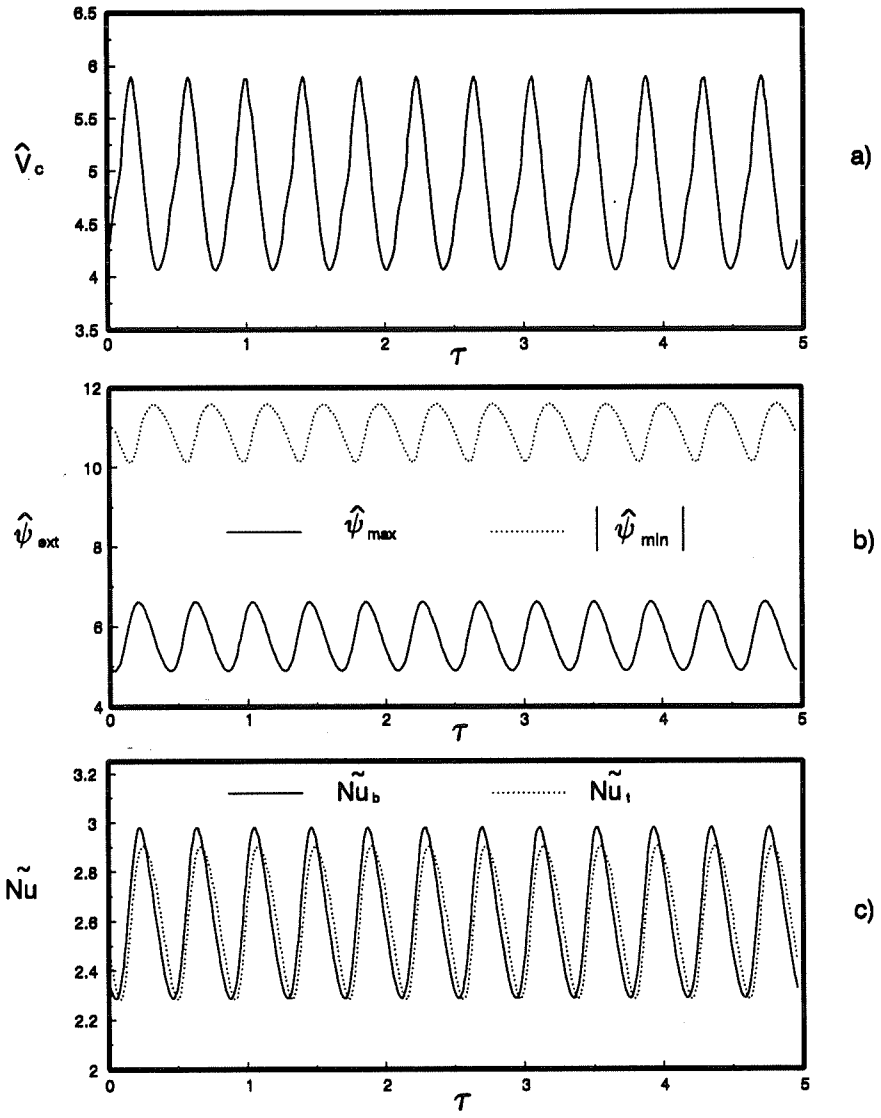

Fig. 6.9 Time dependence of $\hat{V}_c$, $\hat{\Psi}_{max}$, $\hat{\Psi}_{min}$, $\widetilde{Nu}_b$ and $\widetilde{Nu}_t$ ($Ra = 8000$, $V_w = 5$, $\delta = 0.3$)

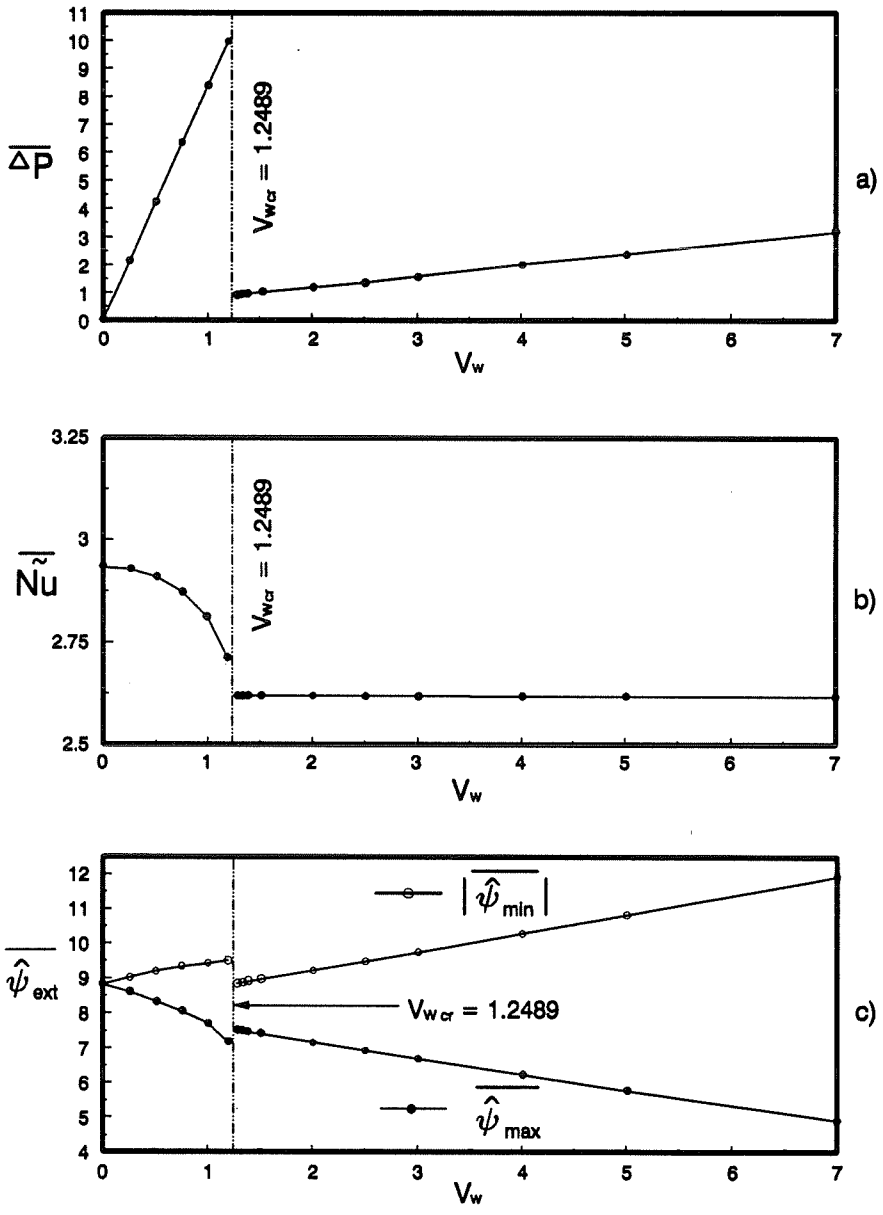

Fig. 6.10 Time average value $\overline{\Delta P}$, $\overline{\widetilde{Nu}}$ and $\overline{\hat{\Psi}_{ext}}$ function of thermal wave velocity V_w ($Ra = 8000$, $\delta = 0.3$)

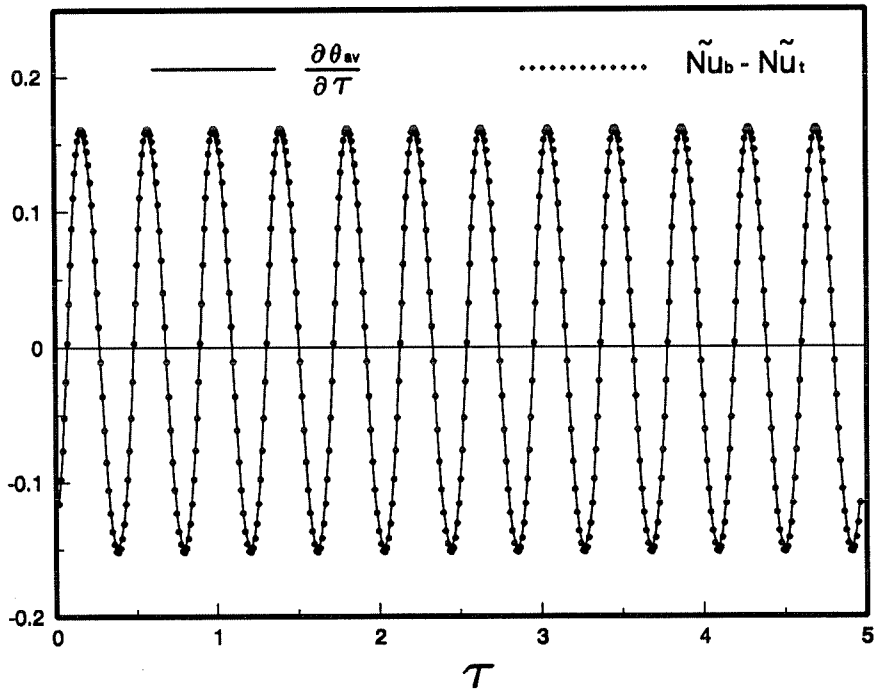

Fig. 6.11 Energy balance ($Ra = 8000$, $V_w = 5$, $\delta = 0.3$)

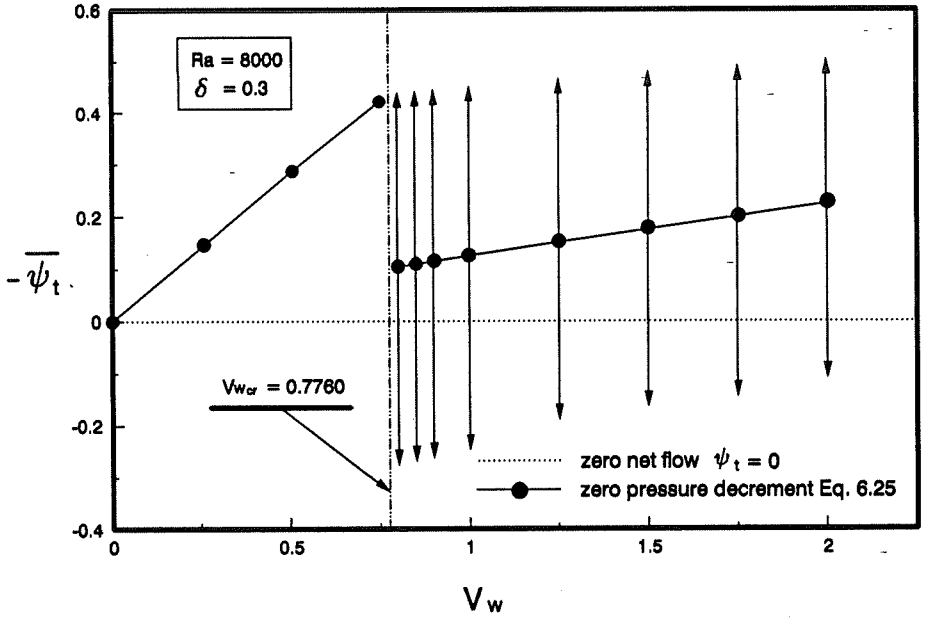

Fig. 6.12 Net flow function of thermal wave velocity

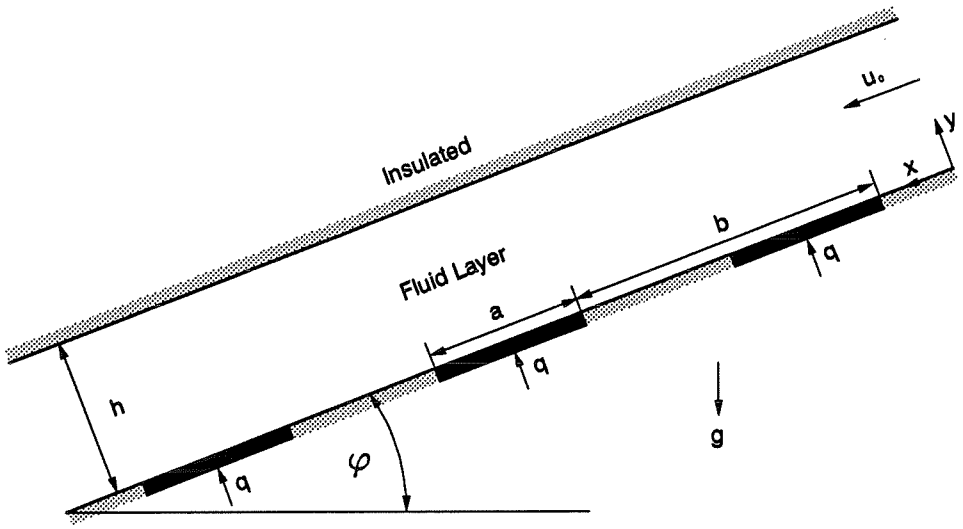

Fig. 7.1 Geometry of the problem

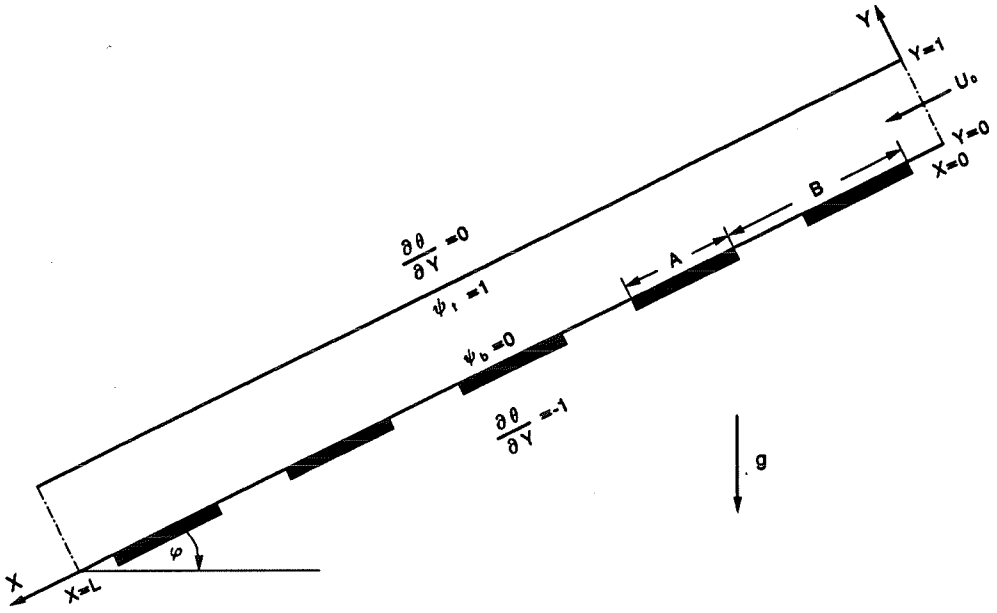

a) Whole channel configuration

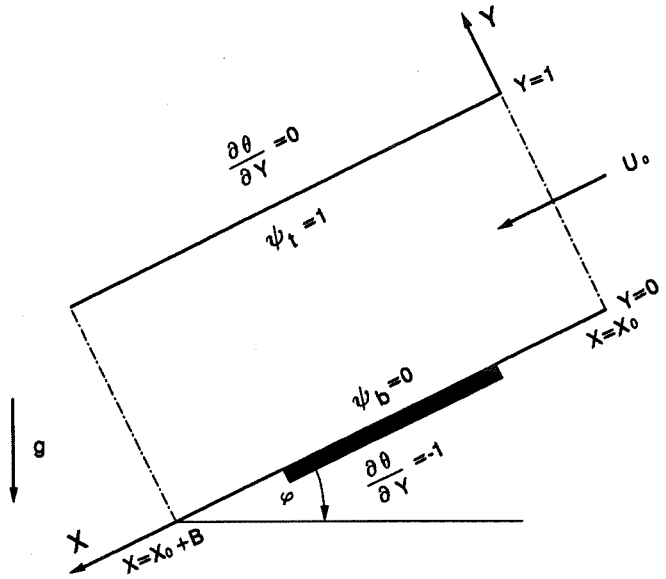

b) One-wavelength configuration

Fig. 7.2 Numerical domain

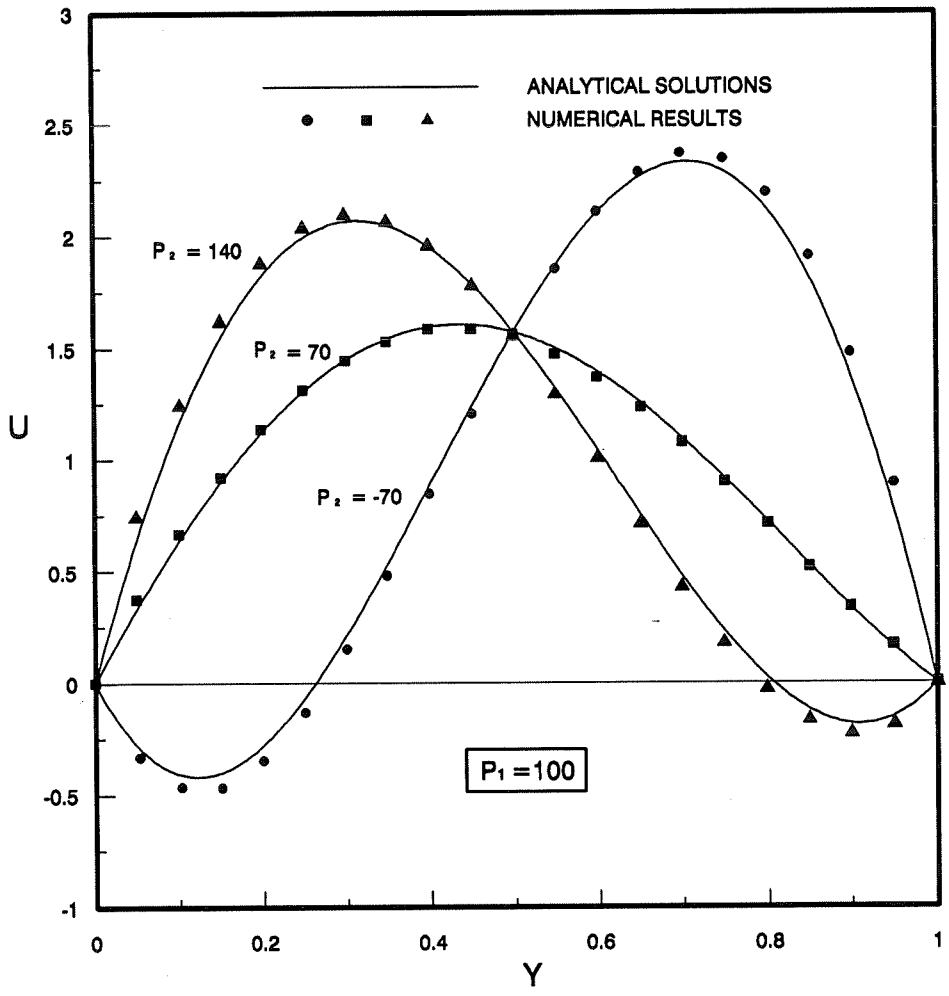

Fig. 7.3 Velocity profiles of entirely heated wall

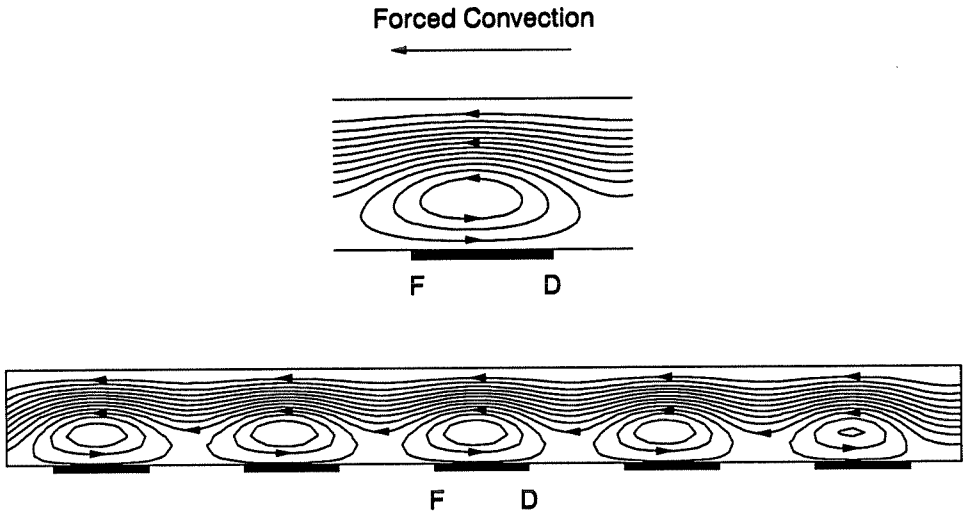

a) Flow field

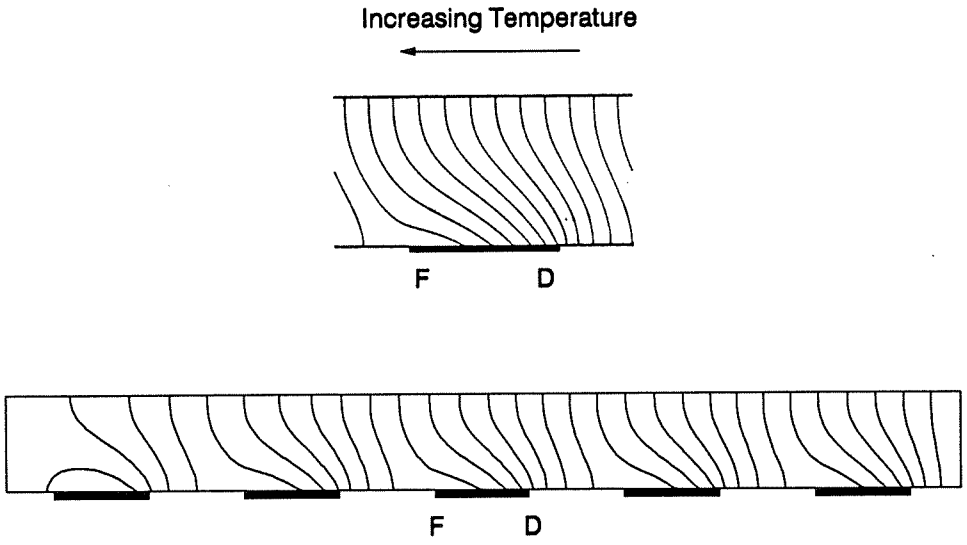

b) Temperature field

Fig. 7.4 Comparison between the one-wavelength configuration and the whole channel configuration ($Ra = 500$, $\varphi = 75^0$)

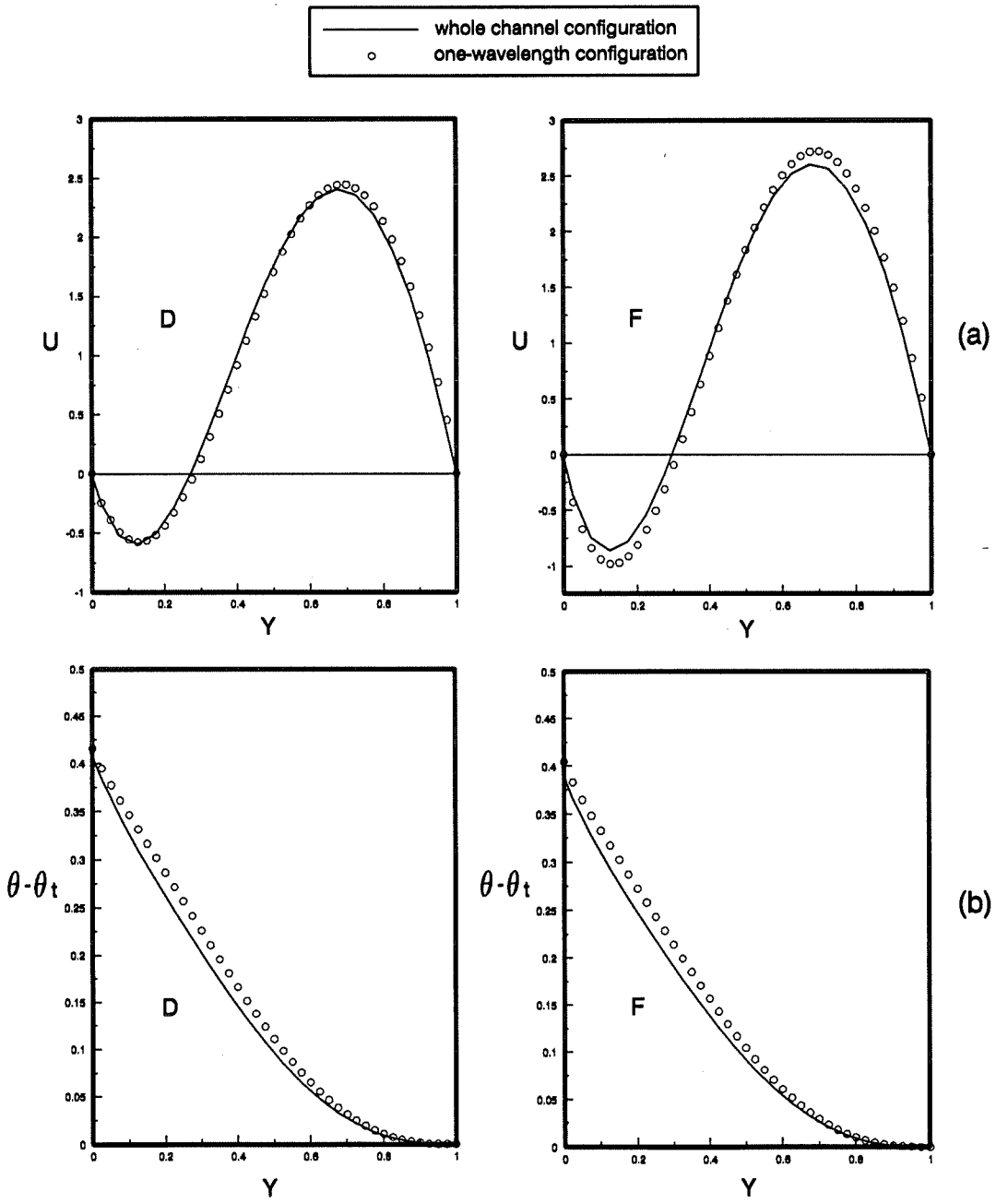

Fig. 7.5 Velocity and temperature profiles at given locations D & F

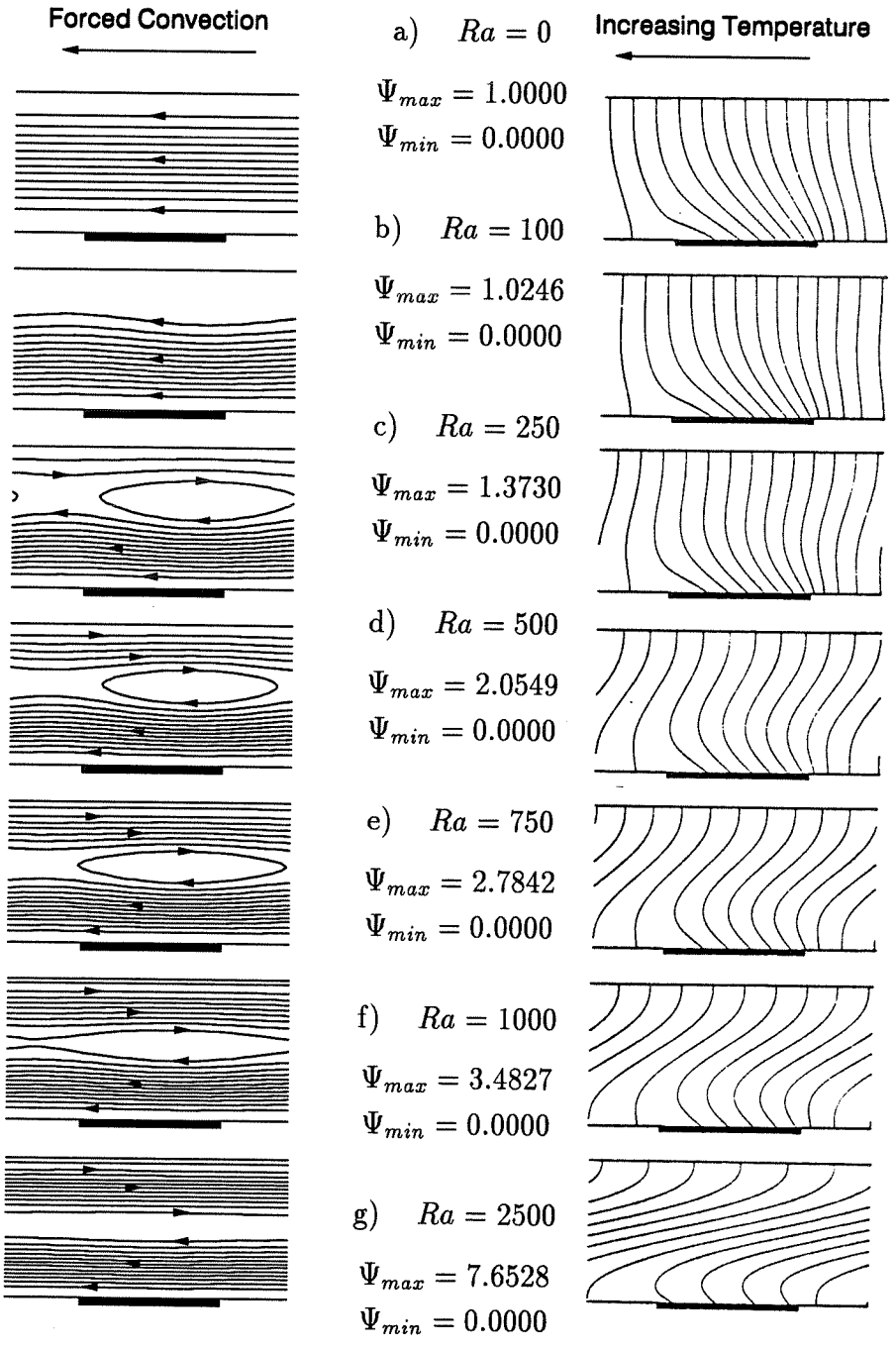

Fig. 7.6 Flow and temperature fields as function of Ra in a horizontal channel ($Re = 1.0$, $\varphi = 0$)

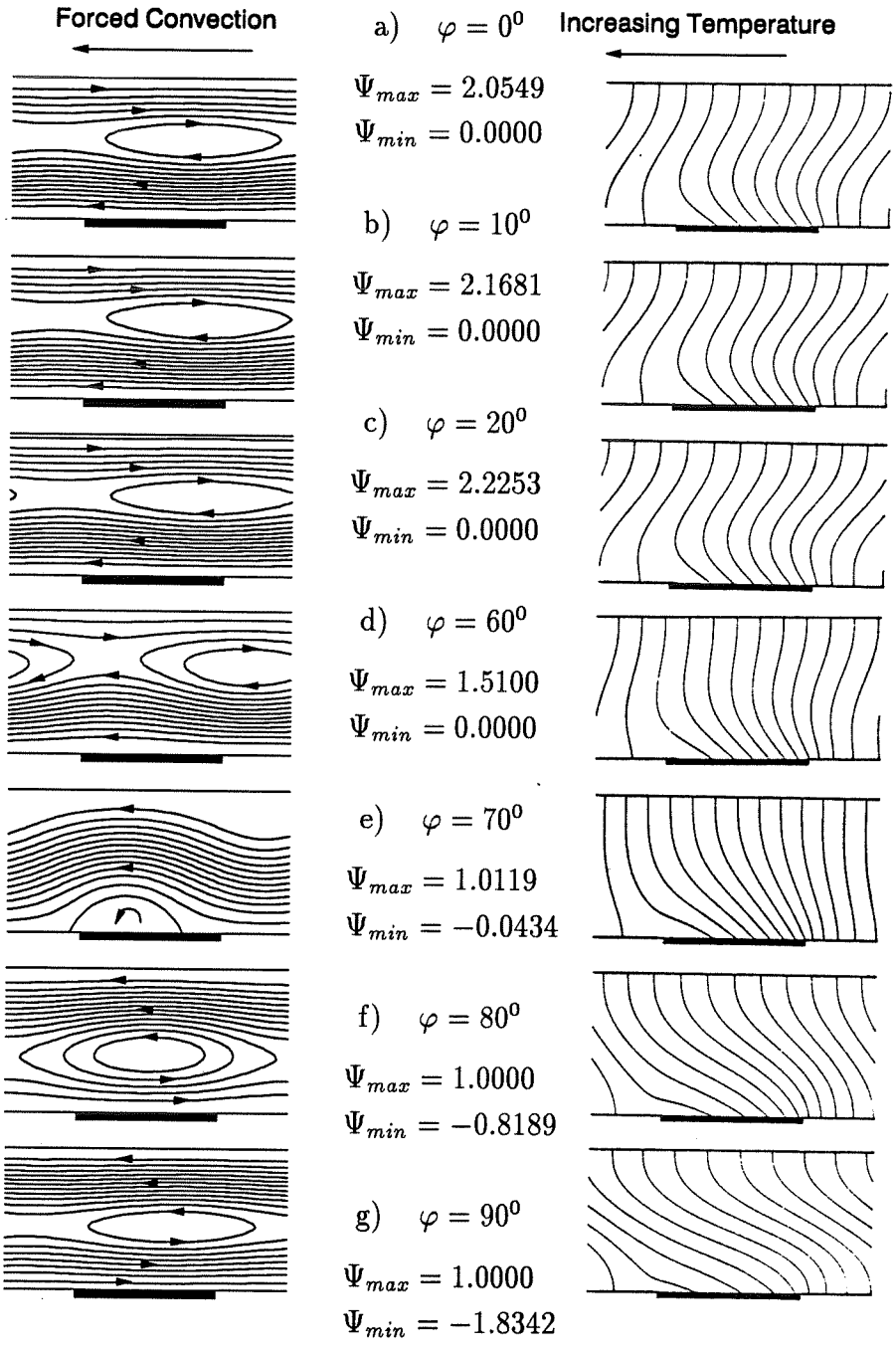

Fig. 7.7 Flow and temperature fields as function of inclination angle ($Ra = 500$, $Re = 1$)

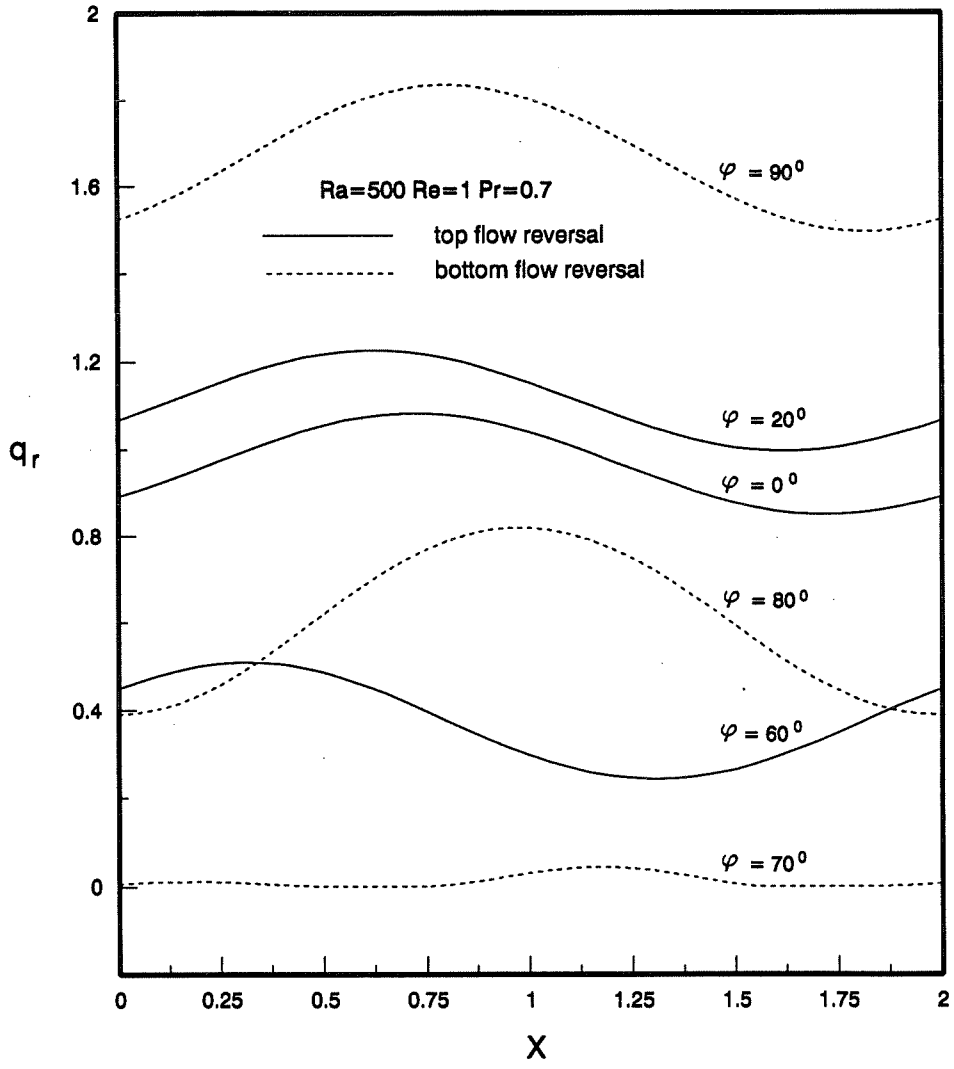

Fig. 7.8 Flow reversal parameter as function of X

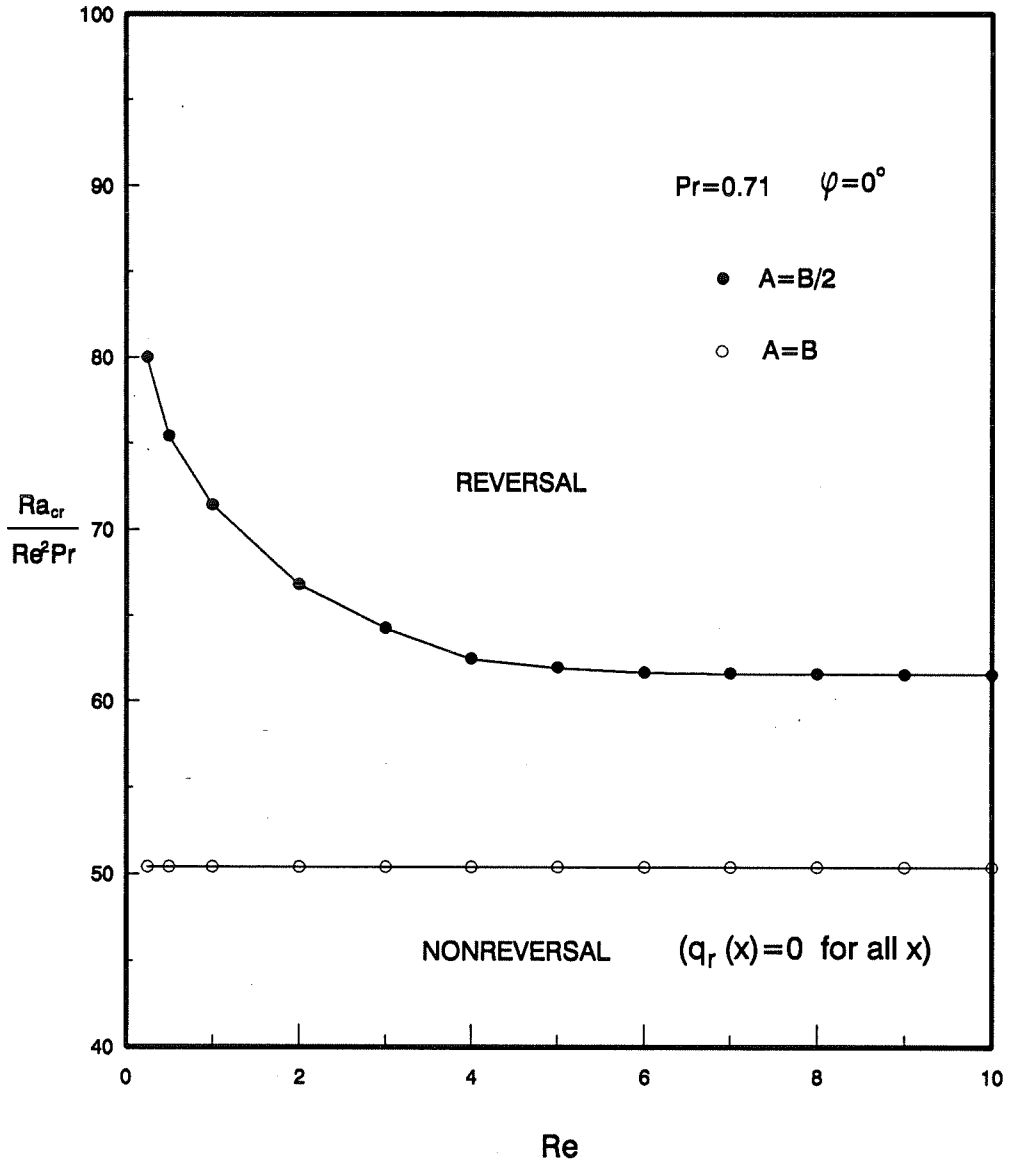

Fig. 7.9 Conditions for flow reversal

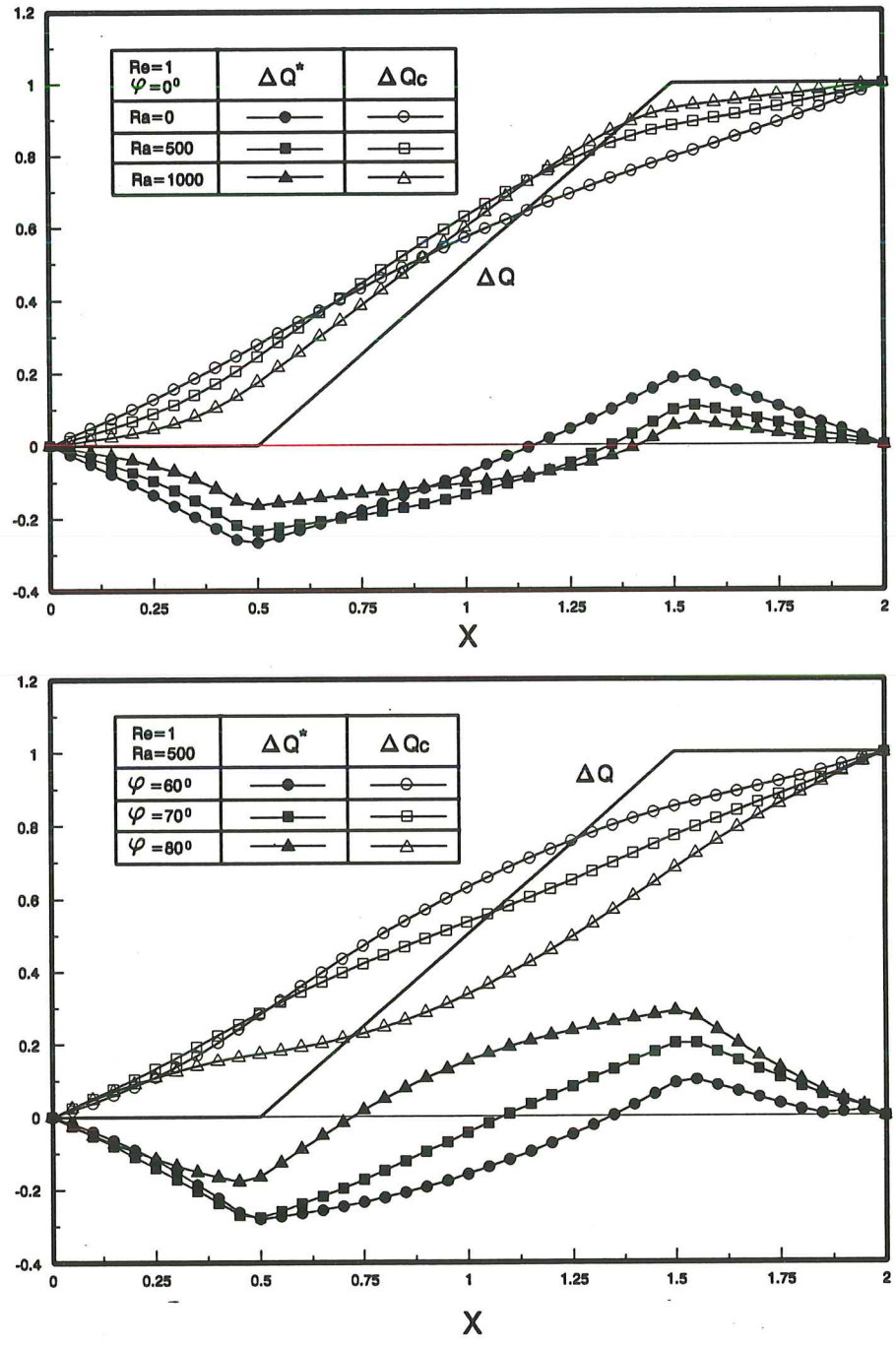

Fig. 7.10 Local heat flux profiles